CHALMERS

Durability of Adhesively-Bonded CFRP/Steel Joints

Modelling of moisture ingress and joint degradation

Master's Thesis in the Master's Programme Structural Engineering and Building Technology

LUIS DURAN JOFRE
ELOY OLAGÜE JULIÁN

Department of Civil and Environmental Engineering
Division of Structural Engineering
Steel and Timber Structures
CHALMERS UNIVERSITY OF TECHNOLOGY
Göteborg, Sweden 2013
Master's Thesis 2013:123

Durability of Adhesively-Bonded CFRP/Steel Joints

Modelling of moisture ingress and joint degradation

Master's Thesis in the Master's Programme Structural Engineering and Building Technology

LUIS DURAN JOFRE

ELOY OLAGÜE JULIÁN

Department of Civil and Environmental Engineering
Division of Structural Engineering
Steel and Timber Structures
CHALMERS UNIVERSITY OF TECHNOLOGY
Göteborg, Sweden 2013

Durability of Adhesively-Bonded CFRP/Steel Joints
Modelling of moisture ingress and joint degradation

Master's Thesis in the Master's Programme Structural Engineering and Building Technology
LUIS DURAN JOFRE
ELOY OLAGÜE JULIÁN

Department of Civil and Environmental Engineering
Division of Structural Engineering
Steel and Timber Structures
Chalmers University of Technology
SE-412 96 Göteborg
Sweden
Telephone: + 46 (0)31-772 1000

Cover:
The configuration of the studied double-lap-shear joint on top, and on the bottom moisture diffusion progress and degradation of the joint as a function of time

Modelling of moisture ingress and joint degradation

Master's Thesis in the Master's Programme Structural Engineering and Building Technology
LUIS DURAN JOFRE
ELOY OLAGÜE JULIÁN
Department of Civil and Environmental Engineering
Division of Structural Engineering
Steel and Timber Structures
Chalmers University of Technology

ABSTRACT

The aim of this study is to model the moisture diffusion and consequently degradation of an adhesively bonded CFRP/steel joint. Different failure modes and diffusion models are investigated, while joint strength degradation with respect to time and exposure is presented. The damage mechanic approach Cohesive Zone Modelling (CZM) is used as a method to describe the adhesive joints strength, the commercial Finite Element Method (FEM) program ABAQUS is used as a tool to simulate and compare the experimental test results. The main methodology of this work consists in using results from laboratory test that gives the traction-separation laws of the adhesive and then apply these parameters to simulate other tests to verify the independency of the models performed in ABAQUS. The tests that are used to get the traction-separation laws and the test that are used to verify the models are strictly independent from each other's. The only relation that exists between them is the type of adhesive and the mechanical behaviour of the joints. The tests that are used to identify the traction-separation law of the adhesive in question are the DCB, ENF and MCB-test. The test that are simulated and also used to verify the models in ABAQUS are the DLS and RTB-test. However, the aim in this work is to predict the joint strength degradation and this is performed in ABAQUS. ABAQUS has been showed to be able to easily perform diffusion analysis by using the well-known analogy and cross-coupling between the heat conduction and moisture diffusion. The moisture profile used in this work is verified by Fick's second law calculations performed in MATLAB. Specifically, the cohesive zone modelling has been used and the respective moisture dependent traction-separation law of the adhesive have conceptually been modelled in ABAQUS. The moisture dependent traction-separation law for the different modes are formulated and described.

Key words: Adhesive, damage mechanics, cohesive zone modelling, CZM, moisture dependent, MMF, gravimetric test, moisture dependent, traction-separation law, ABAQUS, numerical method, continuum mechanics, fracture mechanics, epoxy, failure mode, mode I, mode II, mixed mode.

Contents

Preface

This study is a part of a research project concerning mechanical properties and durability of adhesive bonds in CFRP/steel joints. The project is carried out at the Department of Structural Engineering, Timber and Steel Structures at Chalmers University of Technology, Sweden from January 2013 to July 2013.

We would like to express our deep gratitude to our supervisor, Mohsen Heshmati, for his guidance, support, and inspiring collaboration. This study could have never been conducted without the sense of high quality and professionalism of him.

Göteborg July 2013

Notations

J: Energy release rate

J_c: Critical energy release rate

E: Young modulus

K: Stress intensity factor

K_c: Fracture toughness

$T_{n,max}$: Traction stress in normal direction (Damage initiation)

$T_{s,max}$: Traction stress in shear direction (Damage intiation)

$T_{n,mix}$: Damage initiation in normal direction in Mix-mode

$T_{s,mix}$: Damage initiation in shear direction in Mix-mode

w_c: Critical displacement in normal direction

v_c: Critical displacement in shear direction

δ_c: Mix-mode critical displacement

τ: Shear stress

σ: Normal stress

τ_0: Damage initiation

σ_0: Damage initiation

D: Damage parameter

F: Applied force

θ_A: Rotational angle

ε_s: Swelling strain

CME: Coefficient of moisture expansion

ΔM_t: Moisture uptake

1 Introduction

A large number of steel bridges all over the world need to be repaired or upgraded. There are many bridges that are experiencing advanced levels of deterioration because of the environmental exposure during their service life. The upgrading of old bridges can be motivated by the need for them to be able to take higher load because the transportations vehicles are increasing in both size and load [1].

The rehabilitation of steel bridges using advanced composite materials offers the possibility of a short-term retrofit or long-term solution for bridge owners faced with deficient structures. The high strength-to-weight ratios along with corrosion resistance are appealing factors in favour of the use of Carbon Fibre Reinforced Polymer (CFRP) as a strengthening method of steel structures. The ease of application, if comparing with applying a welded steel plate, introduces cost savings associated with labour, time, and inconvenient to public transportation [2]. In other words, is a social economical alternative for the repair or upgrade of steel bridges that are currently in service [1].

CFRP has shown some unique advantages among other construction materials such as excellent resistance to corrosion and environmental degradation, high longitudinal strength, high fatigue endurance and reduced weight. These features have made the CFRP adequate for reinforcing structures that are being affected by degradation.

Adhesive bonding as a joining technology consist basically of taking a strip of, for example CFRP, and gluing it to the material that need to be reinforced. This easy procedure have as mentioned earlier many advantages in comparison with other joining technics as, for example, welding and bolting. Nevertheless the adhesive material is the weakest link in this joint system when looking at the long-time performance of adhesive joints [1, 2].

The durability of these bonded joints still remains as a disadvantage when the engineer has to take decisions about witch joining technology to use, mainly because of the lack of knowledge concerning the durability of these joints. The lack of long-term and high initial costs is characterised issues of new materials when the technology is relatively new. In this study, the durability issue is investigated with focus on the moisture ingress in bonded joints and how it affects the strength of the joint through its service life [1].

1.1 Aim and Objectives

The aim of this thesis is to predict the failure strength and durability of CFRP/steel joints. The objective is to research the use of CFRP strengthened steel in bridge structures and presents a methodology that can predict the failure load of statically loaded aged and un-aged adhesive joints.

1.2 Method

To realise the objectives of this thesis a literature study about the "state-of-the-art" concerning the mechanical behavior and durability of CFRP/steel joints is performed. A mechanical and numerical approach is chosen based on the literature study. The moisture diffusion of the adhesive and the degradation of an adhesively bonded CFRP/steel joint strength due to moisture concentration is identified and modelled. The mechanical method used consists of performing test that describes the damage

initiation, this is a relation between deformation and strength behaviour of the material, and also gives an energy parameter that describes the damage propagation. This damage initiation and damage propagation is in this work called the traction-separation law of the material. The tests that are used in this work to identify the traction-separation laws of the adhesive used are the DCB, ENF, and MCB-test. Once well obtained the traction-separation laws it is possible to simulate and predict the behaviour of aged and un-aged adhesively bonded specimens. The tests that are used to verify the models are the TRB and DLS-test. The mechanical theory used is the Cohesive Zone modelling (CZM) and the numerical method is the finite element commercial program ABAQUS.
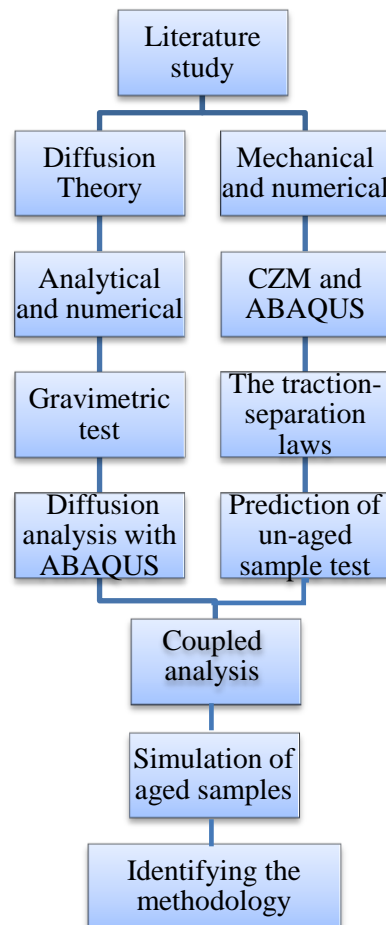
Figure 1 Work Method

1.3 Limitations

Due to the size of this thesis, concerning time and resources, some approaches are going to be taken.

The degradation rate are assumed and described in chapter 6.5.

The interfacial degradation do to wander walls forces and corrosion formation is ignored. Interfacial moisture diffusion is also left out.

Diffusion model is restricted to Fick´s second law.

Temperature over the glass transition, cyclic loads, cyclic temperature and water exposure are all ignored.

1.4 Outline of the Thesis

Figure 2 Outline of the thesis

2 Literature study

2.1 Materials

2.1.1 Carbon Fibre Reinforced Polymer (CFRP)

The Encyclopaedia[3] defines CFRP as:

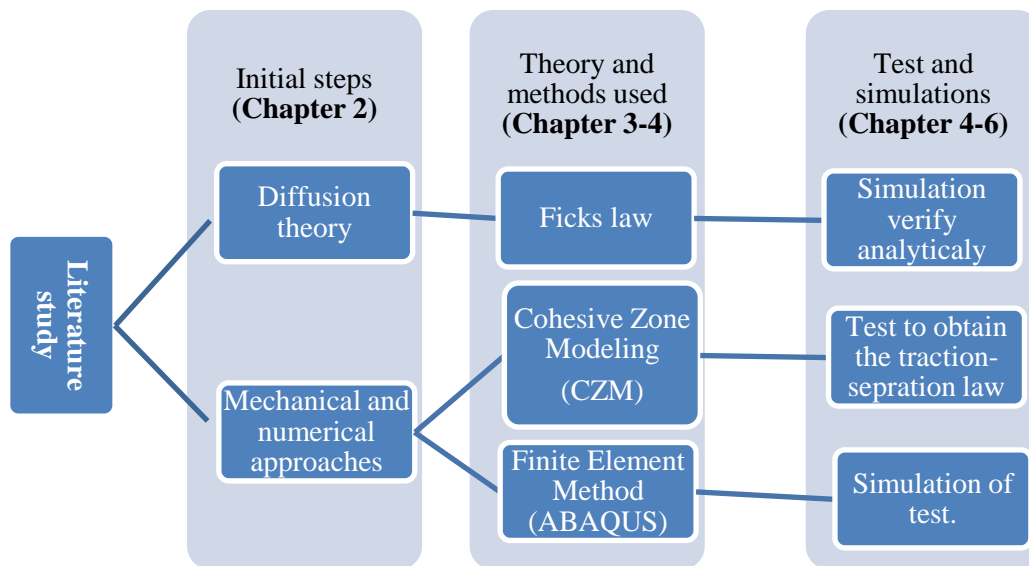"Carbon fibre reinforced Plastic (CFRP) is a strong and light composite material or fibre reinforced polymer. Like glass-reinforced plastic, the composite material is commonly referred to by the name of its reinforcing fibres (carbon fibre). The polymer is most often epoxy, but others plastics, like polyester or vinyl ester, are also sometimes used".

In the context of durability of the CFRP/steel joints, the durability of the CFRP is not the critical point in these joints, because it has shown excellent resistance against hostile environmental exposure in strengthening systems [4-6]. Due to this evidence, the investigation is focusing on the durability of the adhesive between these two materials (steel and CFRP) [7].

2.1.2 Steel

The steel that is used in this work is a S355 structural steel with high strength and low alloy, is a European standard structural steel EN 10025-2004 standard. The typical applications of the S355 steel include:

- Bridge components, components of offshore structures
- Power plants
- Wind tower components
- Mining and earth moving equipment.

2.1.3 Structural Adhesives

R.D. Adams defines in his book (Structural Adhesive Joints in Engineering, R.D. Adams, J. Comyn, W.C. Wake – 1997) the term adhesive as a polymeric material that, when applied to an adherent surface, e.g. a metal adherent or a CFRP material, can join them together and resist separation [8].

In this study, the adhesive used is StoBPE lim 567. It is a two-component, solvent-free structural epoxy adhesive. According to the producer, after a week of curing the adhesive has the following characteristics:

Table 1 Material properties of StoBPE lim 567

E-modulus:	7 GPa
Poisson´s ratio:	0.3
Tensile strength:	26 MPa
Strain to: failure	0.82 %

2.1.4 Adhesives Bonding

Although adhesive joints have important advantages against mechanical joint, e.g. lower structural weight, lower fabrication cost, and improved damage tolerance [9], all adhesives are, to some degree, permeable to water or moisture ingression. The moisture ingression changes with temperature, interfacial strength degradation and bulk properties are all factors that affect the durability of adhesive joints. For these reasons the adhesive material is the weakest link in these joint[10-12].

The moisture is able to change the bulk material properties of the adhesive, e.g. the glass transition temperature, modulus and tensile strength [13]. Different types of adhesives have different diffusion coefficients and moisture influences. This means that the rate of changes, e.g. plasticisation rate of the adhesive due to diffusion varies among the different types of adhesives [14].

Moisture can also act at the interface of the adherent/adhesive joint. When the water molecules are absorbed into the adhesive the moisture transport is concentrated on the metal adherent and this accumulation of water at the interface accelerate the displacement of the adhesive from the metal surface [13]. The appearance of corrosion at the interface of the metallic adherent is also a reason of higher degradation rate of the interface strength [15, 16]. Measures taken in experiments have shown that the loss of strength and stiffness of CFRP/steel are likely due to loss of cross-sectional area which can be represented by the mass loss because of corrosion, and not by degradation of material properties [5].

Pocius and co-workers [17] study showed that there is a critical combination of temperature, humidity and load that produce rapid loss of the adhesive joint strength. They also showed that the durability of steel joints and aluminium joints have an interesting behaviour. The experimental study performed by them showed that the dry lap-shear strengths are similar for both steel and aluminium, however a total different behaviour was found for water exposed lap-shear joints. In lap-shear joints exposed to a humid environment, joint with steel adherent fail after 30 days while the ones with aluminium adherent fail after around 3000 days.

In summary, two main effects that can reduce the strength of CFRP/steel adhesive joints can be identified.

- The properties of the bulk adhesive
- The adhesion properties at the interface

It has been mentioned that a strength recovery of the joints is observed after desorption of moisture [14] . Analysis done in [14] of the failure surfaces revealed that the dry joints failed cohesively in the adhesive layer and that the failure path moved towards the interface after conditioning. The failure mode then reverted back to cohesive failure after moisture desorption. Although, these results are not general for all types of adhesives, the adhesive material does have some recovery properties in some cases.

The properties of the adhesive are strongly dependent of its composition. This means that to change the moisture resistance or the mechanical behaviour the formulator generally must operate on the bulk adhesive. This will occur mainly through modification or change in the bulk polymer and somehow by modification or change of the fillers and additives in the formulation[18].

When studying the mechanical behaviour of the adhesive joints it is commonly to divide the deformation directions of the joint in mode I, mode II and mode III, shown in Figure 3. Mode I being an opening mode of the crack region and is in direct relation to the normal stresses of the crack surface. The mode II is the sliding mode and is in relation to the shear stresses in the crack surface area. Mode III is the same as mode II but mode III being in the respective shear and sliding mode of the second direction of the local coordinate system.
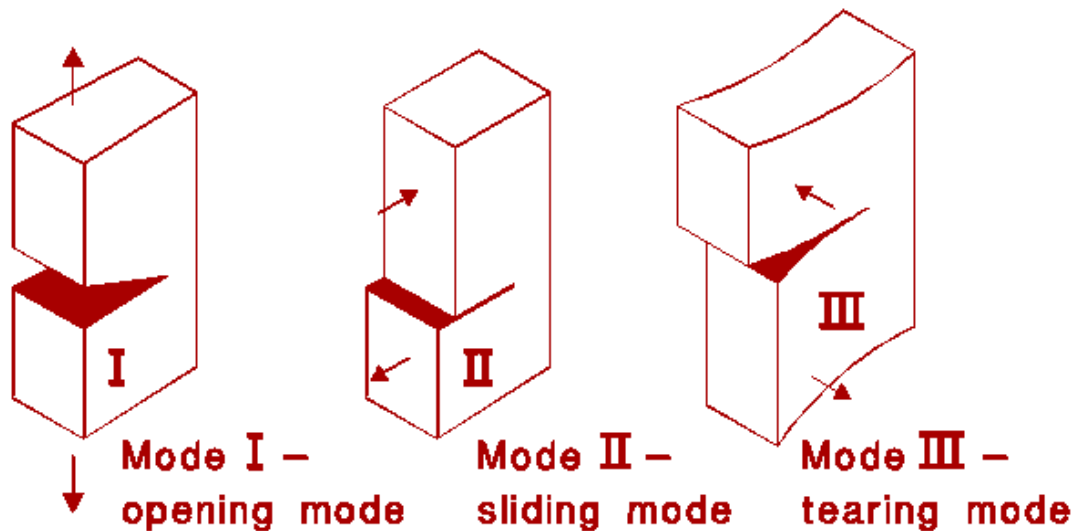

Figure 3 Deformation modes

Independent of the opening mode of the crack region there is a division of the failure mode of the adhesive joint. When the failure is in the adhesive layer it is called cohesive failure and, in the other hand, when the failure is in the transition zone between the material, from adherent to adhesive, then it is called interfacial failure, Figure 4.
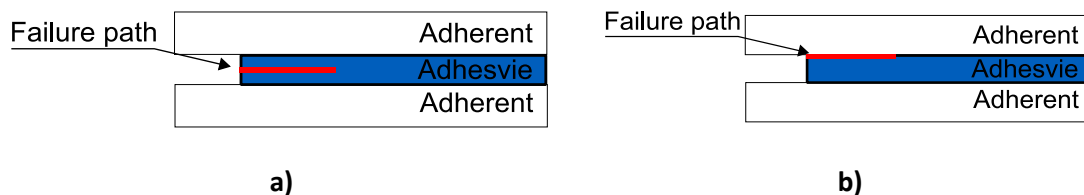

Figure 4 Failure modes. a) Cohesive failure and b) Interfacial failure

To correctly predict and describe the behaviour of the failure models and paths it is first necessary to decide and choose a mechanical and numerical method. Various mechanical and numerical methods have been applied in adhesive joints and the history and developing of the predictive tools have been well summarised by the work of Da Silva[9, 19]. The chapter 2.2 true out 2.3 describe the work of Da Silvia that is a satisfactory "state-of-the-art" of the history of mechanical and numerical methods that have been used for adhesive joints, from the begging of adhesive joint theory to the modern trends and methodology's.

2.2 Numerical Modelling of Adhesive Joints

In [9] Silvia explains the tree numerical methods used to solve differential equations, Finite Element Method (FEM), Boundary Element Method (BEM) and Finite Difference Method (FDM). The work of Silvia is a very interesting "state of the art" of the different numerical methods and gives examples of how the methods are applied to adhesive joints in modern research. All the different numerical methods are described, and examples are given where they are most adapted to be applied. Because there is no perfect theory nowadays that is capable of solving any given problem concerning adhesive joints, the engineer has to be aware of the limitations in each one of the numerical methods [9, 20].

2.2.1 Finite Element Method

The Finite Element Method (FEM) is a numerical analysis procedure that provides an approximate solution. There exist a grand variety of commercial FE analysis programs today and they have the possibility of performing coupling analysis, such as e.g. hydro-thermo-structural problems, and this method is also suitable for complex geometries [9]. To model the joint strength the analyser needs to have the stress distribution and a suitable failure criterion. The stress distribution can be obtained by FE analysis or a closed-form model. There are numerous amounts of approaches for the FEM and the failure criterion. The simplest failure model is the stress, strain or energy limits and it is one of the commonly used in continuum mechanics approaches. The fracture mechanics principal can also be modelled by commercial FEM programs. This can be based on the stress intensity factor approach or the energy release rate approach and finally the damage mechanics that is the combination of the continuum mechanics approach and the fracture mechanic [9] with both damage initiation criteria and propagation criteria, as for example the Cohesive Zone Modelling (CZM).

FEM is basically the discretization of a structure in various sub domains called elements that are joined at their nodes. Each node has a given number of Degree of Freedom (DoF). Now the structure, that is a continuum, is represented by nodes with degrees of freedom. In elasticity problems the solutions for the equilibrium equations is to solve the governing partial differential equation. The variation method is one way of finding approximations and is used in FEM to solve the elasticity differential equation by determining the condition that makes a functional stationary. A functional is a function of another function and in elasticity problems the functional used is the potential energy of the structure. Taking into account internal compatibility and essential boundary conditions, optimal values are searched and those are the ones that minimise the total energy. This process of minimisation gives a system of equations for the field quantity of the nodes and can be described by the Eq. 1.

$$K * \delta = F \hspace{3cm} \text{Eq. 1}$$

Where delta is a vector with the field values, **K** is the stiffness matrix and **F** a vector with the loads on the structure. There are integrals in the stiffness matrix **K** that may be needed to be solved with a numerical integration scheme. Generally, the integral can be computed by using gauss points and multiplying with factors with appropriate values. However, these elements can be made by drawing continuum lines between the nodes and thereby creating a mesh in the structure. The mesh sizes govern the accuracy of the stress gradients over the structure represented by the nodes. Because,

if we have more nodes we also have more elements and that means a finer mesh. In other words, more nodes mean more information about what is going on in the structure. Nevertheless, in adhesive joints there are stress singularities at the ends and the mesh refinement can lead the stresses to infinity. These convergence problems can be avoided by using a correct approach e.g. elasto-plastic and fracture mechanics concepts.
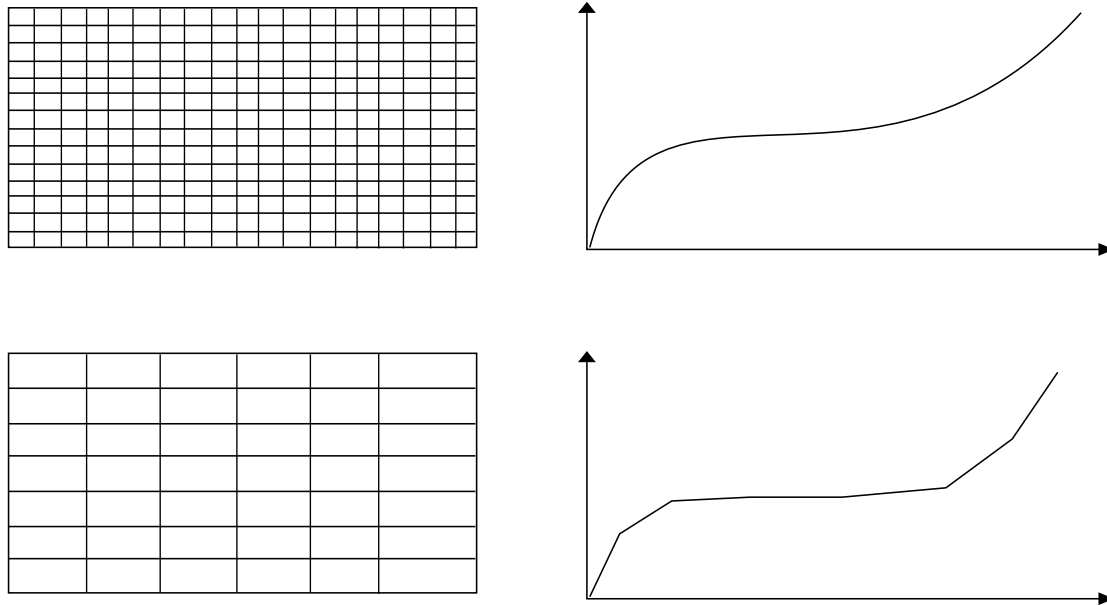

Figure 5 Mesh intensity

The commercial FE programs permit to choose the material model to determine the initial yielding and subsequent plastic deformation in a bonded joint. For the metal adherent the Von Mises yield criterion may be applied and, for the adhesive, a yielding model that takes into account the hydrostatic pressure is generally required. Raghava describe in his work [21] the yielding criteria for polymers that is a version of the Von Mises criterion. This criterion takes into account the differences between tensile and compressive yield strengths and considers any dependence of yielding on the hydrostatic component of the applied stress state. In ABAQUS there exist pre-defined options to use, as for example the Cohesive Zone Model (CZM) that is based on Damage mechanics. The CZM is explained in the Chapter 2.3.3. To use the CZM it is necessary to obtain traction-separation law or cohesive laws. That is the relation between the forces that work against separation and the displacement in a crack or at the interface of an adhesive joint. The form of these traction-separation laws can be defined differently and there exist many different approaches to use to obtain them. However, it is always needed to first establish the initiation and the propagation criterion of the separation rate and this is possible to achieve in the commercial FEM programs, as for example ABAQUS. The traction-separation laws are found by experiments. The use of moisture dependent traction-separation laws need in normal cases a great amount of tests before it is possible to do accurate simulations of the long-time performance of the adhesively bonded joints.

2.2.2 Boundary Element Method

The Boundary Element Method (BEM) is a typically used numerical method in engineering applications and it has been proved to be useful when dealing with fracture mechanics. In FEM the stresses are evaluated inside de elements and in BEM the stresses are evaluated at the boundaries, e.g. at the crack boundary. This representation of stress distribution has been shown to give a good resolution of the stress gradient in the thickness direction of an adhesive joint. Unfortunately, when the stress gradients are along the boundary, as for the interface, then the BEM, like the FEM, requires a refined mesh and the BEM needs to have specialized infinitive boundary element to properly model the interfacial behavior [9].

In the work of Vable [22] the author explain that BE-method can be used effectively in stress analysis of adhesive joints. The result in Vable's work showed that BEM is able to perform parametric study of the joint parameters, such as optimization of mesh. The paper demonstrates the easy way of modeling changes in geometry, e.g. different spew angles. It is also discussed that if a similar stress concentration curves existed for adhesive joint as it exist for design of mechanical fastened joints, the BEM can well become a methodology of choice for stress analysis of adhesively bonded joints.

2.2.3 Finite Difference Method

The Finite Difference Method (FDM) is a numerical technique for approximating the solutions to differential equations, by using finite difference equations to approximate derivatives. Differential equations are well used in both the diffusion analysis and the different types of beam theory approaches used in adhesive joint analysis. So this numerical method is definitely an alternative for the study of durability of adhesively bonded joints.

In the work of Silvia [9] the FDM is discussed and the mayor advantage is the simple computer implementation. Therefore this method is easily used when creating codes and new features are easy added. The main disadvantage is the boundary conditions for complex geometry's and problems with the stiffness matrix, and therefore this method have most been used for simple geometries [23].

2.2.4 Numerical method selection

Although all numerical methods are to some degree applicable to adhesive joints analysis the method in this work is going to be FEM. The main reasons are presented in Table 2. The easy of performing both diffusion analysis and moisture dependent traction-separation laws in ABAQUS is a strong reason for choosing FEM. Another reason is that when performing the literature study of adhesive joint analysis, FEM seem to be the main numerical method used in current research.

Table 2 Pros and cons of different numerical methods concerning adhesive joints.

Finite Element Method	Pros: • Commercial program with predefined options for adhesive joints analysis. • Numerous amounts of approaches for the failure criterion. • Coupled analysis is easy to use in ABAQUS (moisture dependent traction-separation laws) • Diffusion analysis by the analogy of heat analysis (ABAQUS).
	Cons: • Finer mesh takes longer time • ABAQUS traction-separation laws differs from many other traction-separation forms presented in other literature • Subroutines are not as straight forward to use as the predefined options.
Boundary Element Method	Pros: • Give a good resolution of the stress gradient in the thickness direction of an adhesive join • Useful in fracture mechanics • Useful for performing parametric study
	Cons: • Need infinity boundary when analyzing interfacial adhesive joint strength • Not enough rehearse performed with this numerical method
Finite Difference Method	Pros: • Can be used for diffusion analysis • Can be used to solve beam-theory used in adhesive joint analysis
	Cons: • Do not work for complex geometries • Not enough research performed with this numerical method

2.3 Mechanical Modelling Approaches

2.3.1 Continuum Mechanics

A simplified explanation of the continuum mechanics approach consists on comparing the maximum stress, strain or strain energy with the material allowable ones and, thereby, obtaining a failure criterion. Continuum mechanics is one of the simplest approaches to obtain a failure criterion and it can easily be used in the FE analysis [9].

2.3.1.1 Disadvantages and adaptation of continuum mechanics

The continuum mechanics approach has problems in the sharp corners, e.g. singularity problems. This implies that the model is not accurate to model traditional adhesively bonded configurations, as for example, Double Lap Shear joint (DLS-joint), Double Cantilever Beam joint (DCB-joint), Mixed Mode Cantilever Beam joint (MCB-joint) and Tensile Reinforced Bending joint (TRB-joint). Using the continuum mechanics approach give a high mesh-dependency. However, rounding of the sharp corners removes the singularity and reduces the high values of stress, energy, and strain.

Strain criterion has been used to predict failure in some studies but the site of damage initiation and propagation to failure in adhesive joints is highly dependent on the geometry and the edges of the overlap [24].

The maximum stress, strain and energy failure mode has been successively used to predict joint strength with some types of brittle adhesive and with short overlaps. On the other hand, in continuum mechanics it's not appropriate to use a criteria based on stresses when a ductile adhesive is used [9].

The stress, strain and energy failure criterion are all applicable to continuum structure only, and therefore have difficulties when defects are presented or more than one material is analysed. Because continuum mechanics assumes that structures and materials are continuous, consequently e.g. defect in the form of cracks or sharp corners are not properly analysed since discontinuities that gives convergence problem arises in those spots. The problem with the continuum mechanics is in the zone that is cracked, the free surface is absence from stresses and the zone near the crack has the highest stresses, consequently discontinuities and convergence appears. This problem is also presented in bonded joints of two materials with a re-entrant corner, but here only the stress discontinuities exist and the free surface do not. More generally, for the continuum mechanics it's always exist discontinuities if the crack or the material connection is smaller than 180 degrees [9].

2.3.1.2 To take into account before using continuum mechanics

The continuum mechanics approach take only into account the principal stresses in the right direction of the external applied force of a single or double lap test and ignores all the other stresses, e.g. normal stresses existing in the lap joints and therefore overestimates the total joint strength [9]. In the other hand, Adams [25] showed that Poisson's ratio strains in the adherents of a simple adhesive lap joint induce transverse stresses both in the adhesive and adherents. The work by Adams describe that two simultaneous second-order partial-differential equations can be set up to describe the normal stresses along and across an adherent and this equations cud be solved both by an approximate analytical method and a Finite Difference Method (FDM).

The continuum mechanics is a straight forward approach and it does not need any traction-separation parameters from experiments, as for the fracture and damage mechanics. In the other hand, it's important to be aware of the limitations as e.g. the geometry, mechanical behavior and material dependency of the model.
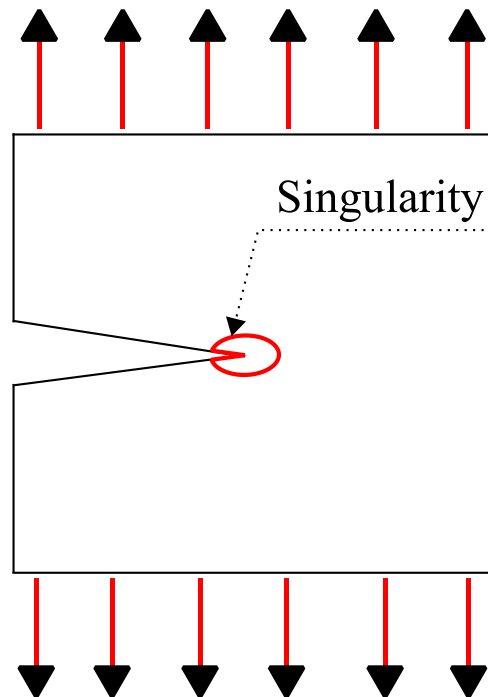

Figure 6 Singularity at the crack tip

2.3.2 Fracture Mechanics

To model the ultimate carrying capacity and the structural integrity it is important to take the discontinuities into account. This need of dealing with this important issues in engineering have developed the fractural mechanics in the form of Linear Elastic Fracture Mechanics (LEFM) to deal with the discontinuities and the Elastic-Plastic Fracture Mechanics (EPFM) to deal with the formation and propagation of material with plastic deformation [26]. The EPFM can also be called yielding fracture mechanics (YFM).

Materials with low fracture resistance fail below their ultimate load and can be analyzed on the basis of continuum mechanics concepts through the use of LEFM. If a body with a crack is subjected to a loading mode I, the material will be considered elastic, naturally following Hooke's law [27]. Fracture will occur when the stresses at the crack tip become too high for the material. As the stress intensity factor (K) determines the entire crack tip stress field. The fracture will occur when K becomes too high for the material. How high the stress intensity is dependent of the material chosen and it must be determined from experimental tests [27]. The material's fracture toughness (Kc) can be recognized as the critical maximum stress intensity (K) which the material can withstand without drastic crack propagation in the material.

In LEFM the crack tip behavior can be characterized by the stress intensity factor (K) that describes the effect of loading at the crack tip region and the resistance of the material and is valid for a small region around the crack tip. LEFM concepts are valid if the plastic zone is much smaller than the singularity zones. In the other hand, in EPFM the crack tip undergoes significant plasticity.

EPFM is applied to materials, generally, in the case of large-scale plastic deformation. Three parameters are generally used: Crack opening displacement (COD) or crack tip opening displacement (CTOD) and the well-used J-integral. These parameters give geometry independent measure of fracture toughness

By idealizing elastic-plastic deformation as non-linear elastic the J-integral characterizes the crack tip stress and crack tip strain and energy release rate. In LEFM the cohesive zone is assumed small in comparing with the crack length. In this approach, the external load can be represented by the stress intensity factor K or energy realize rate J. the fracture toughness is the critical value for the stress intensity factor

This approach does not take into account what is happening in the cohesive zone [28]. The main idea is that the crack propagation is determined by the relation between the release of potential energy and the necessary surface energy to create new surface area as the crack propagates. It was asserted that when a crack grows, the decrease of potential energy is compensated by the increase of the surface energy caused by the tension in the new cracked surface [29].

2.3.2.1 Disadvantages and adaptation of fracture mechanics

In LEFM parameters as, e.g. the Stress intensity factors are difficult to establish when the crack grows at or near an interface. Instead the energy release rate, J, and the critical energy release rate, Jc can be used. However, a strain singularity still exists for ductile materials, even though the stress singularity has disappeared. Linear Elastic Fracture Mechanics (LEFM) has been used to overcome singularity problems and can

be used in different layouts of fillets for bonded joints, but the LEFM do not work when the material have plastic deformation before failure. There exist modifications of the approach but the all need a great amount of parameters to best fit the experimental data[9].

The Elastic-Plastic Fracture Mechanics (EPFM) has been used to model plastic behaviour introducing the J-integral that is used to predict the joint strength of cracked adhesive joints satisfactory. The mayor disadvantage of the use of the J-integral to model adhesive joints is that it's dependent of the interfacial length and therefore the J-integral have to be extrapolated to find the new values and a new mesh have to be establish.

It have been shown that the EPFM need to have a predefined crack path and this imply that the failure mode can be highly complex and doubtful some time [9].

2.3.2.2 To take into account before using fracture mechanics

In the cases where the global stress-strain response of the body is linear and elastic, the use of LEFM is suitable and the stress intensity factor K is used. Many studies dealing with adhesive joints use the strain energy release rate, J, and the critical value of the energy release rate J_c, because is easier than to find the stress intensity factor K and the Fracture toughness, K_c.
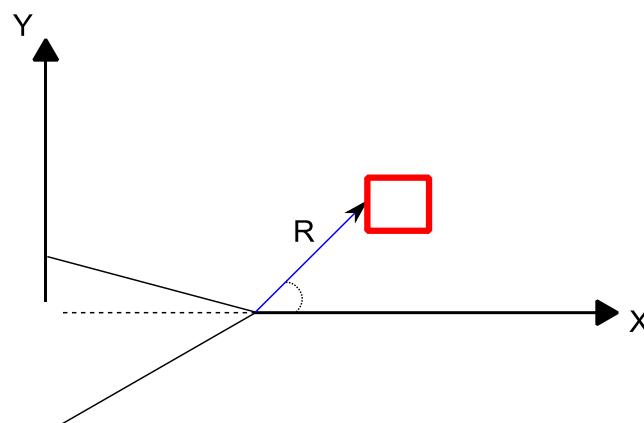

Figure 7 The stress intensity factor is defined from the elastic stress field equations for a stressed element near the tip of a sharp crack under biaxial (or uniaxial) loading in an infinite body.

2.3.3 Damage Mechanics

Damage mechanics is the study of material damage based on damages variables. This damages variables changes with the applied load condition to quantitatively represent the growth of mechanical deterioration of a material component. Structural damage during loading can be found in the form of micro cracks over a finite volume or interface region between bonded components. Damage mechanics permits the simulation of step-by-step damage and fracture at an arbitrarily finite region, up to complete structural failure [8, 9, 26, 27, 30-34].

There exist two main approaches available for damage modelling and they are the local approach and the continuum approach. In the local approach, damage is confined to a zero volume line or a surface, allowing the simulation of an interfacial failure between materials, e.g. between the adhesive bond and the adherent. By the continuum approach, the damage is modelled over a finite region, within solid finite elements of structures to simulate a adhesive failure or along an adhesive strip to model an interfacial failure of the adhesive joint. The Cohesive zone model (CZM) can be used in both approaches (local and continuum) and it can simulate the macroscopic damage along a path by the specification of a traction-separation response between paired nodes on ether sides of a pre-defined crack path. The CZM simulate the fracture process better than traditional fractural mechanics, by extending the concept of continuum mechanics using both strength and energy parameters to characterize the debonding process [9].

2.3.3.1 Disadvantages and Adaptation of Damage Mechanics

This method presents limitations because it is necessary to know beforehand the critical zones where damage is prone to occur and a methodology is needed to characterise the moisture-dependent cohesive zone properties in a satisfactory way.

A traction–separation response is used to model the damage initiation and evolution in the fracture process zone (Cohesive Zone), and for ductile materials the shape of traction-separation laws must be modified which can give convergence problems [9]. In the work of Katnam [31] characterisation of moisture-dependent cohesive zone properties have been identify for a cohesive failure mode. It is also discussed there, that the same approach can also be useful for an interfacial failure mode. Consequently, the critical energies and tractions parameters are related to the degraded interface traction-separation law, rather than the bulk adhesives properties as for the adhesive failure.

In the work of Yang [35] a mode-dependent embedded-process-zone (EPZ) model has been developed and it is used to simulate the mixed-mode fracture of plastically deforming adhesive joints with Mode-I and Mode-II fracture parameters combined with a mixed-mode failure criterion to run quantitative predictions of the deformation and fracture of mixed-mode geometries. These numerical calculations have been shown to provide excellent predictions for geometries that experience large-scale plastic deformation such as single lap-shear joints. Details of the deformed shapes, loads, displacements and crack propagation have all been well predicted by the calculations.

2.3.3.2 To take into account before using Damage Mechanics

When EPFM is used the fracture characterizing parameters are the J-integral or the crack opening displacement (COD). All these fracture characterizing parameters meet both the Griffith energy criterion and the critical stress/strain criterion. The three modes, mode I, mode II and mix-mode of crack propagation are all associated with the fracture energy concepts.

The fracture parameters may be chosen so the model best fits to the experimental data, or they may be prescribed based on some assumed relationship. Fabricating such models will require an increasing number of independent material parameters, which must all be pre-obtained or re-adjusted by experiments. Apart from the amount of experimental work involved, this purely mathematical fracture parameter fitting method does not explain the physical failure mechanism [36].

Further on, the now called the cohesive zone model (CZM) in Damage mechanics was developed, in which the stress in the cohesive zone ahead of the crack is a function of the traction-separation laws, rather than a constant field stress as in traditional fracture mechanics. The concept of traction-separation law relates the tractions in the cohesive zone to the relative displacement. The traction-separation relationship can be modelled in different ways: constant, nonlinear, trapezoidal and bilinear [16, 37, 38].

There exist a large number of studies concerning the numerical aspects of the J-integral near the crack tip and incremental plasticity. These theories, concepts and methods of fracture/damage mechanics, are to some degree today "common" knowledge. However, it has not always been like that, it was a time when the concepts and theory of the J-integral was restricted to a few experts. In the process from just being knowledge of a few people to a "state-of-the-art", unfortunately some of the background information how to apply the respective concepts, the assumptions and restrictions may get lost.

The main assumptions and restrictions are presented in the table below.

1) Time independent processes, no body forces.
2) Small strains.
3) Homogeneous hyper-elastic material.
4) Plane stress and displacement fields, i.e. no dependency on x3.
5) Straight and stress-free crack borders parallel to x1.

Recommendations and comments[39-51]:

1) Choose domain as large as possible but do not touch the boundary of the structure
2) Check if saturated value has been reached, otherwise increase the number of domains.
3) A small-strain analysis will show less path dependency.
4) No difference

2.3.4 Mechanical method selection

The damage mechanics is the model used in this work that describes the behaviour of the adhesive and its influence on moisture diffusion. The CZM have several

advantages when a relation between moisture concentration and degradation of the traction-separation law are desired. The main reasons are presented in Table 3.

Table 3 Pros and cons of different mechanical approaches in adhesive joint analysis

Continuum mechanics	Pros: • simple failure criterion • strain criterion is used to predict correct failure load for brittle adhesives • Describes de normal stresses along and across the adherents involved.
	Cons: • Singularity problems • Mesh dependent • Not apply do describe ductile material • Over estimate the total joint strength
Fracture mechanics	Pros: • Take into account discontinuities • Analysis of both brittle and ductile material is possible • Geometry independent • Stress intensity factors or energy release rates describe the singularity zone
	Cons: • Need experimental test • Does not take into account the cohesive zone • Predefined crack path gives doubtful results some times.
Damage mechanics	Pros: • Simulate of damage initiation and propagation • Interfacial failure and cohesive failure are possible to predict • Various method/approaches exist for both the traction-separation law and the moisture dependency. • Proved to give good predictions of the deformation and failure load • Can be mixed with XFEM
	Cons: • The traction-separation laws are obtained true an empirical process. • The form of the traction-separation law needs to be modified to experimental results. • The re-adjusting of the parameter is not a satisfactory way of modeling • Does not explain the physical failure mechanism

3 Cohesive zone modeling

Because the moisture concentration affects the adhesive bulk properties, moisture dependent traction-separation properties are needed for predicting the durability of adhesive joints. In the work of Katnam [52] the respective experimental test was carried out to find the traction-separation law for the adhesive in question. Focus was on the adhesive because the failure mode was cohesive under both wet and dry situations. Nevertheless, same methodology can be used even if the failure mode is interfacial failure. In this case the critical energies and traction relates to the degraded interface strength rather than the bulk material. The diffusion of water along the interface is often assumed to be faster than in the adhesive material, the interface is more prone in many cases to moisture consequences than the adhesive [52].

The CZM is ably to describe the interfacial debonding of adhesive joints with a nonlinear traction-separation relation that simulates the crack opening and growth. A damage parameter D is used to describe the state of the interface [45].

In the paper [28] Rui Huang discuss the issues of using the CZM for prediction of interfacial debonding of adhesive joint. There is a conscious that the interfacial failure mode has been well established theoretically and has been successfully used and presented in various papers. Nevertheless, the implementation of cohesive elements in ABAQUS has been discussed. The standard form of the implementation of the traction-separation laws in ABAQUS differs from many other traction-separation forms presented in other literate. ABAQUS has the flexibility to use customized implementation through user subroutines, but this way of modeling is not as straight forward, as using standard option in the program. However, in the paper of Rui Huang presents nonlinear traction-separation parameters that are capable of describing both the initiation process and growth of the adhesive interfacial failure [28]. This approach can be used to simulate nonlinear material properties as, e.g. nonlinear viscoelastic and elastic-plastic.

However, to use CZM it's always needed to first have accurate characterization of the specific material traction-separation law used, and this is made true experimental tests. There exist various methodologies how to get the information of the traction-separation laws for a specific adhesive and different researchers have used different approaches and methods. In this paper we are going to use the same methodology as in the work of Liljedahl and Crocombe [7, 14-16, 20, 37, 38, 52, 53] where they first use some test to find the traction-separation law for mode I and mode II and then calibrate the exponential value alpha for the mixed mode case, using ABAQUS. These traction-separation parameters are then used to predict the response of an overlap tests, a different one from the one used to find the traction-separation parameters. In this work the Double cantilever beam test (DCB-test) is used to find the mode I traction separation law, the End notch flexure test (ENF-test) to find the Mode II traction-separation laws and finally the Mixed Mode cantilever beam test (MCB-test) to find a realistic value of the exponential parameters "alpha". In this work the test results from the work of Saeed Salimi [29] are used and explained in chapter 5.

3.1 The traction-separation law:

The traction-separation law describes the relationship between the forces of attraction and the correspondent displacement between the atoms in a material or the adhesively bonded faces of two equal/different materials [16, 29, 31, 33, 34, 53-56]. The background to all the equations presented in this chapter is well described in the work of Saeed Salimi and others [29, 32, 33, 54, 57]. The traction-separation law gives the information of when the material is in the linear-elastic region, damage initiation and material failure is reached. The material is in the linear-elastic region until the stresses or traction reaches $T_{n,max}$. When the stresses are equal to $T_{n,max}$ damage initiation have started. Total failure is presented when deformation is equal to w_c (normal deformation) or v_c (shear deformation).

The model that describes both normal and shear effects acting together is called mix-mode. The damage initiation for mix-mode used in this work is called quadratic nominal stress (QUADS) in ABAQUS and is presented as Eq. 2.

$$QUADS: \left(\frac{\langle T_n \rangle}{T_{n,max}}\right)^2 + \left(\frac{T_s}{T_{s,max}}\right)^2 + \left(\frac{T_t}{T_{t,max}}\right)^2 = 1 \qquad \text{Eq. 2}$$

The following statements are conceptually presented in **Figure 8**.

$$T_{n,max} > T_{n,mix}$$

$$T_{s,max} > T_{s,mix}$$

$$w_c > w_{c,mix}$$

$$v_c > v_{c,mix}$$

$$QUADS \geq T_{n,max} \text{ and } T_{s,max}\delta_c \geq v_c \text{ and } w_c$$

a)   **b)**
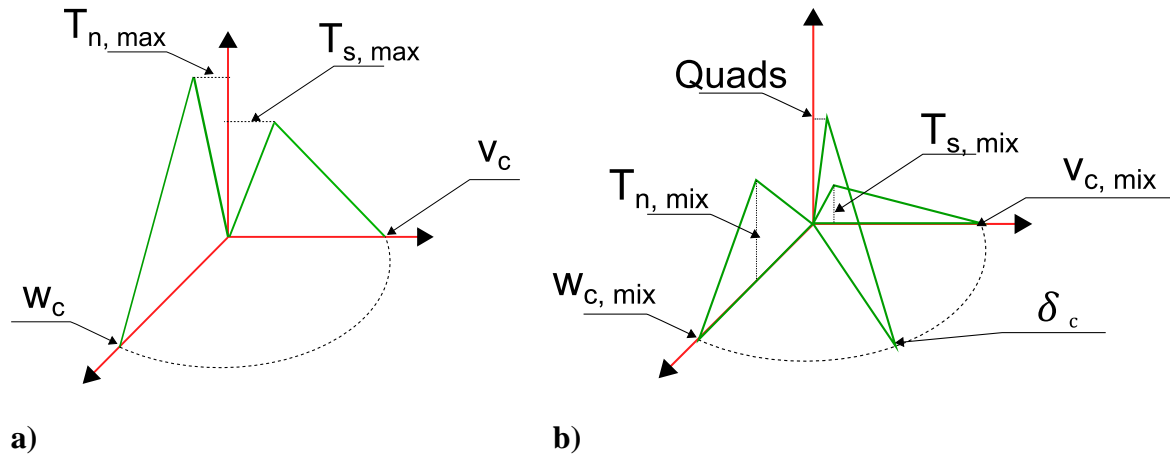
Figure 8 a) Traction-separation law for mode I and mode II. b) Traction-separation law for mix-mode

3.1 Traction-separation for pure Mode I
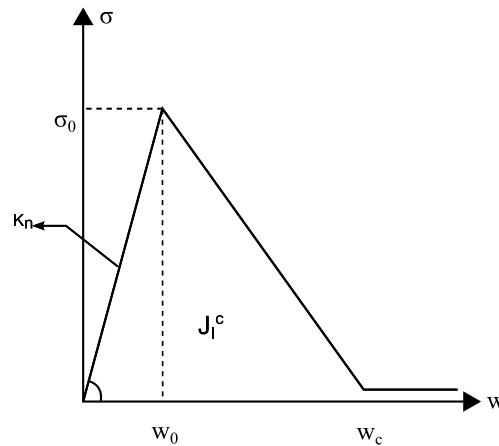
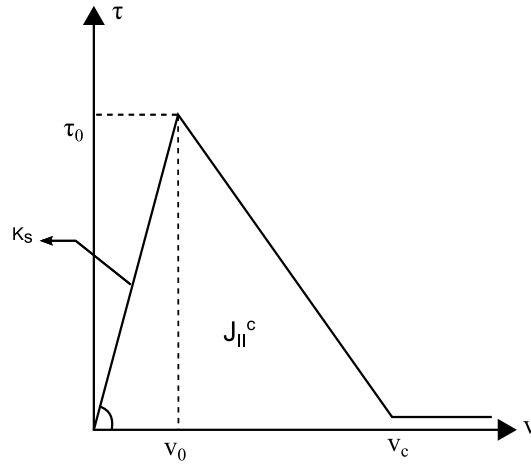**Figure 9** Bilinear traction-separation law for pure mode I.

Damage inititation, propagation and failure (Eq. 3)

$$\sigma = \begin{cases} \frac{\sigma_0}{w_0}w, & (0 \leq w \leq w_0) \\ \frac{\sigma_0}{(w_c - w_0)}(w_c - w), & [w_0 \leq w \leq w_c] \\ 0, & w \geq w_c \end{cases} \qquad \text{Eq. 3}$$

Damage parameter D (Eq. 4)

$$D = \frac{w_c(w_{max} - w_0)}{w_{max}(w_c - w_0)} \qquad \text{Eq. 4}$$

The tensile stress is related to the opening displacement linearly (Eq. 5)

$$\sigma = (1 - D)K_n w \qquad \text{Eq. 5}$$

Eq. 6 is the same as Eq. 5 expresses in terms of the initial (w_0) and critical (w_c) displacement

$$\sigma = \sigma_0 \frac{w_c - w}{w_c - w_0} \qquad \text{Eq. 6}$$

From Eq. 5 and Eq. 6 it is noticed that the stress decreases linearly with the displacement and obviously when $w \geq w_c \rightarrow D = 0 \; and \; \sigma = 0$ which indicates that the traction-separation element is fully fractured. During unloading, w_{max} and D remain constant. Therefore, the stress decreases linearly as the opening displacement decreases, with the slop $K_n = (1 - D)K_n$.

The energy release rate is the area under the traction-separation curve (Eq. 7) for pure mode I.

$$J_I^C = 0.5(1 - \Psi)K_n w_c w_0 \qquad \text{Eq. 7}$$

The experimental test that is well used to obtain the traction-separation for pure mode I is the DCB-test. The methodology used between the mechanical theory and the experimental test are well described in the work of Saeed Salimi [29] and is here summarised in chapter 5. The principal equations are presented below for completeness.

The form of energy release rate, also called the J-integral that is used for the pure model I for a thick adhesive layer is presented as (Eq. 8)

$$J_{DCB} = \frac{2F\theta_A}{b} \qquad \text{Eq. 8}$$

$$b: with\ of\ specimen$$
$$F: Forze\ applied\ on\ speciement$$
$$\theta_A: Rotational\ angle$$

A second expression is used to obtain the traction normal stresses for mode I. This expression is obtained by differentiating J with respect to the peel deformation w and is presented as (Eq. 9)

$$\sigma = \sigma(w) = \frac{\partial J}{\partial w} = \frac{\partial}{\partial w}\left\{\frac{2F}{b}\theta_A\right\} \qquad \text{Eq. 9}$$

These two equations (Eq. 8 and Eq. 9) are used to obtain the traction-separation law for pure mode I. The equation Eq. 8 is used to get the value of the energy release rate and the stress equations is used to finally get the values of the damage initiation for pure mode I. However, it is first necessary to perform the DCB-test and get the values of the force (F), the rotation angle (θ_A) and the normal deformation (w).

3.2 Traction-separation for pure Mode II

The traction-separation behaviour for mode II is basically the same as for the mode I.

Figure 10 Bilinear traction-separation law for pure mode II.

Damage inititation, propagation and failure (Eq. 10)

$$\tau = \begin{cases} \dfrac{\tau_0}{v_0} v, & [0 \leq v \leq v_0] \\ \dfrac{\tau_0}{(v_c - v_0)} (v_c - v), & [v_0 \leq v \leq v_c] \\ 0, & v \geq v \end{cases} \qquad \text{Eq. 10}$$

The damage parameter (Eq. 11)

$$D = \frac{v_c(v_{max} - v_0)}{v_{max}(v_c - v_0)} \qquad \text{Eq. 11}$$

The shear stress is related to the displacement linearly (Eq. 12)

$$\tau = (1 - D)K_s v_s \qquad \text{Eq. 12}$$

The critical energy release rate is the area under the traction-separation curve in Figure 12 and the expression (Eq. 13)

$$J_{II}^C = 0.5(1 - \Psi)K_s v_c v_0 \qquad \text{Eq. 13}$$

To obtain the traction-separation law for pure mode II, as for mode I, it is first necessary to perform experimental tests. The test that is used for this purpose is the ENF-test. Just the results are is used in this work, more information can be found in the work of Saeed Salimi [29].

In comparison to the expression of the J-integral for mode I, the analytical formulation of the en integral is a bit more complicated. However the most of the values in the expression are constant that are dimensions of the ENF-test.

The J-integral that is used for the pure model I for a thick adhesive layer is presented as (Eq. 14)

$$J_{ENF} = J_0 + J_1 \qquad\qquad \text{Eq. 14}$$

The first part of the (Eq. 14) is the (Eq. 15)

$$J_0 = \left[\frac{\left(1 + \frac{t}{h}\right)^2}{1 + \frac{3}{2}\frac{t}{h} + \frac{3}{4}\left(\frac{t}{h}\right)^2} \right] \frac{9}{16} \frac{P^2 a_0^2}{E b^2 h^3} \qquad\qquad \text{Eq. 15}$$

The second part of the (Eq. 14) is the Eq. 16

$$J_1 = \left[\frac{1 + \frac{t}{h}}{1 + \frac{3}{2}\frac{t}{h} + \frac{3}{4}\left(\frac{t}{h}\right)^2} \right] \frac{3}{8} \frac{Pv}{bh} \qquad\qquad \text{Eq. 16}$$

The following expression is used to obtain the traction shear stresses for mode II. This expression is obtained by differentiating J with respect to the peel deformation v and is presented as (Eq. 17)

$$\tau = \tau(v) = \frac{\partial}{\partial v} \left[\frac{9}{16}\frac{P^2 a^2}{E b^2 h^3}\left(1 + \frac{t}{h}\right) + \frac{3}{8}\frac{Pv}{bh} \right] \frac{\left(1 + \frac{t}{h}\right)}{1 + \frac{3}{2}\frac{t}{h} + \frac{3}{4}\left(\frac{t}{h}\right)^2} \qquad\qquad \text{Eq. 17}$$

3.3 Mixed Mode (Mode I and Mode II)

There exist a relation between the shear and normal deformation and this can be called, the direction variable. The direction variable can be seen as the respective portions of the total deformation δ of the shear (v) and normal deformation (w) in Figure 11. The total deformation is: $\delta = \sqrt{w^2 + v^2}$ And the direction variable for shear (Eq. 26) and tensile (Eq. 27) deformation can be expressed like:

$$\sqrt{\Psi} = \frac{v}{\delta} \qquad \textit{Shear portion} \qquad \text{Eq. 18}$$

$$\sqrt{1 - \Psi} = \frac{w}{\delta} \qquad \textit{Tensile portion} \qquad \text{Eq. 19}$$
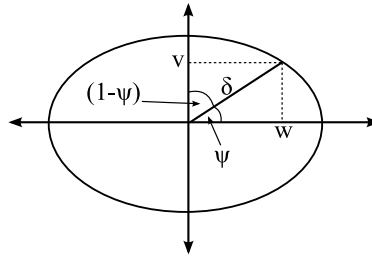
Figure 11 Direction variable concept

Therefore the shear and tensile deformation can be expressed as in (Eq. 20) and (Eq. 21)

$$v = \sqrt{\Psi}\, \delta \qquad \text{Eq. 20}$$

$$w = \sqrt{1 - \Psi}\, \delta \qquad \text{Eq. 21}$$

The damage initiation under mixed mode loading can occur before the shear and tensile components reach there critical value ($\sigma_0 \ and \ \tau_0$), therefore the damage initiation is expressed as in (Eq. 22and is called the quadratic nominal stress criterion

$$\left(\frac{\langle \sigma \rangle}{\sigma_0}\right)^2 + \left(\frac{\tau}{\tau_0}\right)^2 = 1 \qquad \text{Eq. 22}$$

Or the power law used in ABAQUS, where the exponential value alpha is a variable that can be identify by experimental test ore re-adjusted to best fit experimental data.

$$\left(\frac{\langle \sigma \rangle}{\sigma_0}\right)^\alpha + \left(\frac{\tau}{\tau_0}\right)^\alpha = 1 \qquad \text{Eq. 23}$$

And the damage initiation for the mixed mode (Eq. 24)

$$\delta_0 = \frac{v_0 w_0}{\sqrt{v_0 + \Psi(w_0^2 - v_0^2)}}$$

Eq. 24

The damage parameter for mixed-mode is determined by (Eq. 25)

$$D = \frac{\delta_c(\delta_{max} - \delta_0)}{\delta_{max}(\delta_c - \delta_0)}$$

Eq. 25
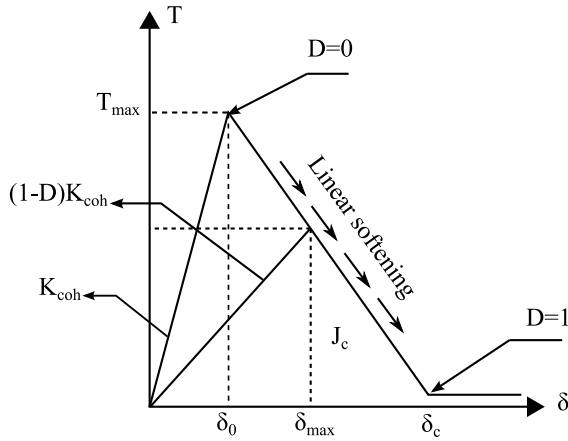
Figure 12 Bilinear traction-separation law for mix-mode

Where δ_c is the critical effective displacement, depending on the mixed mode of Mode I and Mode II of the traction-separation law and δ_{max} is the maximum Mixed Mode separation displacement during the hole loading history.

Under Mixed Mode loading, both the strength and toughness depend on the direction of the variable. The Mixed Mode strength depends on the normal and shear strenght and consequently the mixed mode toughness depends on the Mode I and Mode II toughness. Toghether at least five parameters are needed to describe the fracture.

- Stiffness (K_{coh}), (Eq. 26)

- Normal and shear strength σ_0, τ_0. (Eq. 12) and (Eq. 9)

- Toughness J_{IC} and J_{IIC} given the mixed mode energy release rate (Eq. 27)

$$K_{coh} = \begin{bmatrix} K_n & 0 \\ 0 & K_s \end{bmatrix}$$

Eq. 26

$$J_C = J_I^C + J_{II}^C \qquad\qquad \text{Eq. 27}$$

One form of expressing the mixed mode energy relase rate is shown in (Eq. 28)

$$J_C = \left\{ \left(\frac{\frac{J_I^C}{J_c}}{J_{IC}} \right)^\alpha + \left(\frac{\frac{J_{II}^C}{J_c}}{J_{IIC}} \right)^\alpha \right\}^{\frac{-1}{\alpha}} \qquad\qquad \text{Eq. 28}$$

where J_{IC} and J_{IIC} Critical energy release rate for pure mode I and mode II

Expressing the critical energy release rate with the direction variable (Eq. 29)

$$J_C = \left\{ \left(\frac{K_s \Psi}{K_{coh} * J_{IIC}} \right)^\alpha + \left(\frac{K_n(1 - \Psi)}{K_{coh} * J_{IC}} \right)^\alpha \right\}^{\frac{-1}{\alpha}} \qquad\qquad \text{Eq. 29}$$

And the critical separation displacement with respect to the direction variable in mixed mode (Eq. 30)

$$\delta_C = \frac{2}{K_{coh} \delta_0} \left\{ \left(\frac{K_s \Psi}{K_{coh} * J_{IIC}} \right)^\alpha + \left(\frac{K_n(1 - \Psi)}{K_{coh} * J_{IC}} \right)^\alpha \right\}^{\frac{-1}{\alpha}} \qquad\qquad \text{Eq. 30}$$

In CZM in ABAQUS the direction variable is defined locally at each point or for each interface element. Therefore the mode mix may change along the interface and during the loading process. Too model the critical energy release rate with respect to the direction variable Ψ it is necessary to use the power law fracture criterion:

$$\left\{ \frac{J_I^c}{J_{Ic}} \right\}^\alpha + \left\{ \frac{J_{II}^c}{J_{IIc}} \right\}^\alpha = 1 \qquad\qquad \text{Eq. 31}$$

The necessary experimental tests to be performed for the traction-separation parameters in mixed-mode are in principal a test that describes the behavior of both modes together.

The test results used in this work are from a MCB-test performed by Saeed Salimi [29]. The equations that are needed together with the MCB-tests are:

Vertical force at the crack tip, where S is the applied force with angle beta (Eq. 32).

$$V = S \sin(\beta) \qquad\qquad \text{Eq. 32}$$

Normal force at the crack tip (Eq. 33)

$$N = S \cos(\beta)$$ Eq. 33

Moment at the crack tip (Eq. 34).

$$M_{1,2} = V a_0 \pm N \frac{h + t}{2}$$ Eq. 34

The energy release rate for the MCB-test is(Eq. 35).

$$J_{MCB} = \frac{V}{b}(\theta_1 - \theta_2) + \frac{6 (M_1^2 + M_2^2)}{E b^2 h^3} + \frac{N^2}{E b^2 h}$$ Eq. 35

Inserting the sectional forces and moment in to the expression of J_{MCB} gives (Eq. 36)

$$J_{MCB} = \frac{S \sin(\beta)}{b} (\theta_1 - \theta_2) + \frac{12(S \sin(\beta))^2 a_0^2}{E b^2 h^3} + \frac{4 (S \cos(\beta))^2}{E b^2 h^3} \left[1 + \frac{3}{2} \frac{t}{h} + \frac{3}{4} \left(\frac{t}{h} \right)^2 \right]$$ Eq. 36

4 Modeling of moisture distributions in adhesive joints

In this study, one of the main objectives is to analyse the effects of moisture in adhesive joints, and be able to quantify the degradation induced by the adhesive, and the corrosion of the steel in contact with the adhesive. Therefore, a good model to find the moisture concentration in the adhesive joint with respect to time in a specific environment is needed. As the moisture diffusion depends on the moisture concentration, and the moisture concentration varies in each dimension of the adhesive, we are taking in consideration two kind of moisture diffusion: adhesive layer diffusion and interface diffusion.

For this study, 3 different kinds of environments have been used: one with 23ºC and immersed one with 43 º C and immersed and one with 43ºC and with 95% Relative humidity, trying to simulate critical spots in the bridge where water could accumulate. To increase the effect of corrosion, all the environmental chambers have a 5% of NaCl content. This is justified because in countries with cold climates, salt is used to prevent the freezing of the road. Eventually, this salt falls off to the steel structure of the bridge, and it expected that 5% of salt content is a good approximation of this effect.

4.1 Theory background

4.1.1 Fickan model

Moisture diffusion is analogous to heat transfer, since both are caused by random molecular motions. Fick adopted Fourier's mathematical expression for heat conduction to quantify the diffusion [58]. Fick's first law is:

$$F_x = -D\frac{\partial C}{\partial x}$$

Eq. 37

Where F_x is the diffusion flux in the x direction, D is the diffusion coefficient, and $\frac{\partial C}{\partial x}$ is the concentration gradient. The expression is negative because diffusion occurs in the opposite direction of increasing concentration. Also, this equation is only valid for isotropic medium.

Fick's second law describes the nonsteady state of diffusion and can be derived from Fick's first law. Crank [59] has shown that for a constant diffusion coefficient, it is obtained:

$$\frac{\partial C}{\partial t} = D\left(\frac{\partial^2 C}{\partial x^2} + \frac{\partial^2 C}{\partial y^2} + \frac{\partial^2 C}{\partial z^2}\right)$$

Eq. 38

where C is the concentration of the diffusing substance and D is the diffusion coefficient. The previous expression can be simplified for a one-dimensional diffusion to:

$$\frac{\partial C}{\partial t} = D\left(\frac{\partial^2 C}{\partial x^2}\right) \qquad \text{Eq. 39}$$

The solution for this one-dimensional equation that calculates the concentration of a diffusing substance in an isotropic plane sheet of finite thickness depending on time and space is:

$$\frac{C(x,t)}{C_\infty} = 1 - \frac{4}{\pi}\sum_{n=0}^{\infty}\frac{(-1)^n}{2n+1}\exp\left[\frac{-D(2n+1)^2\pi^2 t}{4l^2}\right]\cos\frac{(2n+1)\pi x}{2l} \qquad \text{Eq. 40}$$

where D is the diffusion coefficient, l is the half-thickness of the sheet ($-l<x<l$), C is the concentration of the diffusing substance at position x and time t, and C_∞ is the saturation concentration of the absorbed substance. This equation assumes that the concentration at the borders is the saturation concentration, the initial concentration of the diffusing substance is zero, and the diffusion coefficient remains constant. An analogous expression based on mass diffused, according to Crank [59] is:

$$\frac{M_t}{M_\infty} = 1 - \frac{8}{\pi^2}\sum_{n=0}^{\infty}\frac{1}{(2n+1)^2}\exp\left[\frac{-D(2n+1)^2\pi^2 t}{h^2}\right] \qquad \text{Eq. 41}$$

where D is the diffusion coefficient, h is the total sheet thickness, M_t is the total mass absorbed by the sample at a time t, and M_∞ is the equilibrium mass of the absorbed substance.

4.1.2 Two dimensional equation

The diffusion of moisture in the adhesive can't be considered as one-dimensional, because in this case our adhesive layer is free in 2 axes. Therefore, a two dimensional equation is needed in order to calculate the ingress of moisture by the faces of the adhesive that are exposed to the environment.

The concentration of moisture, depending on 2 space variables (x,y) and time, being the adhesive layer a rectangle with thickness in the z axis, can be written as:

$$\frac{C(x,y,t)}{C_\infty} = 1 - \frac{16}{\pi^2} \sum_{j=0}^{\infty} \sum_{n=0}^{\infty} \frac{(-1)^n(-1)^j}{(2n+1)(2j+1)} \exp\left[\frac{-D\pi^2 t}{4l^2}\left(\frac{2n+1}{x_0}\right)^2\left(\frac{2j+1}{y_0}\right)^2\right] \cos\frac{(2n+1)\pi x}{2l} \cos\frac{(2j+1)\pi y}{2l}$$

Eq. 42

where x and y are the distances from the centre of the adhesive layer, x_0 and y_0 are the total dimensions of the adhesive layer in that direction, l is the half-thickness of the sheet, D is the diffusion coefficient and t is the time.

4.1.3 Different mass uptake equations

4.1.3.1 Non Fickian

It has been observed that polymers present non-Fickian behaviour when the temperature is below the glass transition temperature (T_g) [58], where the diffusion process differs from Fickian behaviour after initial uptake. The two mechanisms of the dual Fickian model are considered to be working in parallel. The one-dimensional equation for the non-Fickian behaviour [59] that determinates the concentration is:

$$C(x,t) = \left(1 - \frac{4}{\pi}\sum_{n=0}^{\infty}\frac{(-1)^n}{2n+1}\exp\left[\frac{-D_1(2n+1)^2\pi^2 t}{4l^2}\right]\cos\frac{(2n+1)\pi x}{2l}\right) \times C_{1\infty}$$
$$+ \left(1 - \frac{4}{\pi}\sum_{n=0}^{\infty}\frac{(-1)^n}{2n+1}\exp\left[\frac{-D_2(2n+1)^2\pi^2 t}{4l^2}\right]\cos\frac{(2n+1)\pi x}{2l}\right)$$
$$\times C_{2\infty}$$

Eq. 43

where $C_{1\infty}$ and $C_{2\infty}$ are fractions of saturated concentration C_∞, D_1 and D_2 are the diffusion coefficients and l is the length of the diffusion path.

The mass uptake equation in the non-Fickian model is:

$$M_t = \left(1 - \frac{8}{\pi^2}\sum_{n=0}^{\infty}\frac{1}{(2n+1)^2}\exp\left[\frac{-D_1(2n+1)^2\pi^2 t}{h^2}\right]\right) \times M_{1\infty}$$
$$+ \left(1 - \frac{8}{\pi^2}\sum_{n=0}^{\infty}\frac{1}{(2n+1)^2}\exp\left[\frac{-D_2(2n+1)^2\pi^2 t}{h^2}\right]\right) \times M_{2\infty}$$

Eq. 44

where $M_{1\infty}$ and $M_{2\infty}$ are fractions of saturated mass uptake M_∞.

4.1.3.2 Relaxation of the adhesive

At high temperatures, and for adhesives immersed in liquids, a phenomenon of polymer relaxation takes place. This mechanism increases the water uptake of the adhesive. According to [58] the equation that considers the polymer relaxation is:

$$M_t = M_{\infty,F}\left\{1 - \exp\left[-7.3\left(\frac{Dt}{h^2}\right)^{0.75}\right]\right\} + M_{\infty,R}1 - \exp(-kt)$$

Eq. 45

This equation considers both the Fickian behaviour and the polymeric relaxation taking place in the adhesive. The first part considers the Fickian diffusion and when the curve starts to bend over, and then the relaxation part has the dominance of the moisture ingress. The final moisture saturation level M_∞ is the sum of the absorption during Fickian process, $M_{\infty,F}$ and the maximum absorption due to polymer relaxation, $M_{\infty,R}$.

4.1.3.3 Delayed dual Fickian model

Sometimes, the experimental data doesn't fit with any of the previous models explained before when there is a secondary uptake. To incorporate the secondary uptake in the analytical model, a dual Fickian model with a Heaviside step function can be used. This model is called delayed dual Fickian model, where the secondary uptake is modelled by power law [59]. The expression is:

$$\begin{aligned}M_t = &\left(1 - \frac{8}{\pi^2}\sum_{n=0}^{\infty}\frac{1}{(2n+1)^2}\exp\left[\frac{-D_1(2n+1)^2\pi^2t}{h^2}\right]\right) \times M_{1\infty} \\ &+ \left(1 - \frac{8}{\pi^2}\sum_{n=0}^{\infty}\frac{1}{(2n+1)^2}\exp\left[\frac{-D_2(2n+1)^2\pi^2t}{h^2}\right]\right) \times M_{2\infty} \\ &+ \Phi(t - t_1)(at^b + c)\end{aligned}$$

Eq. 46

where Φ is the Heaviside step function, t_1 is the start time of secondary uptake as determined experimentally and a,b and c are toe power law constants determined by curve fitting.

4.2 Experimental test and results

4.2.1 Gravimetric test

For this moisture diffusion in the adhesive layer, a gravimetric test has been performed in order to obtain the diffusion coefficient (D). This test method covers the determination of the relative rate of absorption of water by plastics when immersed, and has two chief functions: first, as a guide to the proportion of water absorbed by a material; and second, as a control test on the uniformity of a product. Ideal diffusion of liquids into polymers is a function of the square root of immersion time. Time to saturation is strongly dependent on specimen thickness. The experiment consisted in immersing an adhesive specimen of 60x60x1 mm in water, according to the ASTM D 570 – 98 standard[36], and then measures of the water uptake are taken.

4.2.2 Gravimetric test results

As this thesis aim is to develop a methodology and not to go into tests and values, it is going to be assumed a value of D, the one that was obtained in the work of Nguyen [32], with a value of $2.07 \cdot 10^{-7}$ mm^2/s.

4.3 Verification of our model

4.3.1 Finite element method and analytical method

To prove the accuracy of the ABAQUS results, Fickian concentration equation was modelled in MATLAB (see Appendix A), so a comparison between a numerical solution and an analytical solution could be done. The 2D diffusion equation was used in MATLAB, while the Mass Diffusion module was used in ABAQUS. Both methods need as an input the diffusion coefficient and the maximum concentration, which can be obtained from a gravimetric test.
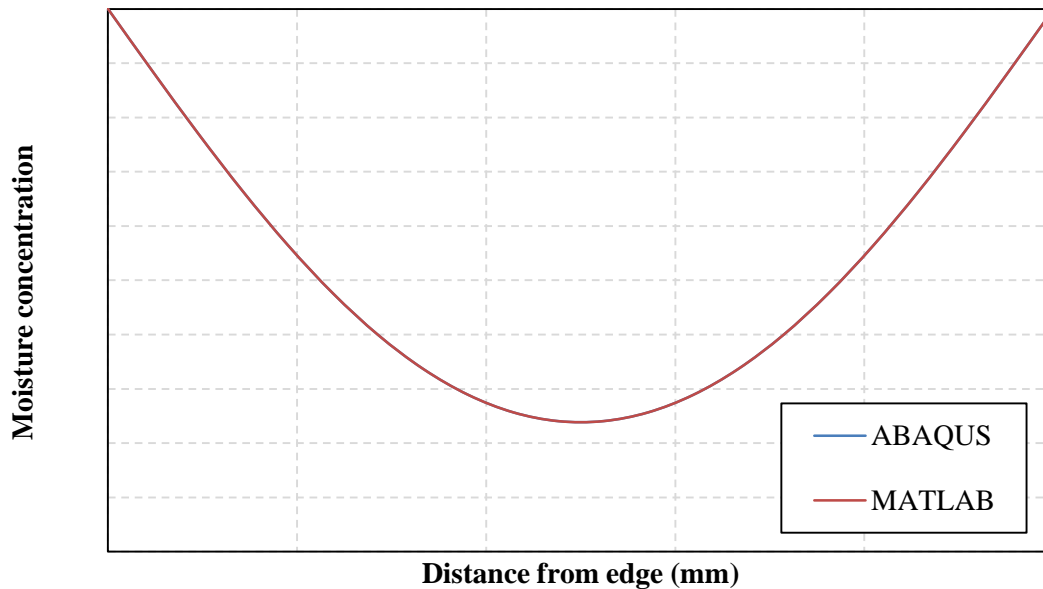
Figure 13 Comparison of diffusion profile performed by MATLAB and ABAQUS

As it can be appreciated in the previous graphic, the ABAQUS (FEM) and the MATBAL (analytical) solutions are the same, therefore the FEM model is validated.

4.3.2 Analogy between heat and moisture

The Finite Element program ABAQUS can´t do a coupled stress-mass diffusion analysis. In order to perform this analysis, an analogy between heat transfer and mass diffusion shall be done. According to Fourier's law of heat conduction:

$$\mathbf{q} = -\mathbf{k}\nabla\mathbf{T}$$
<div align="right">Eq. 47</div>

where $q(W\ m^{-2})$ is the heat flux, $k(W\ m^{-1}K^{-1})$ is the conductivity, $\nabla T(K\ m^{-1})$ is the temperature gradient. From this equation, Fick developed his first law of diffusion:

$$\mathbf{F_x} = -\mathbf{D}\frac{\partial \mathbf{C}}{\partial \mathbf{x}}$$
<div align="right">Eq. 48</div>

where F_x is the diffusion flux in the direction x, D is the diffusion coefficient and $\partial C/\partial x$ is the concentration gradient. To relate these two equations, a transformation is needed to make the heat conduction to be heat diffusion, to be like the Fick's law. In order to do that, the conductivity parameter k has to be converted into a diffusion parameter, D_T. Using Lewis formula:

$$\beta = \frac{\alpha_c}{\rho_\alpha c_{p\alpha}} \qquad \text{Eq. 49}$$

where α_c is the convective heat transfer coefficient, $\rho(kg\ m^{-3})$ is the density and $c_p(J\ kg^{-1}\ K^{-1})$ is the heat capacity. Using this formula, the conductivity $k(W\ m^{-1}\ k^{-1})$ becomes a diffusion coefficient $D_T(m^2\ s^{-1})$ as follows:

$$D_T = \frac{k}{\rho c_p} \qquad \text{Eq. 50}$$
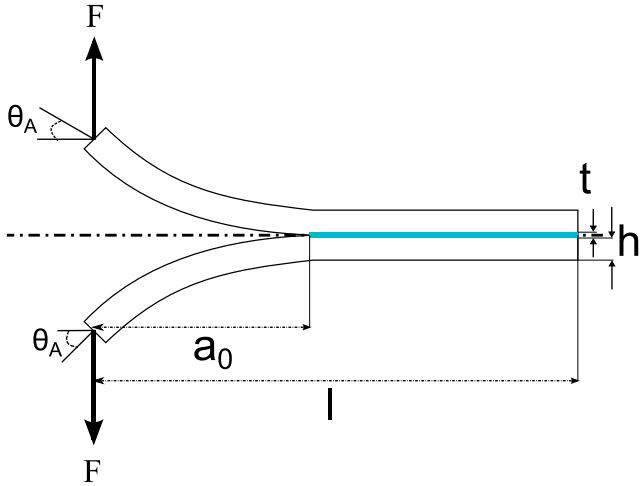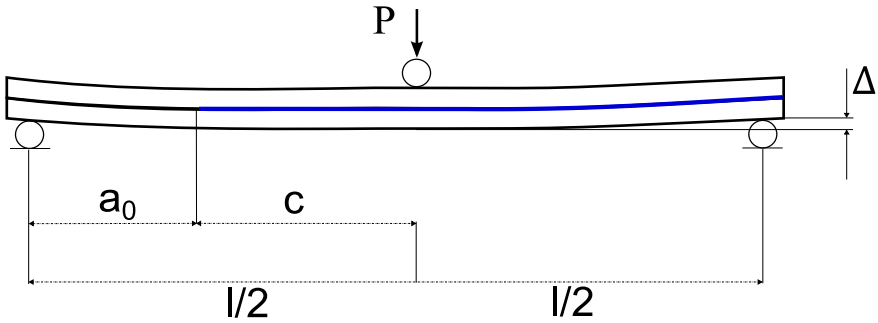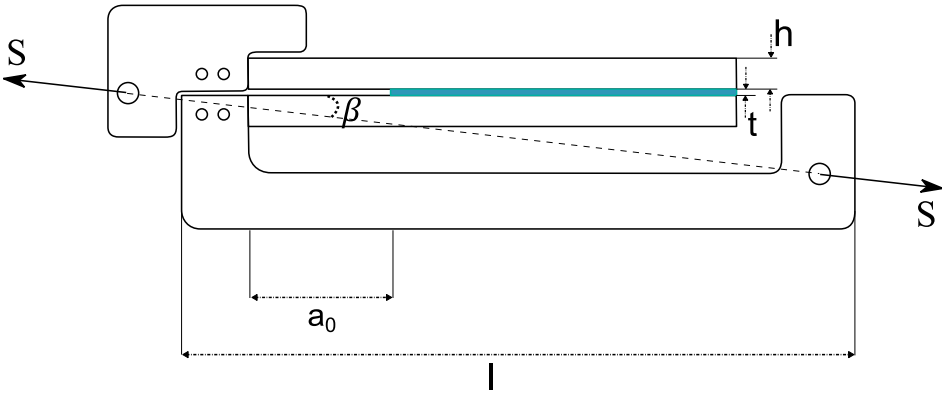
In ABAQUS, to model the mass diffusion, the solubility, the concentration and the diffusion are needed to be introduced. In order to get the same results in the heat transfer analysis, the conductivity of the adhesive is introduced as the diffusivity, and both the density and the specific heat are introduced as 1. It is important, though, to introduce a really low value of the heat capacity in both the CFRP and the steel (for example 1e-06) in order to avoid the heat to diffuse through this materials.

With this method, both the mass diffusion module and the heat transfer module give the same results, and as the mass diffusion was validated with the analytical solution, this means that the heat transfer solution is also correct.

5 Experiments

As it was discussed in chapter 3, when the choice is to use CZM to predict an adhesive joint behavior it is first necessary to perform tests to obtain the traction-separation laws for the actual adhesive in question. The traction-separation law for pure mode I, mode II and the exponential value alpha for the power law are obtained true the test described in the table below Table 4. Mode III is assumed to be equal to mode II.

Table 4 Test that is used to obtain the traction-separation law for mode I, mode II and mix-mode.

The test used for mode I is the DCB-test, for mode II the ENF-test and for the exponential value alpha the MCB-test Table 4. The dimensions used for these different tests are presented in table Table 5. The TRB and DLS test are made for the verification of the ABAQUS models and are shown in Table 6 and the corresponding dimensions are presented in Table 7.

Table 5 Dimensions of test used and performed in this work.

Type	h [mm]	a_0 [mm]	b [mm]	l [mm]	t [mm]	No. of specimen
DCB	6.6	80	8.3	200	2.4	3
ENF	16.6	350	16.6	1000	2.4	3
MCB	10	25	4	125	2.4	6

Table 6 RTB and DLS-joint

TRB-joint

DLS-joint, taking 1/4 of the total geometry for simplicity
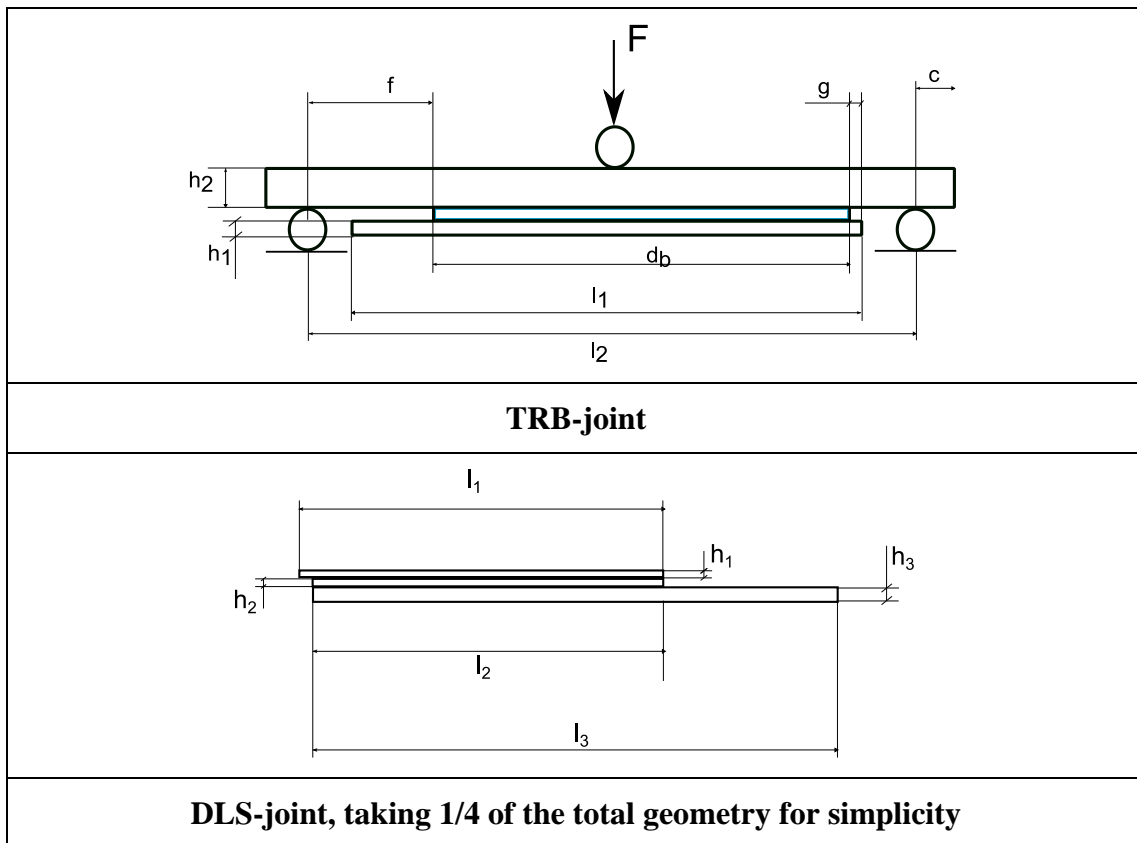
Table 7 Dimensions for the RTB and DLS-joint
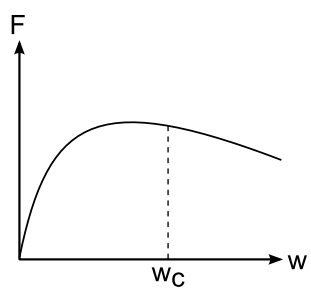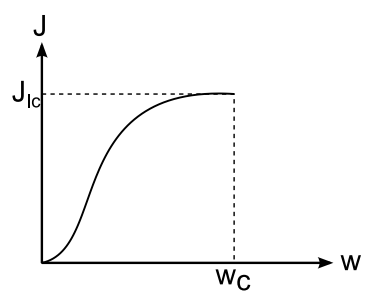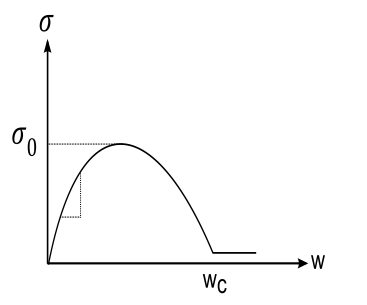
TRB	h1	h2	t	f	g	d_b	c	L1	L2
Dim.	10	4	2.4	90	10	215	10	280	330
DLS	h1	h2	h3	l1	l2	l3	b_{steel}	b_{CFRP}	$b_{adhesive}$
Dim.	1.25	1.45	5	205	200	300	60	50	50

The steel used for TRB-joints haves an elastic modulus of 196 GPa.

5.1 DCB-test results

As in the work of Saeed Salimi [29] the results from the DCB-test are used to find the traction-separation law for pure mode I. The experimentally measured value of F, w and theta together with the corresponding equations gives the characteristic curves that are wanted.

Table 8 Process from the experimental outcome to the traction-separation law

Experimental output: Force and deflection (F and w)	J-w curve from the use of the equation J_{DCB} and the experimental output. $$J_{DCB} = \frac{2F\theta_A}{b}$$	Differentiation of J_{DCB} to obtain the curve: stress vs. deformation $$\sigma = \sigma(w)$$ $$= \frac{\partial J}{\partial w}$$ $$= \frac{\partial}{\partial w}\left\{\frac{2F}{b}\theta_A\right\}$$

The differentiation of J_{DBC} to obtain $\sigma(w)$ causes a substantial scatter, consequently, the $J_{DBC} = J(w)$ data is fitted with a polynomial of order k ore a Prony-series with k terms.

$$J(w) = \sum_{i=0}^{k} A_i w^i$$

Polynomial-series

$$J(w) = \sum_{i=0}^{k} A_i e^{\left(-\frac{kw}{iw_c}\right)}$$

Prony-series
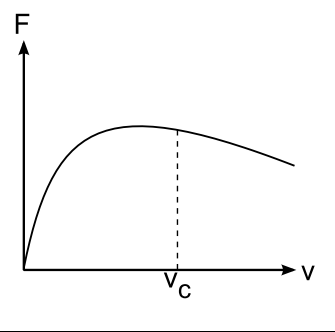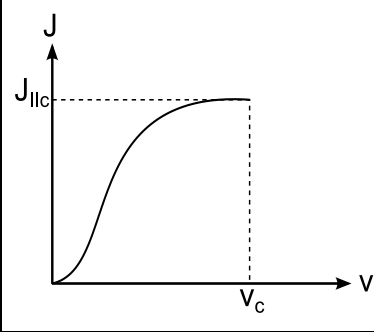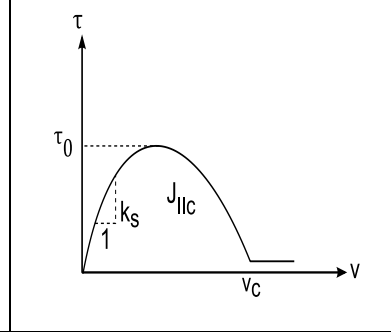
Table 9 Traction-separation law from the test and analytical expressions.

Experiment No.	$J_{IC} \left[\dfrac{J}{m^2}\right]$	$\sigma_0 \, [MPa]$	$w_c \, [\mu m]$	$K_n \, [MPa/\mu m]$
1	930	24	52	2.6
2	1010	20	69	2.1
3	1020	23	69	4.2
Mean value	987	22	63	3

5.2 ENF-test results

As for the DCB-test, the same methodology is used for the ENF-test. The experimentally measured value of F and v together with the corresponding equations gives the characteristic curves that are wanted.

Table 10 Process from the experimental outcome to the traction-separation law

Experimental output: Force and deflection (F and w.	J-v curve from the use of the equation J_{ENF} and the experimental results.	Differentiation of J_{ENF} to obtain the curve: shear vs. deformation $\tau(v)$

The differentiation of J_{ENF} to obtain $\tau(v)$ causes a substantial scatter, consequently, the $J_{ENF} = J(v)$ data is fitted with a polynomial of order k ore a Prony-series with k terms

$$J(v) = \sum_{i=0}^{k} A_i v^i \qquad\qquad J(v) = \sum_{i=0}^{k} A_i e^{\left(-\frac{kv}{iv_c}\right)}$$

Polynomial-series   Prony-series

Table 11 Traction-separation law from the test and analytical expressions.

Experiment No.	$J_{IIC}\left[\frac{KJ}{m^2}\right]$	$\tau_0\,[MPa]$	$v_c\,[\mu m]$	$K_s\,[MPa/\mu m]$
1	2.99	28.4	264	1.1
2	3.57	26.6	211	1.1
3	4.35	28.2	255	1.2
Mean value	3.64	27	243	1

5.3 MCB-test results

The outcomes from the MCB-test are recorded with the ARAMIS 4M system. The displacement of four point at the crack tip are measured in order to determinate the shear and peel deformation of the adhesive layer and the rotation of the adherent. The displacement is measured in both x and y directions and the rotation are evaluated with equations showed in Figure 14.

$$\theta_u = \frac{u_{x,1} - u_{x,2}}{y_1 - y_2}$$

$$\theta_l = \frac{u_{x,3} - u_{x,4}}{y_3 - y_4}$$

$$\theta_m = \frac{\theta_u + \theta_l}{2}$$

a)   b)
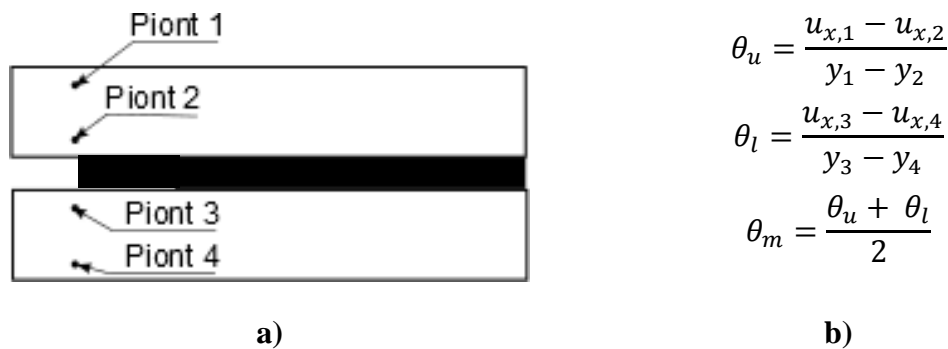
Figure 14 a) Positions of the points used to record the displacement at the crack tip. b) Equations used to evaluate the rotation
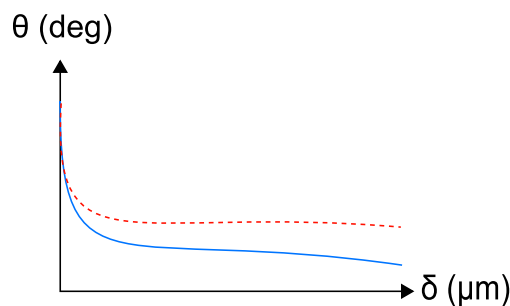
Figure 15 Rotational angel of the over (blue) and under (red) adherents vs. the displacement

In the work of Saeed Salimi [29] it is shown that when comparing the MCB simulation results in ABAQUS with the experimental results presented above the best value of the exponential parameter alpha in Eq. 2 is 0.8. When defining the material properties in edit material in ABAQUS, damage initiation (QUADS DAMAGE) and in the damage propagation option (DAMAGE EVOLUTION) the power law is chosen as the mix mode behavior and the exponential value as 0.8.
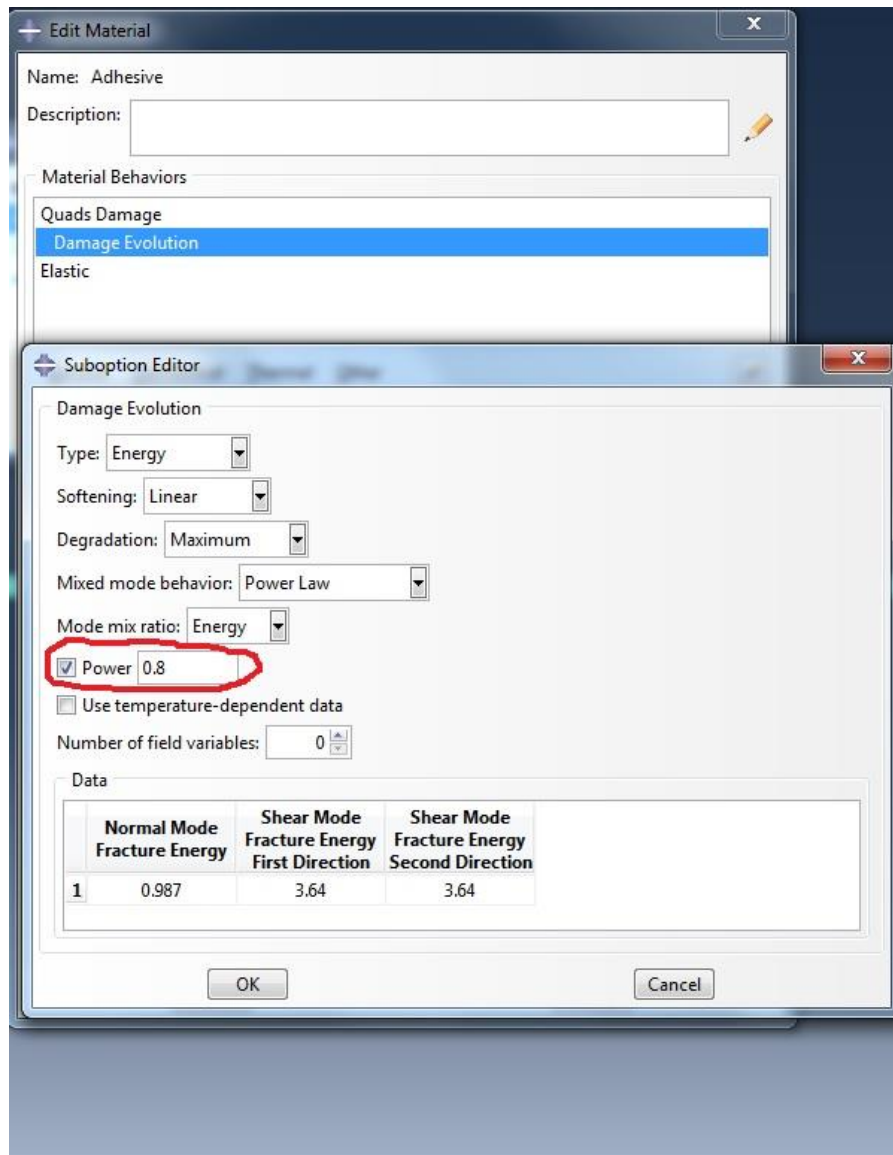
Figure 16 Exponential value alpha in ABAQUS

In the MCB-test the shear and peel deformation is recorded with the help points shown in Figure 14 and Eq. 51 and Eq. 52. The shear and peel deformation is conceptually presented in Figure 17 and the results from the test are compare with the simulation in ABAQUS with different values of alpha. This iteration process gives an indication of witch value of alpha to use for the prediction of failure load for the test specimens presented in chapter 5.5 and 5.6.

$$v = u_{x,2} - u_{x,3} + \theta_m \left(u_{y,3} - u_{y,2} \right) \qquad \text{Eq. 51}$$

$$w = u_{y,2} - u_{y,3} + \theta_m \left(u_{x,3} - u_{x,2} \right) \qquad \text{Eq. 52}$$
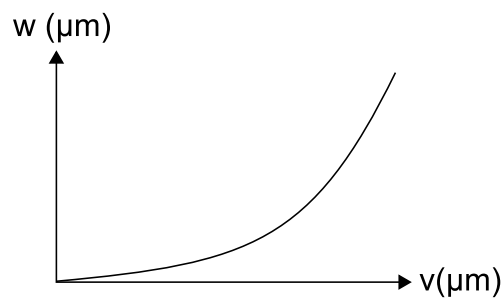
Figure 17 shear and peel deformation
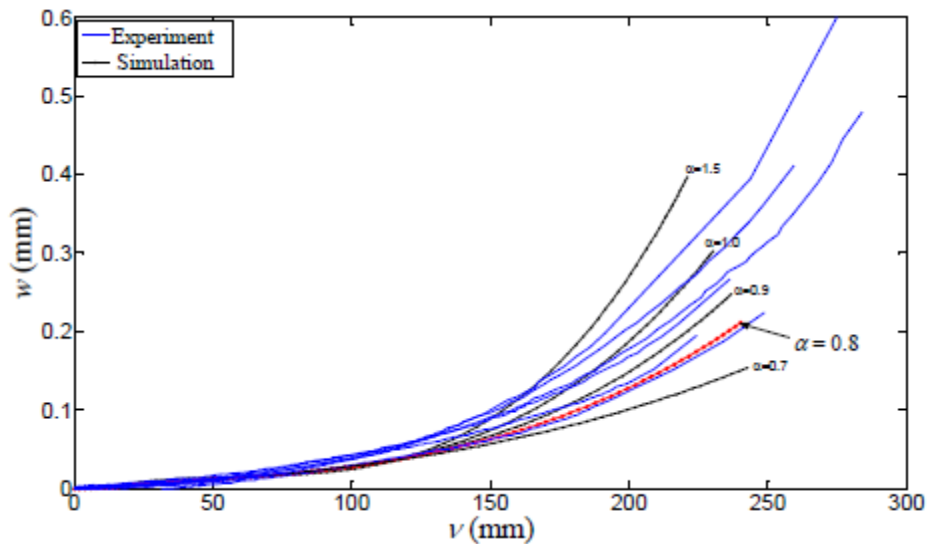
Figure 18 shears and peel deformation, experimental versus simulations with different alpha values.

Another comparison that is maid between the simulation in ABAQUS and test results is the force versus displacement. The conceptual relation is shown in Figure 19.
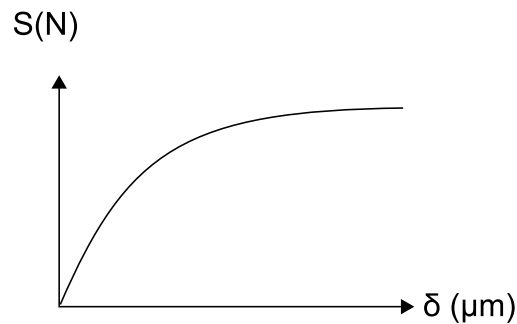
Figure 19 Force vs. displacement at crack tip. Where S is the applied external force on the joint specimen.
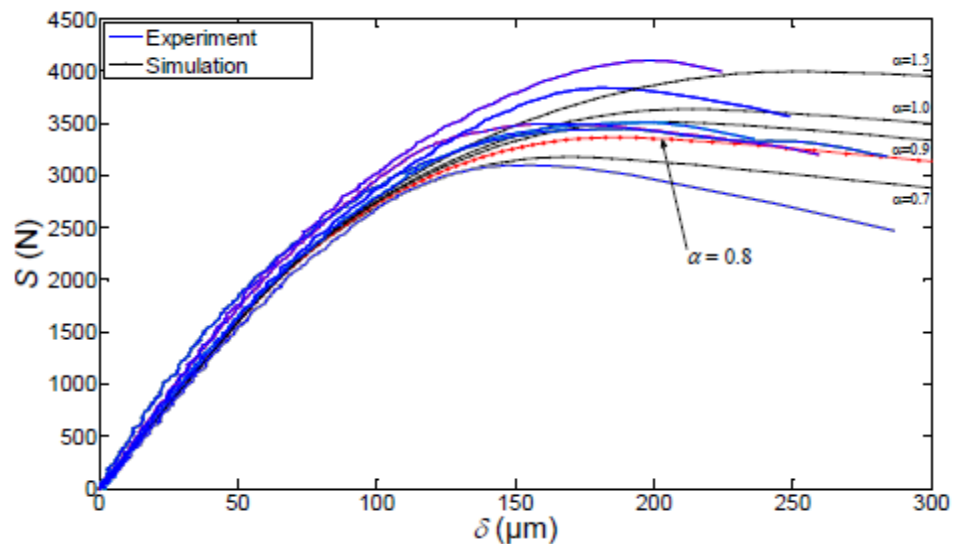
Figure 20 Force vs. displacement, experimental versus simulations with different alpha values.

Finally a comparison is maid between the energy release rate and displacement is done and the conceptual relation is shown in Figure 21. Inserting the sectional forces and moment in to (Eq. 36) gives the experimental results and is presented in Figure 22, this is also compared with different values of alpha.
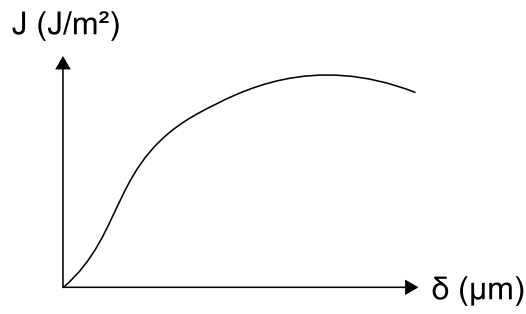
Figure 21 Energy release rate vs. displacement at the crack tip.
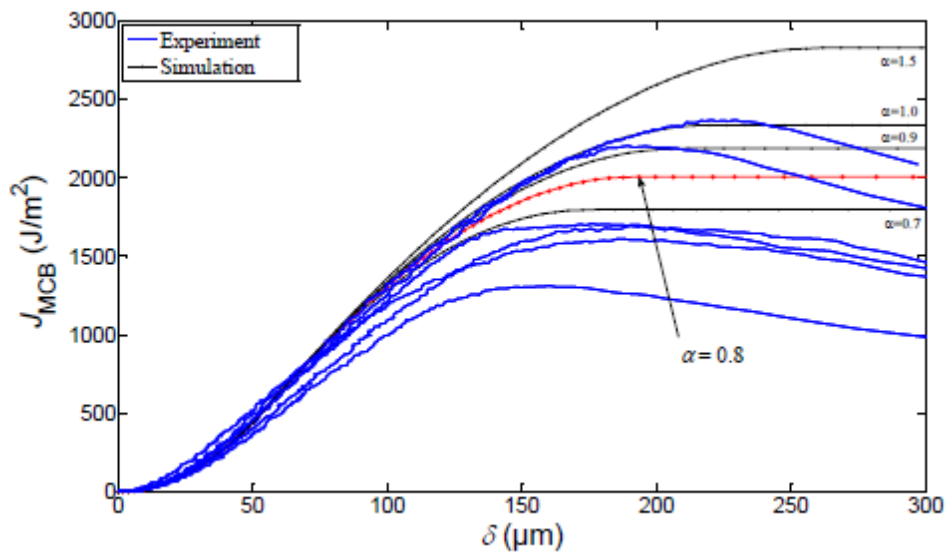
Figure 22 Energy release rate vs. displacement, experimental versus simulations with different alpha values.

5.4 TRB-test

The TRB-test results are used to compare the failure load obtained in the simulation of the TRB-joint analysis performed in ABAQUS. In this Chapter the TRB-joint test performance is described and the results are summarized. Three test specimens are used and the results are shown in Figure 25 and Table 12 TRB test results.

For the set of specimens, due to a technical problem with the internal LVDT, an external LVDT was used to measure the displacement of the loading point Δ, as shown in figure below. The displacement rate of the loading point has been set at 2mm /min for all experiments.

Figure 23 TRB specimen being tested

Figure 24 TRB specimen being tested
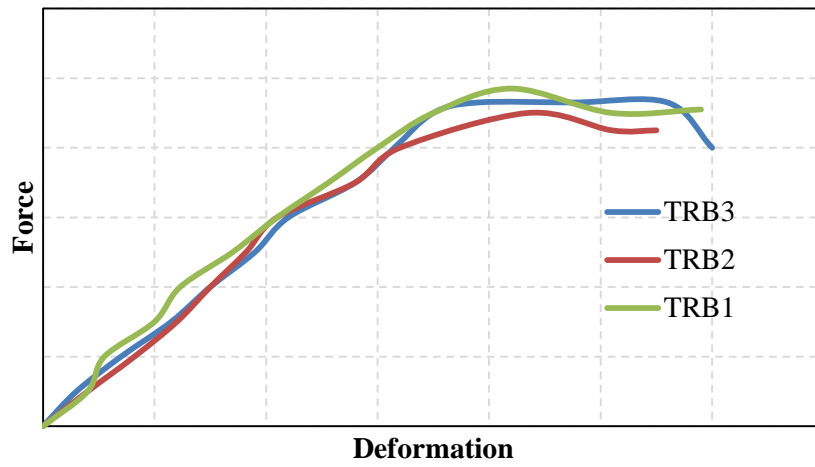
Figure 25 Experimental results for TRB

Table 12 TRB test results

Test specimen	Failure load (N)	Failure deformation (mm)
TRB1	4850	4.1
TRB2	4500	4.0
TRB3	4500	4.2

5.5 DLS test

The DLS-test is performed to verify the methodology presented in this work. In this Chapter the DLS-joint manufacturing process is presented and the results are summarized at the end. The comparison of test results and the simulation in ABAQUS are well described in Chapter 6.

Two test specimens where tested. The test specimens are named CSt1 and CSt2.

To perform the DLS tests, wood molds were first created in order to maintain the geometry of the samples. The adhesive was poured inside this mold and a constant thickness of 1.5mm was achieved applying pressure in the upper part of the mold, as the excess of adhesive was being removed from the sample.
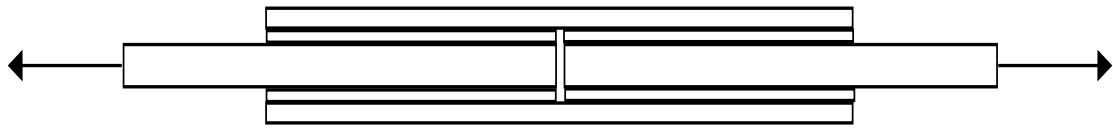
Figure 26 DLS-joint
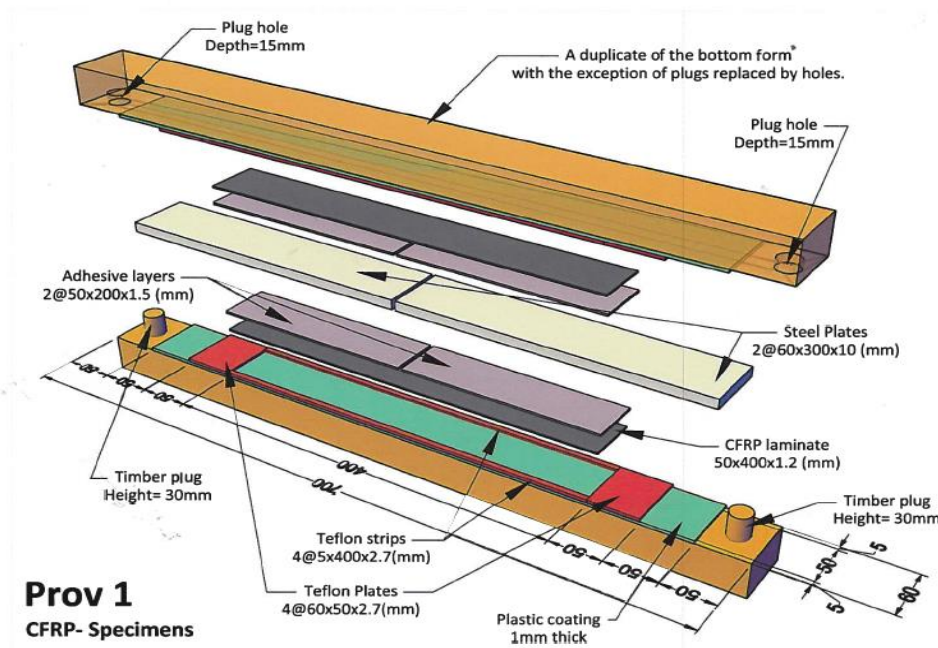
Figure 27 DLS mould configuration
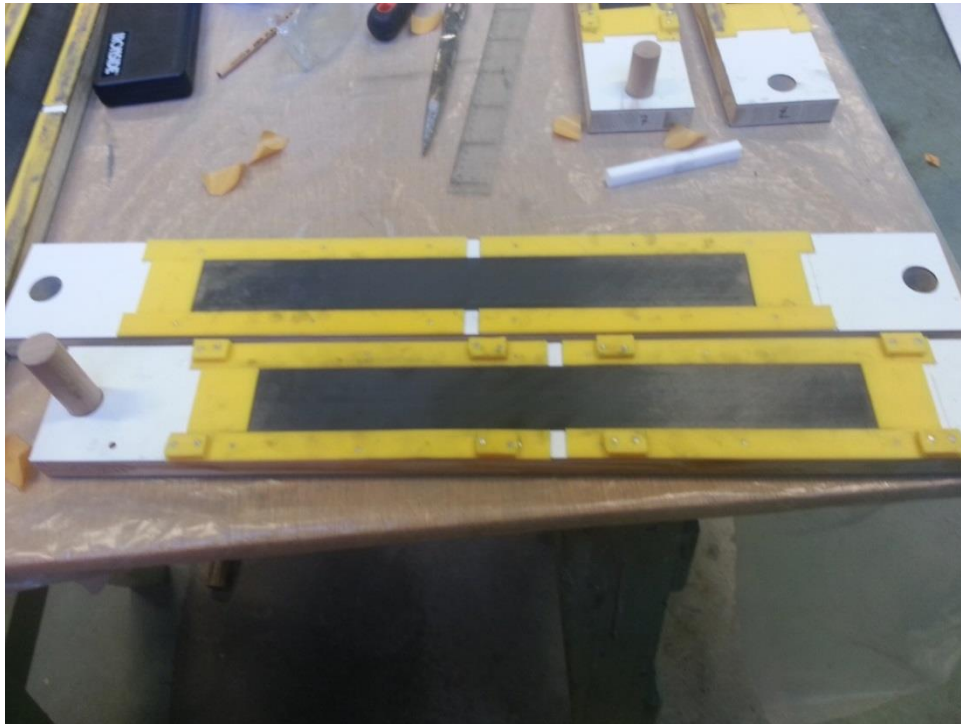
Figure 28 DLS molds with the CFRP in place

After making the specimens in the mold, they were left inside the mold for 2 days. After that, they were taken outside de mold and left for 1 week for curing. Next image shows a finished DLS sample.

Figure 29 DLS specimen curing

After curing, the samples were pulled, and a load-displacement curve was obtained. The speed of pulling was 0.1 mm/min.

Figure 30 DLS specimen being pulled

Figure 32 Cohesive failure in the specimens

Figure 31 Specimens after the test

Table 13 Results of failure loads and failure modes for the tested DLS-joint samples.

Test specimen	Failure mode	Failure load (N)	Failure deformation (mm)
Exp 1	mix-mode	140000	1.5
Exp 2	mix-mode	135000	1.4
Exp 3	mix-mode	125000	1.1
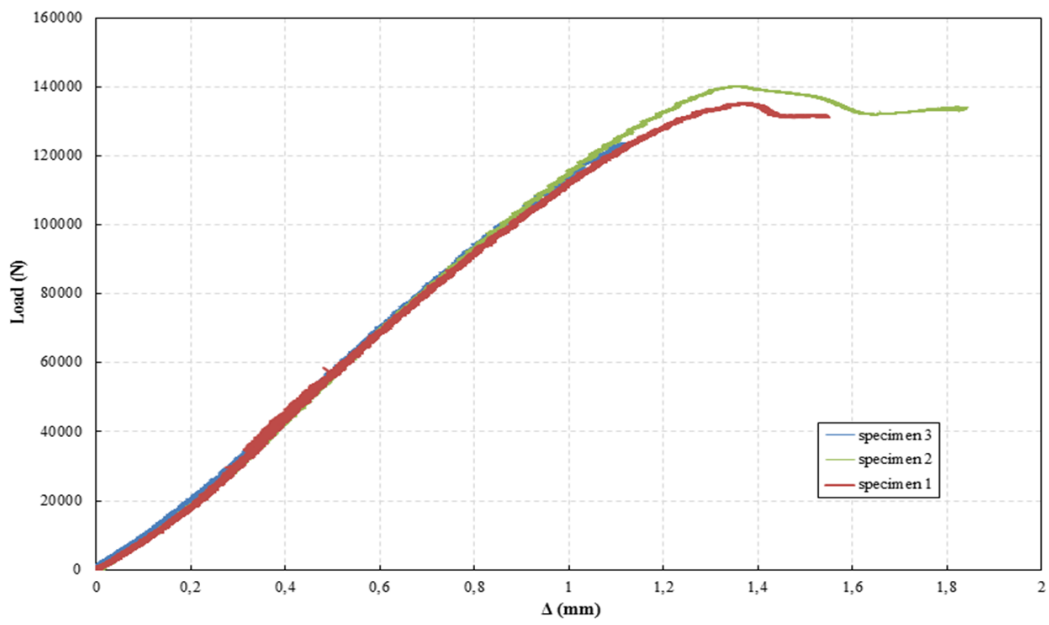
Figure 32 DLS-test results

6 Finite element modeling and analysis

It is now possible to use the traction-separation law obtained from the experimental test. The traction-separation laws for mode I and II from DCB and ENF-tests, and the estimated value of the exponential value alpha for the power law from the MCB-test. This is now all used and applied the finite element analysis program. The aim is to predict the failure load of the dry DLS-test and TRB-test and compare them with experimental data and in that way verifying the CZM approach.

The finite element analysis program ABAQUS version 6.11-1 was used for numerical modeling.

6.1 Material properties

Typical steel mechanical properties (E=210 GPa and ν=0.29) were used for the steel plates. To model the CFRP, the elastic parameters E=135 GPa and ν=0.3 were defined. When the adhesive is not completely considered as a cohesive element, its properties are E=7 Gpa and ν=0.3.

6.2 CZM parameters

To simulate the specimens in ABAQUS (both the TRB and the DLS) using the Cohesive Zone Modeling approach, ABAQUS uses cohesive elements. Using cohesive elements imply that the choice of material properties and section type is consistent with the type of cohesive element. The material properties of the adhesive-cohesive layer are chosen as traction, and have defined a damage initiation (QUADS DAMAGE in ABAQUS) and in the damage propagation option (DAMAGE EVOLUTION in ABAQUS) the power law is chosen as the mix mode behavior and the exponential. The section type is also set as cohesive. In this analysis the type of stress-strain relation is the uncoupled and is as follow:

$$\begin{Bmatrix} t_n \\ t_s \\ t_t \end{Bmatrix} = \begin{bmatrix} K_{nn} & 0 & 0 \\ 0 & K_{ss} & 0 \\ 0 & 0 & K_{tt} \end{bmatrix} * \begin{Bmatrix} \varepsilon_n \\ \varepsilon_s \\ \varepsilon_t \end{Bmatrix} \qquad \text{Eq. 53}$$

For the uncoupled behavior each traction component depends only on its conjugate nominal strain. The Eq. **53** has the quantities of the nominal tractions in the normal and in the two local shear directions at the left side of the equation. The matrix is the elasticity in terms of traction and separations for cohesive elements and the corresponding nominal strains are in the right side of the matrix.

To simulate the tests ABAQUS need the following input:

Elastic properties of the adhesive layer are set to traction Table 14. The Damage initiation definition is presented in Table 15 and the damage propagation in Table 16. The damage Stabilization (VISCOSITY COEFFICIENT) is set to 0.0001.

Table 14 Elastic properties

E or Knn	G1 or Kss	G2 or Ktt
3000 $[MPa/\mu m]$	1000 $[MPa/\mu m]$	1000 $[MPa/\mu m]$

Table 15 Damage initiation (QUADS DAMAGE)

Nominal stress normal-only mode	Nominal stress first direction	Nominal stress second direction
22 $[MPa]$ (Damage initiation for pure mode I)	27 $[MPa]$ (Damage initiation for pure mode II)	27 $[MPa]$ (Damage initiation for pure mode II)

Table 16 Damage propagation (DAMAGE EVOLUTION)

Normal mode Fracture energy	Shear mode Fracture energy first direction	Shear mode Fracture energy Second direction
0.987 $\left[\frac{J}{m^2}\right]$	3.64 $\left[\frac{J}{m^2}\right]$	3.64 $\left[\frac{J}{m^2}\right]$

6.3 TRB-joint simulation

6.3.1 Description of the models
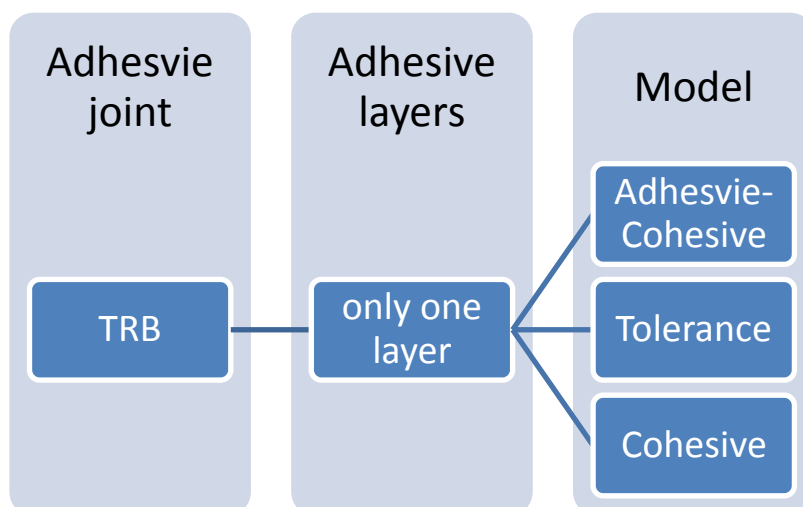
Figure 33 different models that are used for the TRB simulation

6.3.1.1 Adhesive-Cohesive model

Material properties: In this 2 dimensional model, a thin cohesive layer (0.1 mm) is modeled in the middle of the adhesive, as the failure is expected to be cohesive. To model this, the section of the cohesive layer is assigned as cohesive, while the rest are assigned as solid homogeneous.

Step module: In the step module, the Nlgeom was on, the automatic stabilization was set as Specify dissipated energy fraction (with a value of 0.0002), and the use of adaptive stabilization was also on.

Meshing and element type: For the meshing part, the steel plates were modeled with a free mesh, with a 4-node bilinear plane stress quadrilateral, incompatible modes elements (CPS4I). The adhesive layer was modeled as structured mesh with a 4-node bilinear plane strain quadrilateral, incompatible modes (CPE4I). The cohesive layer was modeled with a sweep mesh and a 4-node two-dimensional cohesive element, with element degradation set on Yes and max degradation set as 1. In all the element types, the viscosity was set as 0.0001 to stabilize the process. The mesh at the edge of the adhesive where the crack initiates was 0.2x0.1mm.
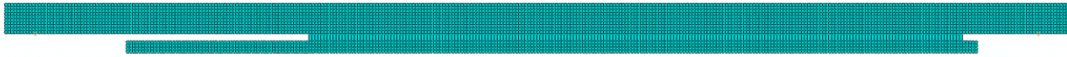

Figure 34 TRB adhesive-cohesive mesh

Loading and boundary conditions: A displacement was applied in the middle of the specimen, while there were vertical restrains in both sides of the specimens (10 mm from the edges) and one horizontal restrain in the left side of the specimen.
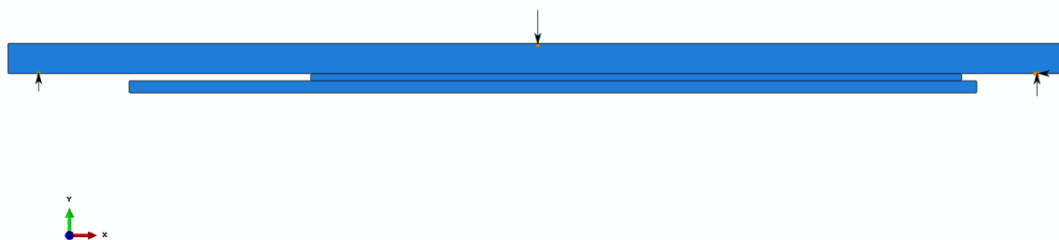

Figure 35 TRB loads and boundaries

6.3.1.2 Tolerance model

Material properties: The steel was modeled as solid homogeneous, while the adhesive layer was modeled completely as cohesive elements. In this model, to avoid assigning viscosity to the material, a tolerance of 0.2 is chosen.

Step module: In the step module, the Nlgeom was on, the automatic stabilization was set as Specify dissipated energy fraction (with a value of 0.0002) and the use of adaptive stabilization was also on.

Meshing and element type: For the meshing part, the steel plates were modeled with a structured mesh, with a 4-node bilinear plane stress quadrilateral, reduced integration, hourglass control elements (CPS4R). The cohesive layer was modeled with a sweep mesh and a 4-node two-dimensional cohesive element, with all the options set as default. There was only 1 element in the thickness of the adhesive layer. The overall mesh was 1mm.
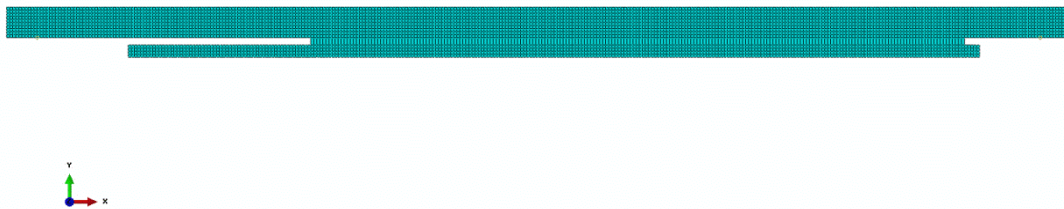
Figure 36 TRB tolerance mesh

Loading and boundary conditions: A displacement was applied in the middle of the specimen, while there were vertical restrains in both sides of the specimens (10 mm from the edges) and one horizontal restrain in the left side of the specimen.

6.3.1.3 Cohesive model

Material properties: The steel was modeled as solid homogeneous, while the adhesive layer was modeled completely as cohesive elements.

Step module: In the step module, the Nlgeom was on, the automatic stabilization was set as Specify dissipated energy fraction (with a value of 0.0002) and the use of adaptive stabilization was also on.

Meshing and element type: For the meshing part, the steel plates were modeled with a structured mesh, with a 4-node bilinear plane stress quadrilateral, incompatible modes elements (CPS4I). The cohesive layer was modeled with a sweep mesh and a 4-node two-dimensional cohesive element (COH2D4), with element degradation set on Yes and max degradation set as 1. In all the element types, the viscosity was set as 0.0001 to stabilize the process. There was only 1 element in the thickness of the adhesive layer. The overall mesh was 1mm.
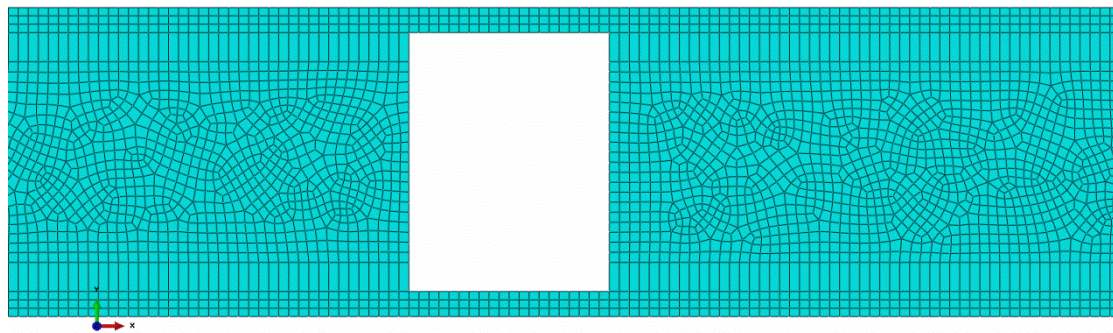
Figure 37 TRB cohesive mesh

Loading and boundary conditions: A displacement was applied in the middle of the specimen, while there were vertical restrains in both sides of the specimens (10 mm from the edges) and one horizontal restrain in the left side of the specimen.
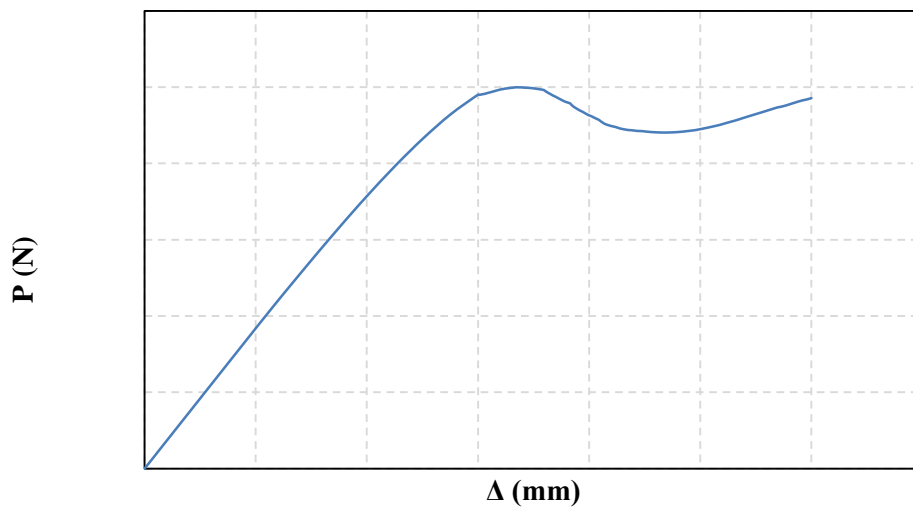
Figure 38 Test and simulation results for TRB

6.4 DLS-joint simulation

To model the DLS samples, a 2D model was firstly used, and finally a 3D model was also performed to compare the results. For the 2D models, 3 different hypotheses were tested: all the adhesive layers may fail, just one side of the DLS may fail or 2 adhesive layers in diagonal may fail.

6.4.1 Description of the 2D models
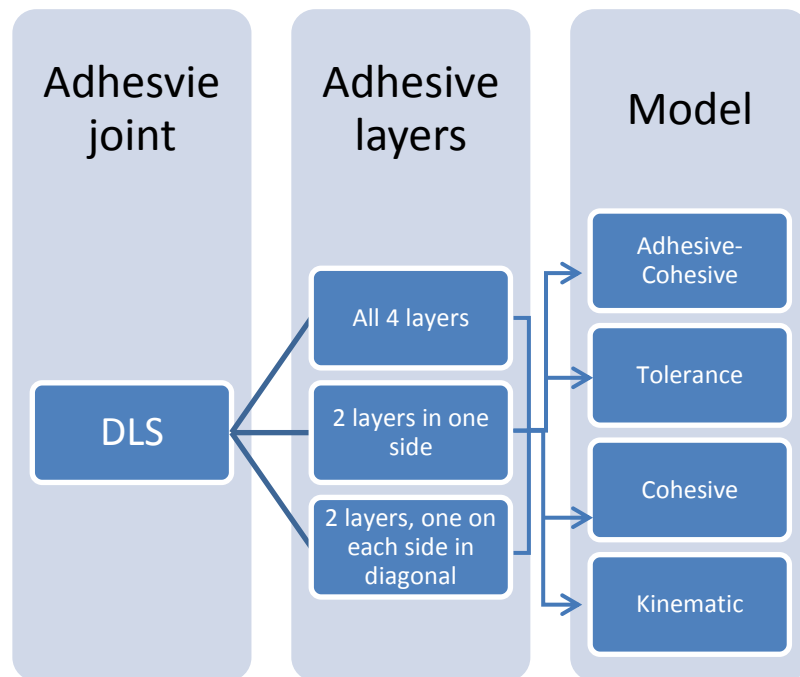
Figure 39 Different models that are used for the DLS simulation

6.4.1.1   Four cracks model

6.4.1.1.1   Cohesive model
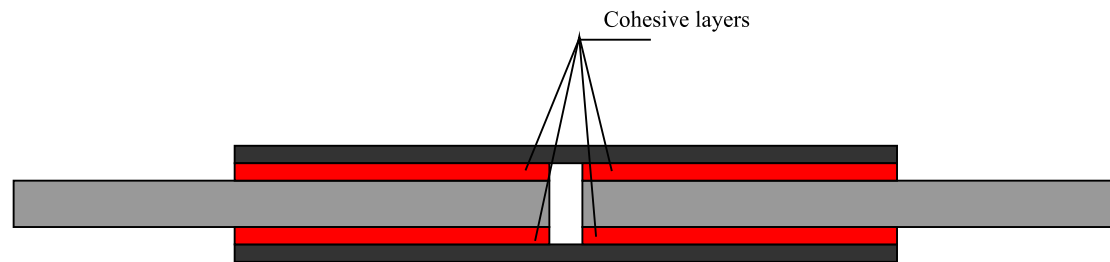
Cohesive layers

Figure 40 DLS 4 cracks cohesive

Material properties: The steel and the CFRP were modeled as solid homogeneous, while all the adhesive layers were modeled completely as cohesive elements.

Step module: In the step module, the Nlgeom was on, the automatic stabilization was set as Specify dissipated energy fraction (with a value of 0.0002) and the use of adaptive stabilization was also on.

Meshing and element type: For the meshing part, the steel plates were modeled with a structured mesh, with a 4-node bilinear plane stress quadrilateral, incompatible modes elements (CPS4I). The cohesive layer was modeled with a sweep mesh and a 4-node two-dimensional cohesive element (COH2D4), with element degradation set on Yes and max degradation set as 1. In all the element types, the viscosity was set as 0.0001 to stabilize the process. There was only 1 element in the thickness of the adhesive layer. The overall mesh was 0.5 mm.

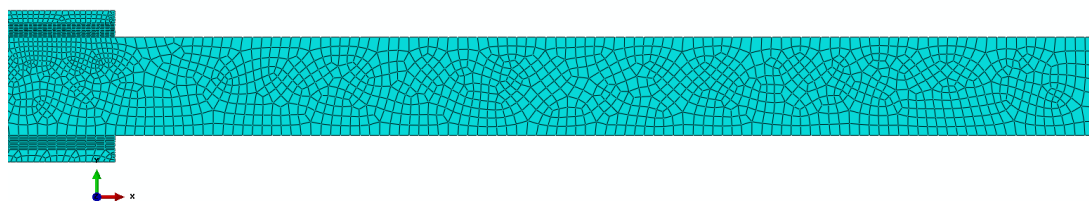**Figure 41** DLS cohesive mesh

Loading and boundary conditions: The DLS sample was fixed in one side and was being pulled from the other, so the boundary conditions assigned in this model were fixing all the displacements in one edge and assigning a displacement to the other edge. The reaction forces were obtained by summing the value of the RF in all the nodes that were fixed.

Fixed surface

Displacement
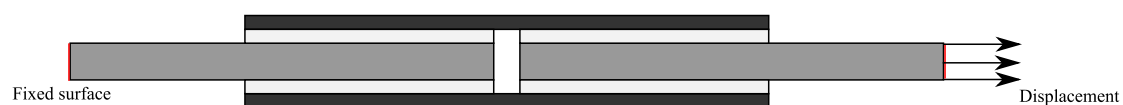
Figure 42 Standard boundary conditions

6.4.1.1.2 Adhesive-Cohesive model
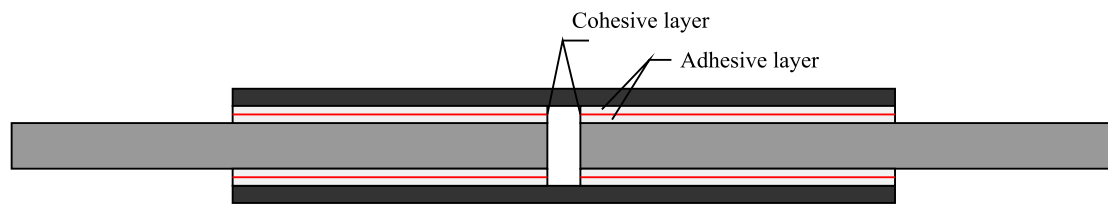
Figure 43 DLS 4 cracks adhesive-cohesive

Material properties: The steel and the CFRP were modeled as solid homogeneous, while the adhesive layers were modeled as 2 layers of solid homogeneous material with a thin layer of cohesive elements in the middle.

Step module: In the step module, the Nlgeom was on, the automatic stabilization was set as Specify dissipated energy fraction (with a value of 0.0002) and the use of adaptive stabilization was also on.

Meshing and element type: For the meshing part, the steel plates were modeled with a structured mesh, with a 4-node bilinear plane stress quadrilateral, incompatible modes elements (CPS4I). The adhesive layer was modeled as structured mesh with a 4-node bilinear plane strain quadrilateral, incompatible modes (CPE4I). The cohesive layer was modeled with a sweep mesh and a 4-node two-dimensional cohesive element (COH2D4), with element degradation set on Yes and max degradation set as 1. In all the element types, the viscosity was set as 0.0001 to stabilize the process. The mesh size in the important points was 0.2x0.2 mm, and it grew till 1.5 mm at the edges of the steel plates.

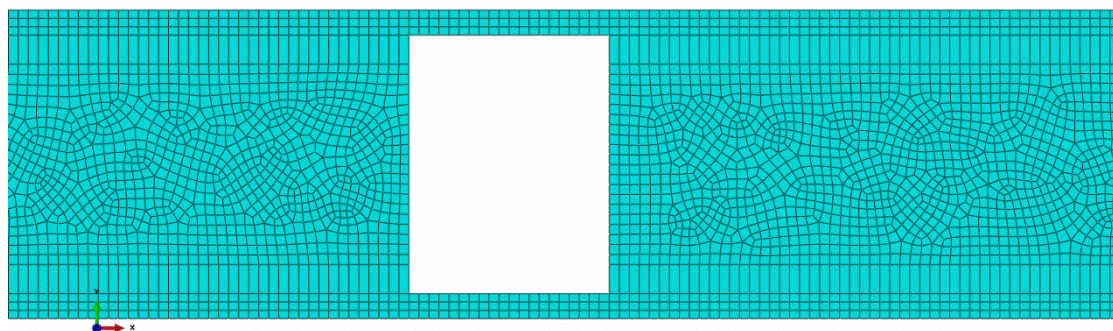**Figure 44** DLS 4 cracks adhesive-cohesive mesh centre

Figure 45 DLS 4 cracks adhesive-cohesive side

Loading and boundary conditions: The DLS sample was fixed in one side and was being pulled from the other, so the boundary conditions assigned in this model were fixing all the displacements in one edge and assigning a displacement to the other edge.

6.4.1.1.3 Tolerance model
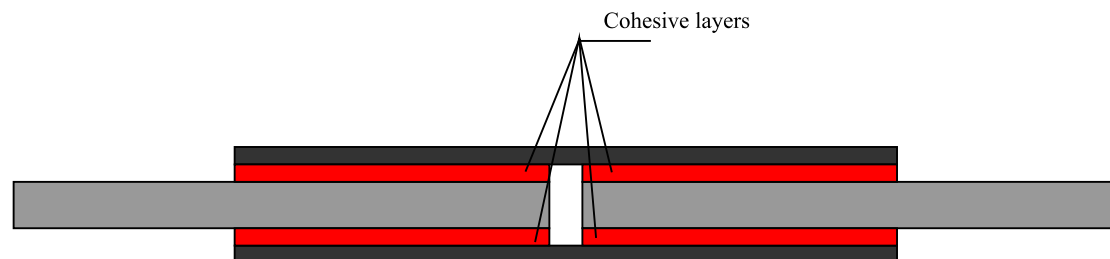
Figure 46 DLS 4 cracks tolerance

Material properties: The steel and the CFRP were modeled as solid homogeneous, while all the adhesive layers were modeled completely as cohesive elements. In material properties, the cohesive elements have a tolerance of 0.2 instead of the default 0.05.

Step module: In the step module, the Nlgeom was on, the automatic stabilization was set as Specify dissipated energy fraction (with a value of 0.0002) and the use of adaptive stabilization was also on.

Meshing and element type: For the meshing part, the steel plates were modeled with a structured mesh, with a 4-node bilinear plane stress quadrilateral, incompatible modes elements (CPS4I). The cohesive layer was modeled with a sweep mesh and a 4-node two-dimensional cohesive element (COH2D4), with element degradation set on Yes and max degradation set as 1. Instead of entering a viscosity as an input, the tolerance is the one that stabilizes the process. There was only 1 element in the thickness of the adhesive layer. The overall mesh was 0.5 mm.

Figure 47 DLS 4 cracks tolerance mesh

Loading and boundary conditions: The DLS sample was fixed in one side and was being pulled from the other, so the boundary conditions assigned in this model were fixing all the displacements in one edge and assigning a displacement to the other edge. The reaction forces were obtained by summing the value of the RF in all the nodes that were fixed.
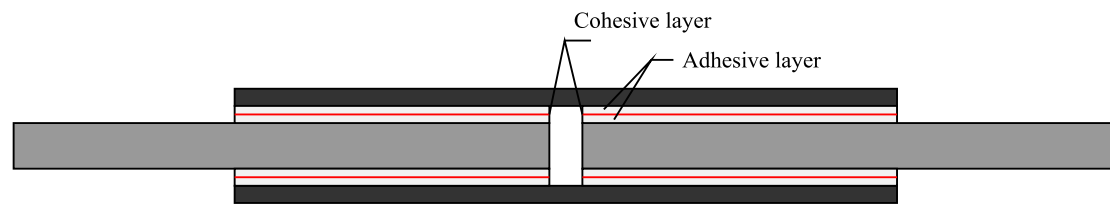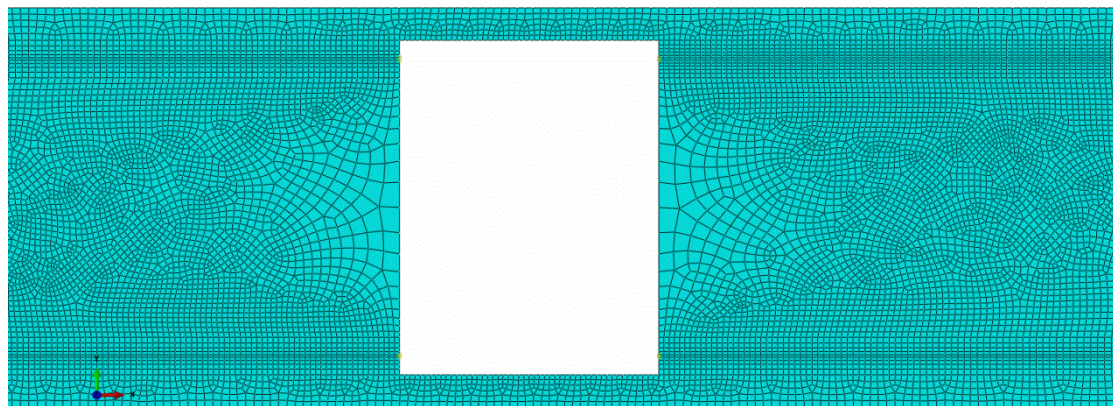
6.4.1.1.4 Kinematic model

Figure 48 DLS 4 cracks kinematic

Material properties: The steel and the CFRP were modeled as solid homogeneous, while the adhesive layers were modeled as 2 layers of solid homogeneous material with a thin layer of cohesive elements in the middle.

Step module: In the step module, the Nlgeom was on, the automatic stabilization was set as Specify dissipated energy fraction (with a value of 0.0002) and the use of adaptive stabilization was also on.
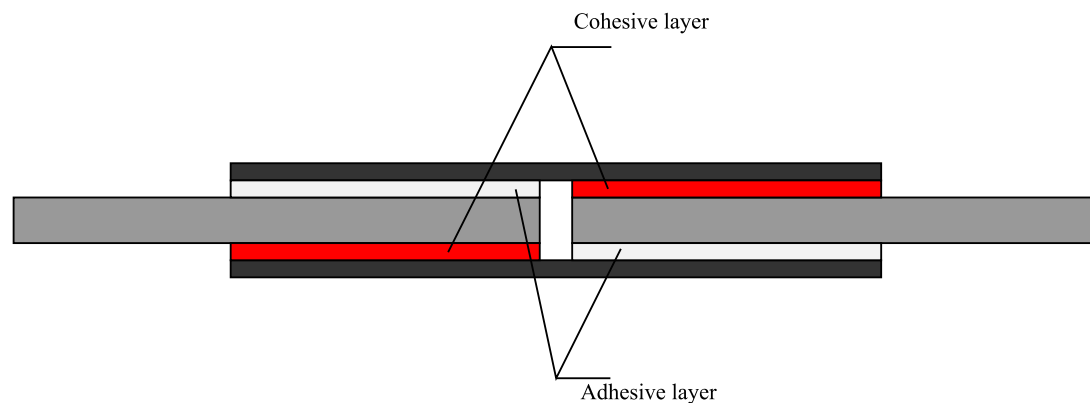
Meshing and element type: For the meshing part, the steel plates were modeled with a structured mesh, with a 4-node bilinear plane stress quadrilateral, incompatible modes elements (CPS4I). The adhesive layer was modeled as structured mesh with a 4-node bilinear plane strain quadrilateral, incompatible modes (CPE4I). The cohesive layer was modeled with a sweep mesh and a 4-node two-dimensional cohesive element (COH2D4), with element degradation set on Yes and max degradation set as 1. In all the element types, the viscosity was set as 0.0001 to stabilize the process. The mesh size in the important points was 0.2x0.2 mm, and it grew till 1.5 mm at the edges of the steel plates.

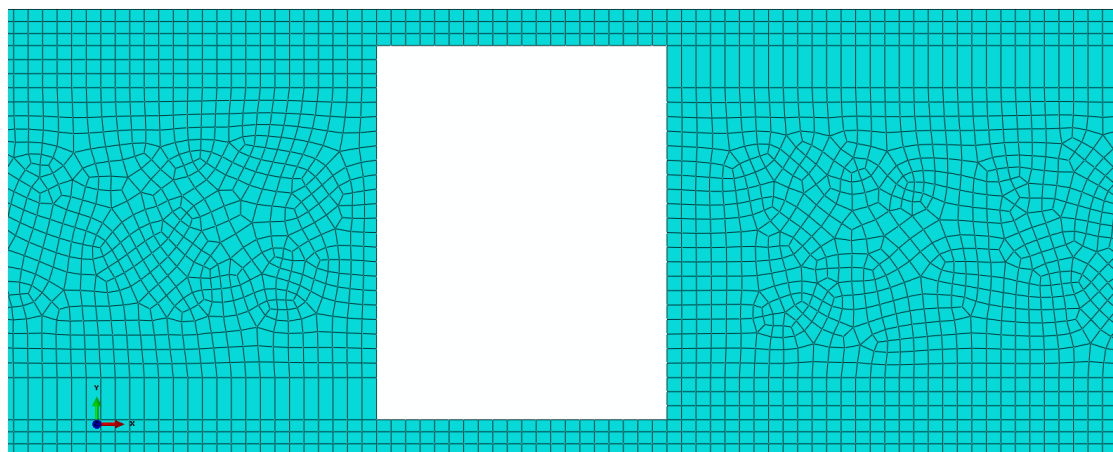**Figure 49DLS 4 cracks kinematic mesh centre**
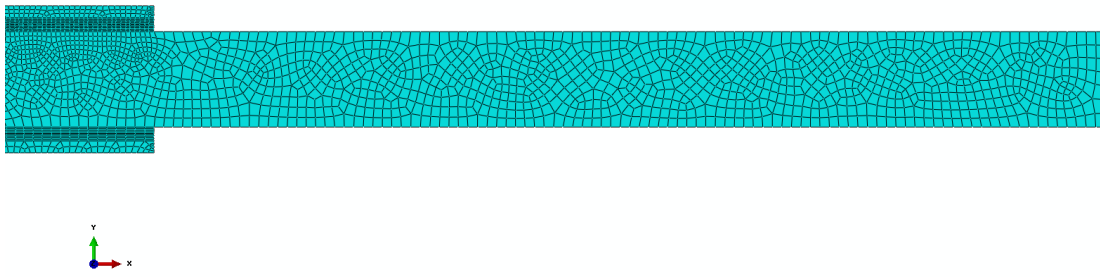
Figure 50 DLS 4 cracks kinematic mesh side

Loading and boundary conditions: The DLS sample was fixed in one side and was being pulled from the other, so the boundary conditions assigned in this model were fixing all the displacements in one edge and assigning a displacement to the other edge. In the displacement side, instead of selecting the whole surface and get the values of RF for each node, in this model a constraint was included, selecting the bottom point of the surface as control point and assigning a kinematic coupling to the surface, so the RF was monitored my only checking this node.

Figure 51 Kinematic model boundaries

6.4.1.1.5 Results
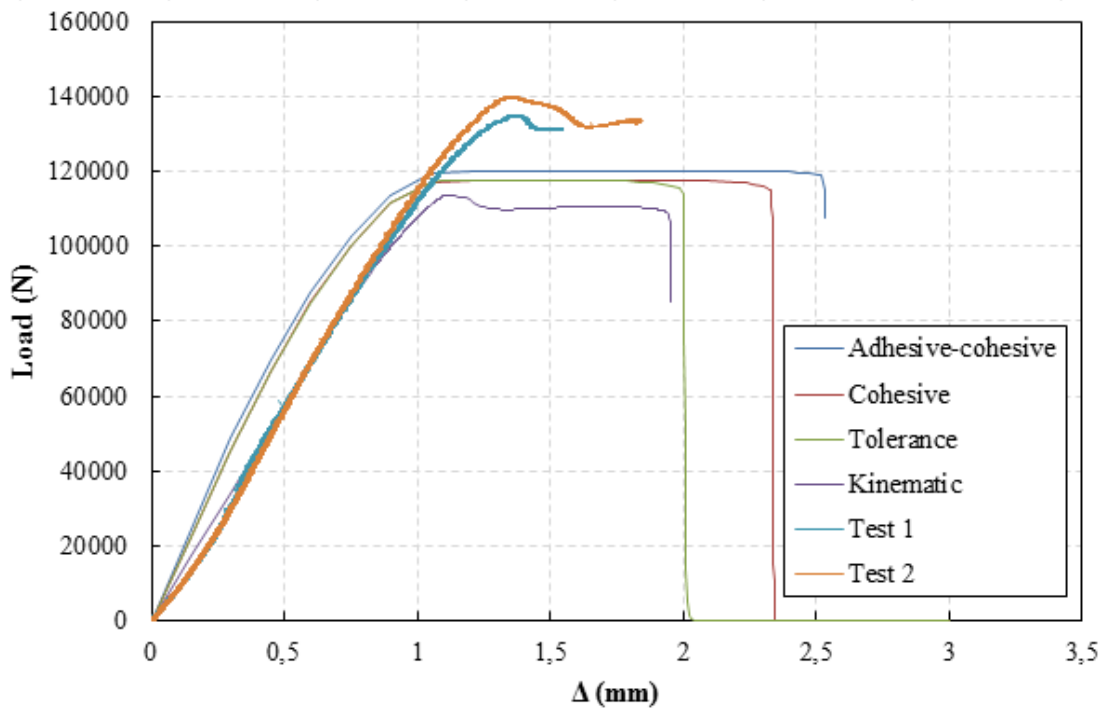
Figure 52 Test and simulation results for the 4 cracks models

6.4.1.2   Two cracks diagonal model

6.4.1.2.1   Cohesive model

Figure 53 DLS 2 cracks diagonal cohesive

Material properties: The steel and the CFRP were modeled as solid homogeneous, while 2 adhesive layers where considered completely as cohesive elements and the other ones as adhesive with solid homogeneous properties.

Step module: In the step module, the Nlgeom was on, the automatic stabilization was set as Specify dissipated energy fraction (with a value of 0.0002) and the use of adaptive stabilization was also on.

Meshing and element type: For the meshing part, the steel plates were modeled with a structured mesh, with a 4-node bilinear plane stress quadrilateral, incompatible modes elements (CPS4I). The cohesive layer was modeled with a sweep mesh and a 4-node two-dimensional cohesive element (COH2D4), with element degradation set on Yes and max degradation set as 1. In all the element types, the viscosity was set as 0.0001 to stabilize the process. There was only 1 element in the thickness of the adhesive layer. The overall mesh was 0.5 mm.

Figure 54 DLS 2 cracks diagonal cohesive mesh

Loading and boundary conditions: The DLS sample was fixed in one side and was being pulled from the other, so the boundary conditions assigned in this model were fixing all the displacements in one edge and assigning a displacement to the other edge. The reaction forces were obtained by summing the value of the RF in all the nodes that were fixed.
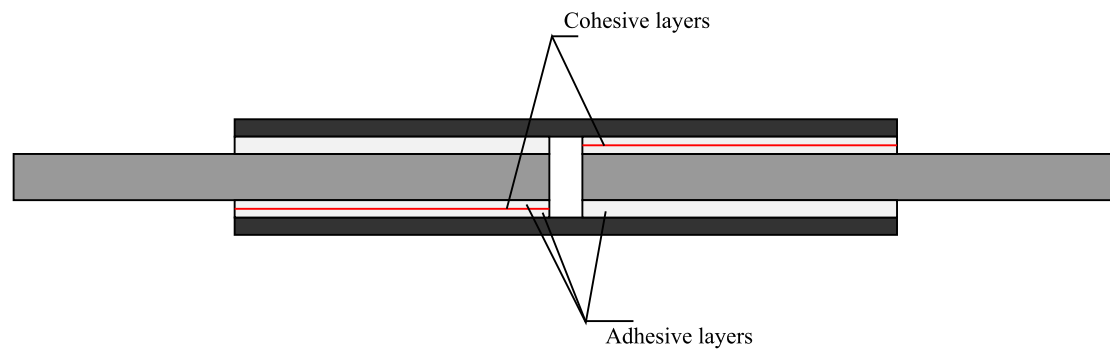
6.4.1.2.2 Adhesive-Cohesive model

Figure 55 DLS 2 cracks diagonal adhesive-cohesive

Material properties: The steel and the CFRP were modeled as solid homogeneous, 2 of the adhesive layers were modeled as 2 layers of adhesive with a cohesive element in the middle, while the other 2 were completely modeled as adhesive layers.

Step module: In the step module, the Nlgeom was on, the automatic stabilization was set as Specify dissipated energy fraction (with a value of 0.0002) and the use of adaptive stabilization was also on.

Meshing and element type: For the meshing part, the steel plates were modeled with a structured mesh, with a 4-node bilinear plane stress quadrilateral, incompatible modes elements (CPS4I). The adhesive layer was modeled as structured mesh with a 4-node bilinear plane strain quadrilateral, incompatible modes (CPE4I). The cohesive layer was modeled with a sweep mesh and a 4-node two-dimensional cohesive element (COH2D4), with element degradation set on Yes and max degradation set as 1. In all the element types, the viscosity was set as 0.0001 to stabilize the process. The mesh size in the important points was 0.2x0.2 mm, and it grew till 1.5 mm at the edges of the steel plates.
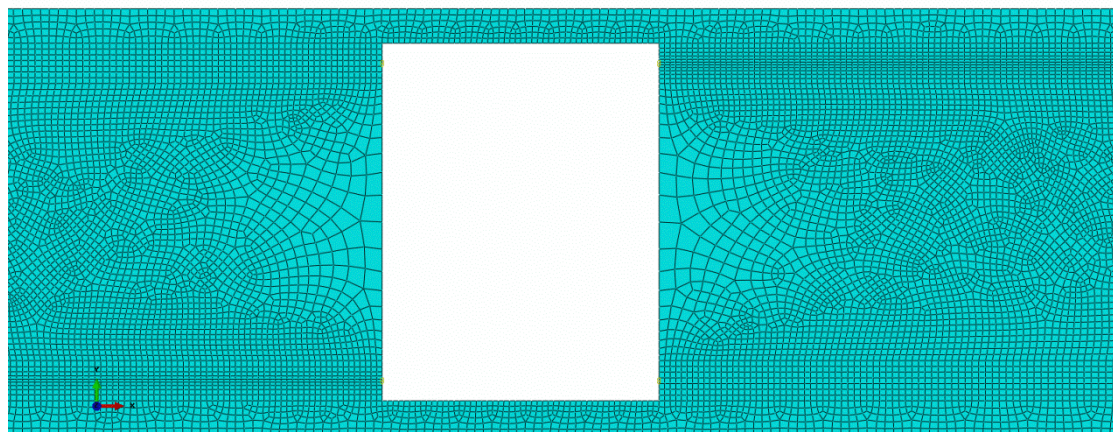

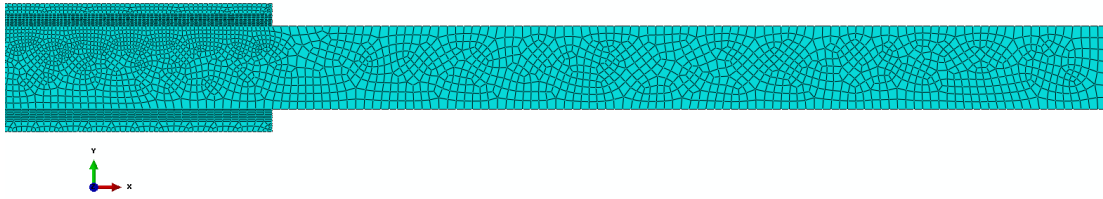**Figure 56** DLs 2 cracks diagonal adhesive-cohesive mesh

Figure 57 DLS 2 cracks diagonal adhesive-cohesive side

Loading and boundary conditions: The DLS sample was fixed in one side and was being pulled from the other, so the boundary conditions assigned in this model were fixing all the displacements in one edge and assigning a displacement to the other edge.
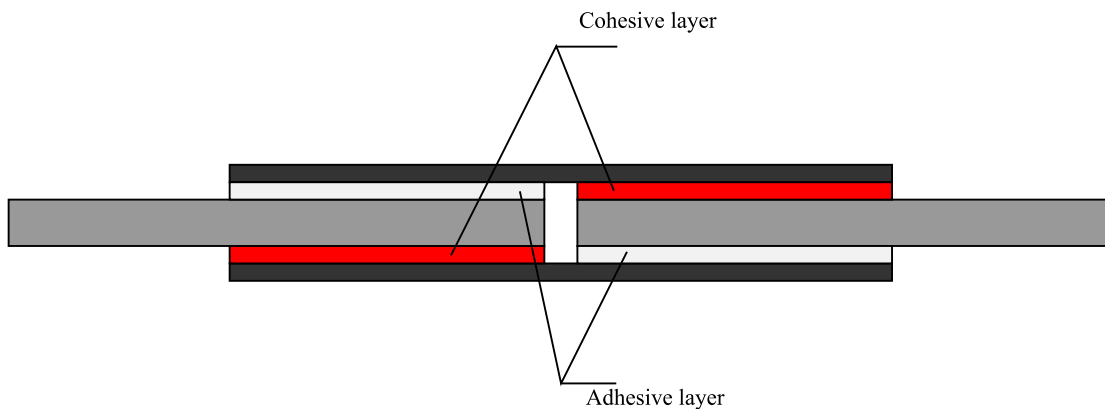
6.4.1.2.3 Tolerance model

Figure 58 DLS 2 cracks diagonal tolerance

Material properties: The steel and the CFRP were modeled as solid homogeneous, while 2 adhesive layers where considered completely as cohesive elements and the other ones as adhesive with solid homogeneous properties. In material properties, the cohesive elements have a tolerance of 0.2 instead of the default 0.05.

Step module: In the step module, the Nlgeom was on, the automatic stabilization was set as Specify dissipated energy fraction (with a value of 0.0002) and the use of adaptive stabilization was also on.

Meshing and element type: For the meshing part, the steel plates were modeled with a structured mesh, with a 4-node bilinear plane stress quadrilateral, incompatible modes elements (CPS4I). The cohesive layer was modeled with a sweep mesh and a 4-node two-dimensional cohesive element (COH2D4), with element degradation set on Yes and max degradation set as 1. Instead of entering a viscosity as an input, the tolerance is the one that stabilizes the process. There was only 1 element in the thickness of the adhesive layer. The overall mesh was 0.5 mm.
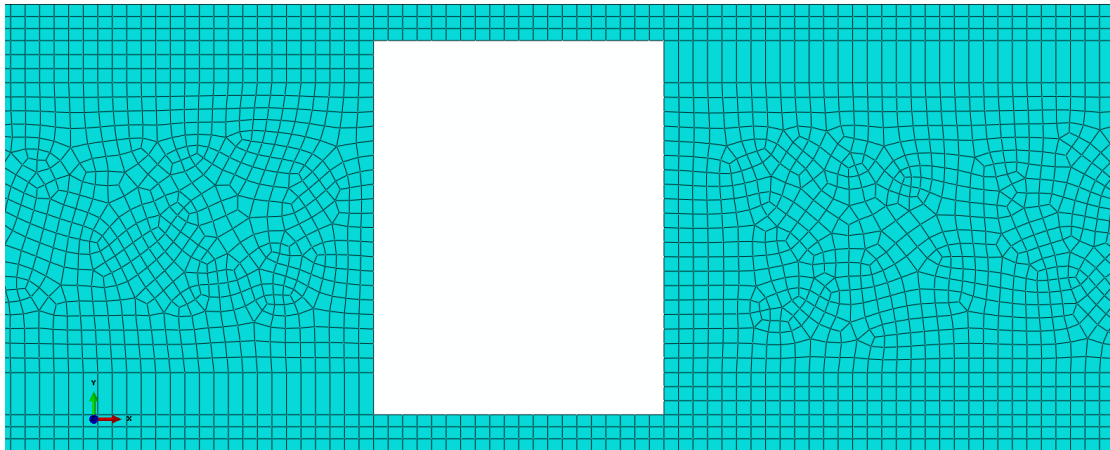
Figure 59 DLS 2 cracks diagonal tolerance mesh

Loading and boundary conditions: The DLS sample was fixed in one side and was being pulled from the other, so the boundary conditions assigned in this model were fixing all the displacements in one edge and assigning a displacement to the other edge. The reaction forces were obtained by summing the value of the RF in all the nodes that were fixed.
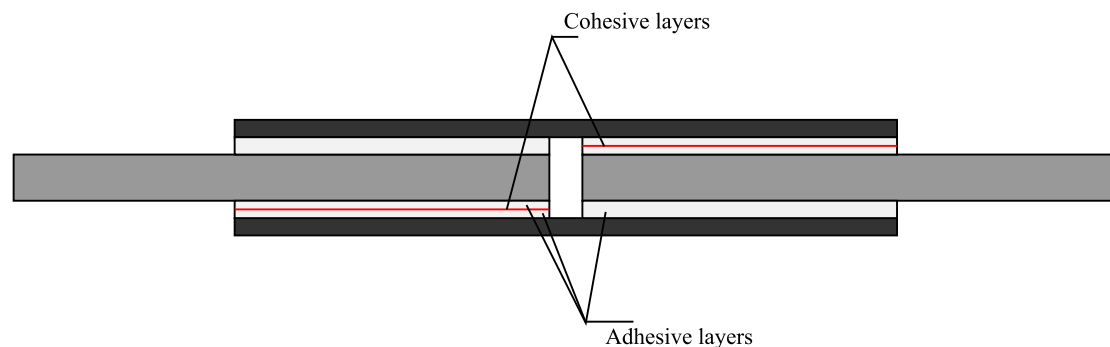
6.4.1.2.4 Kinematic model

Figure 60 DLS 2 cracks diagonal kinematic

Material properties: The steel and the CFRP were modeled as solid homogeneous, 2 of the adhesive layers were modeled as 2 layers of adhesive with a cohesive element in the middle, while the other 2 were completely modeled as adhesive layers.

Step module: In the step module, the Nlgeom was on, the automatic stabilization was set as Specify dissipated energy fraction (with a value of 0.0002) and the use of adaptive stabilization was also on.

Meshing and element type: For the meshing part, the steel plates were modeled with a structured mesh, with a 4-node bilinear plane stress quadrilateral, incompatible modes elements (CPS4I). The adhesive layer was modeled as structured mesh with a 4-node bilinear plane strain quadrilateral, incompatible modes (CPE4I). The cohesive layer was modeled with a sweep mesh and a 4-node two-dimensional cohesive element (COH2D4), with element degradation set on Yes and max degradation set as 1. In all the element types, the viscosity was set as 0.0001 to stabilize the process. The

mesh size in the important points was 0.2x0.2 mm, and it grew till 1.5 mm at the edges of the steel plates.
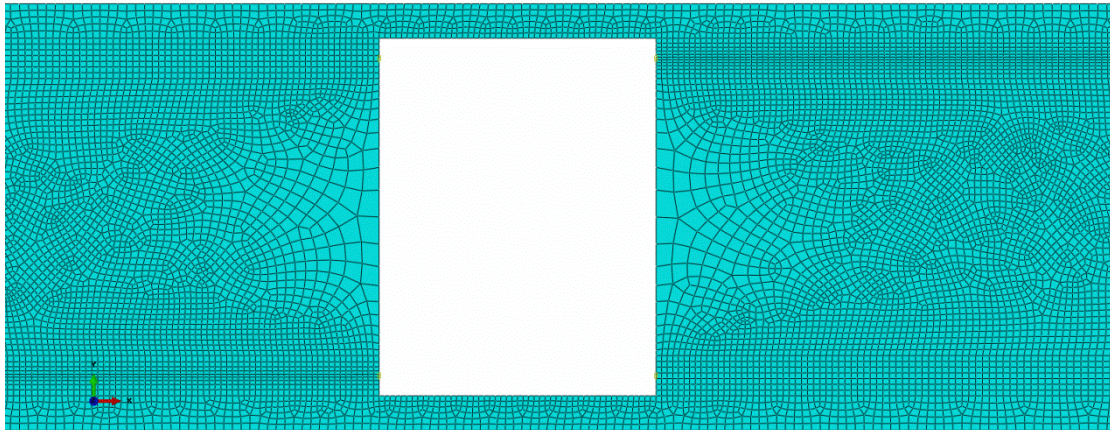

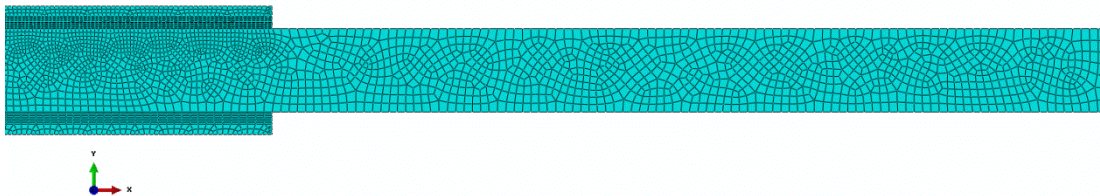**Figure 61** DLS 2 cracks diagonal kinematic mesh centre

Figure 62 DLS 2 cracks diagonal kinematic mesh side

Loading and boundary conditions: The DLS sample was fixed in one side and was being pulled from the other, so the boundary conditions assigned in this model were fixing all the displacements in one edge and assigning a displacement to the other edge. In the displacement side, instead of selecting the whole surface and get the values of RF for each node, in this model a constraint was included, selecting the bottom point of the surface as control point and assigning a kinematic coupling to the surface, so the RF was monitored my only checking this node.

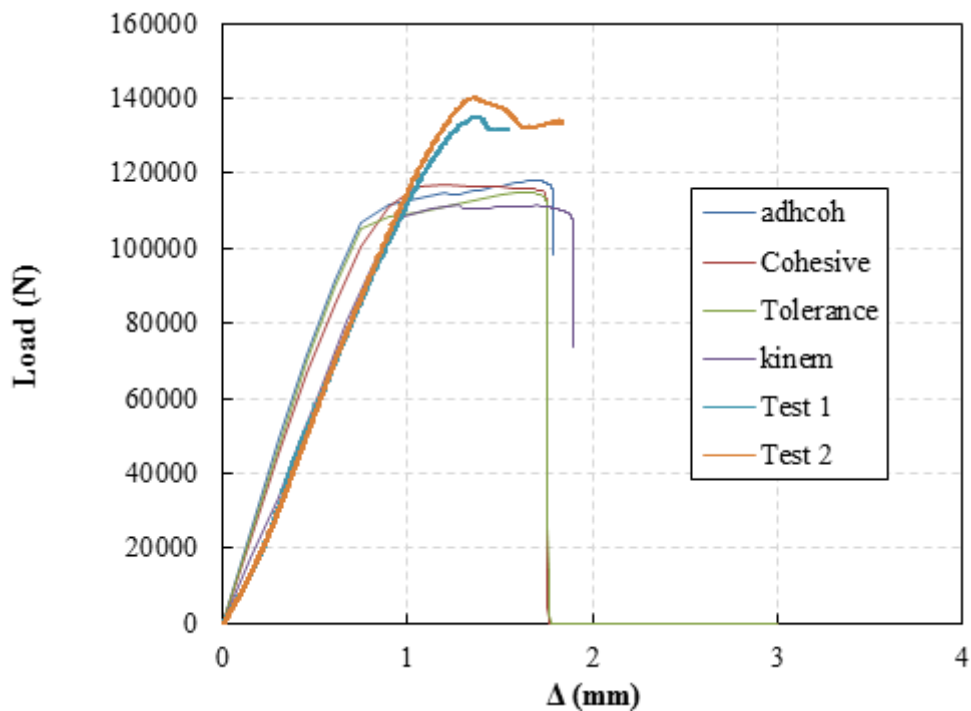**Figure 63** Kinematic model boundaries

6.4.1.2.5 Results

Figure 64 Test and simulation results for the 2 cracks diagonal models

6.4.1.3 Two cracks same side model

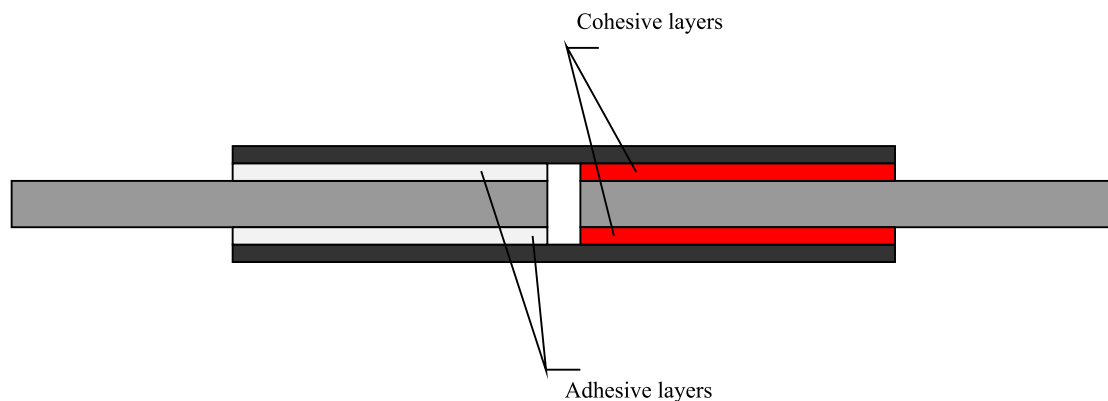### 6.4.1.3.1 Cohesive model

Figure 65 DLS 2 cracks same side cohesive

Material properties: The steel and the CFRP were modeled as solid homogeneous, while 2 adhesive layers where considered completely as cohesive elements and the other ones as adhesive with solid homogeneous properties.

Step module: In the step module, the Nlgeom was on, the automatic stabilization was set as Specify dissipated energy fraction (with a value of 0.0002) and the use of adaptive stabilization was also on.

Meshing and element type: For the meshing part, the steel plates were modeled with a structured mesh, with a 4-node bilinear plane stress quadrilateral, incompatible modes elements (CPS4I). The cohesive layer was modeled with a sweep mesh and a

4-node two-dimensional cohesive element (COH2D4), with element degradation set on Yes and max degradation set as 1. In all the element types, the viscosity was set as 0.0001 to stabilize the process. There was only 1 element in the thickness of the adhesive layer. The overall mesh was 0.5 mm.
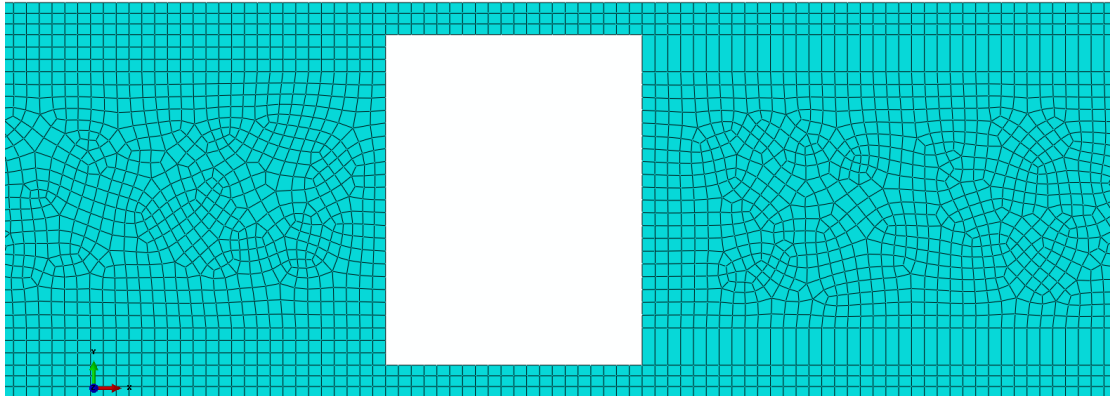

Figure 66 DLS 2 cracks same side cohesive mesh

Loading and boundary conditions: The DLS sample was fixed in one side and was being pulled from the other, so the boundary conditions assigned in this model were fixing all the displacements in one edge and assigning a displacement to the other edge. The reaction forces were obtained by summing the value of the RF in all the nodes that were fixed.
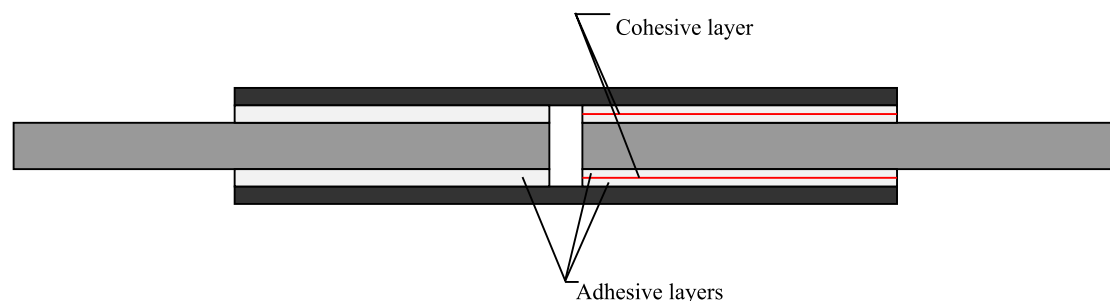
6.4.1.3.2 Adhesive-Cohesive model

Figure 67 DLS 2 cracks same side adhesive-cohesive

Material properties: The steel and the CFRP were modeled as solid homogeneous, 2 of the adhesive layers were modeled as 2 layers of adhesive with a cohesive element in the middle, while the other 2 were completely modeled as adhesive layers.

Step module: In the step module, the Nlgeom was on, the automatic stabilization was set as Specify dissipated energy fraction (with a value of 0.0002) and the use of adaptive stabilization was also on.

Meshing and element type: For the meshing part, the steel plates were modeled with a structured mesh, with a 4-node bilinear plane stress quadrilateral, incompatible modes elements (CPS4I). The adhesive layer was modeled as structured mesh with a 4-node bilinear plane strain quadrilateral, incompatible modes (CPE4I). The cohesive layer was modeled with a sweep mesh and a 4-node two-dimensional cohesive element (COH2D4), with element degradation set on Yes and max degradation set as

1. In all the element types, the viscosity was set as 0.0001 to stabilize the process. The mesh size in the important points was 0.2x0.2 mm, and it grew till 1.5 mm at the edges of the steel plates.
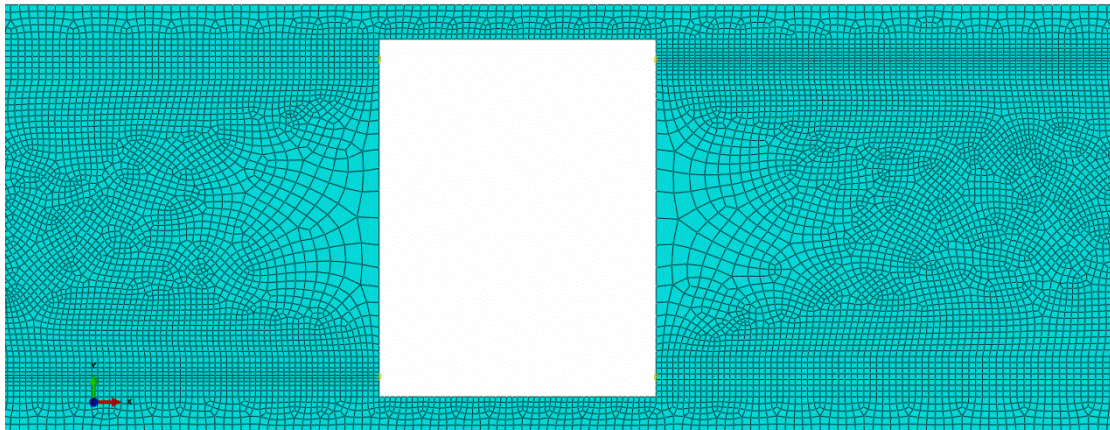

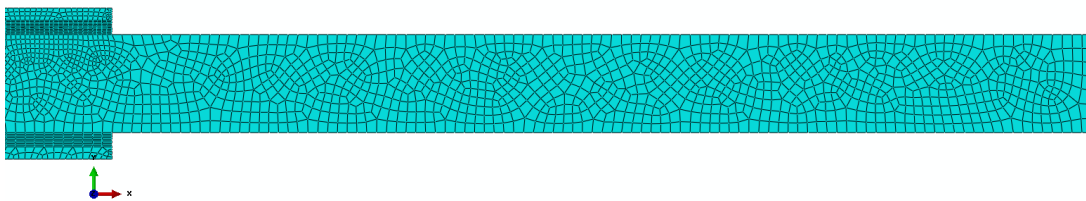**Figure 68** DLS 2 cracks same side adhesive-cohesive mesh centre

Figure 69 DLS 2 cracks adhesive-cohesive mesh side

Loading and boundary conditions: The DLS sample was fixed in one side and was being pulled from the other, so the boundary conditions assigned in this model were fixing all the displacements in one edge and assigning a displacement to the other edge.
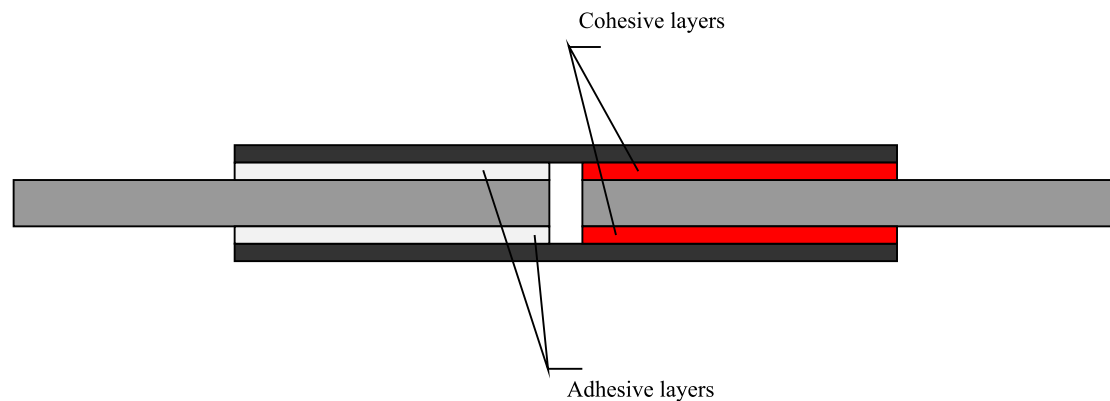
6.4.1.3.3 Tolerance model

Figure 70 DLS 2 cracks same side tolerance

Material properties: The steel and the CFRP were modeled as solid homogeneous, while 2 adhesive layers where considered completely as cohesive elements and the other ones as adhesive with solid homogeneous properties. In material properties, the cohesive elements have a tolerance of 0.2 instead of the default 0.05.

Step module: In the step module, the Nlgeom was on, the automatic stabilization was set as Specify dissipated energy fraction (with a value of 0.0002) and the use of adaptive stabilization was also on.

Meshing and element type: For the meshing part, the steel plates were modeled with a structured mesh, with a 4-node bilinear plane stress quadrilateral, incompatible modes elements (CPS4I). The cohesive layer was modeled with a sweep mesh and a 4-node two-dimensional cohesive element (COH2D4), with element degradation set on Yes and max degradation set as 1. Instead of entering a viscosity as an input, the tolerance is the one that stabilizes the process. There was only 1 element in the thickness of the adhesive layer. The overall mesh was 0.5 mm.
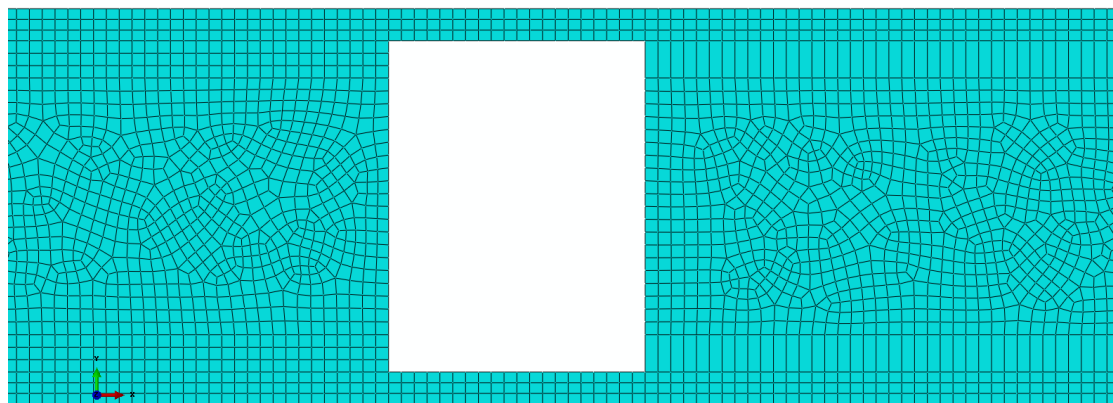

Figure 71 DLS 2 cracks same side tolerance mesh

Loading and boundary conditions: The DLS sample was fixed in one side and was being pulled from the other, so the boundary conditions assigned in this model were fixing all the displacements in one edge and assigning a displacement to the other edge. The reaction forces were obtained by summing the value of the RF in all the nodes that were fixed.
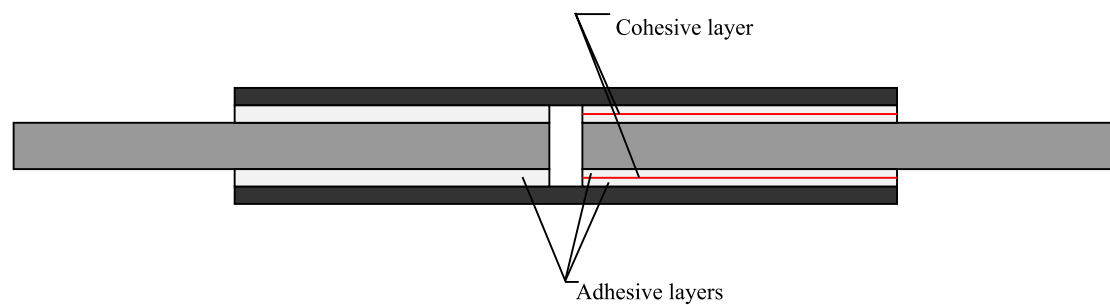
6.4.1.3.4 Kinematic model

Figure 72 DLS 2 cracks same side kinematic

Material properties: The steel and the CFRP were modeled as solid homogeneous, 2 of the adhesive layers were modeled as 2 layers of adhesive with a cohesive element in the middle, while the other 2 were completely modeled as adhesive layers.

Step module: In the step module, the Nlgeom was on, the automatic stabilization was set as Specify dissipated energy fraction (with a value of 0.0002) and the use of adaptive stabilization was also on.

Meshing and element type: For the meshing part, the steel plates were modeled with a structured mesh, with a 4-node bilinear plane stress quadrilateral, incompatible modes elements (CPS4I). The adhesive layer was modeled as structured mesh with a 4-node bilinear plane strain quadrilateral, incompatible modes (CPE4I). The cohesive layer was modeled with a sweep mesh and a 4-node two-dimensional cohesive element (COH2D4), with element degradation set on Yes and max degradation set as 1. In all the element types, the viscosity was set as 0.0001 to stabilize the process. The mesh size in the important points was 0.2x0.2 mm, and it grew till 1.5 mm at the edges of the steel plates.
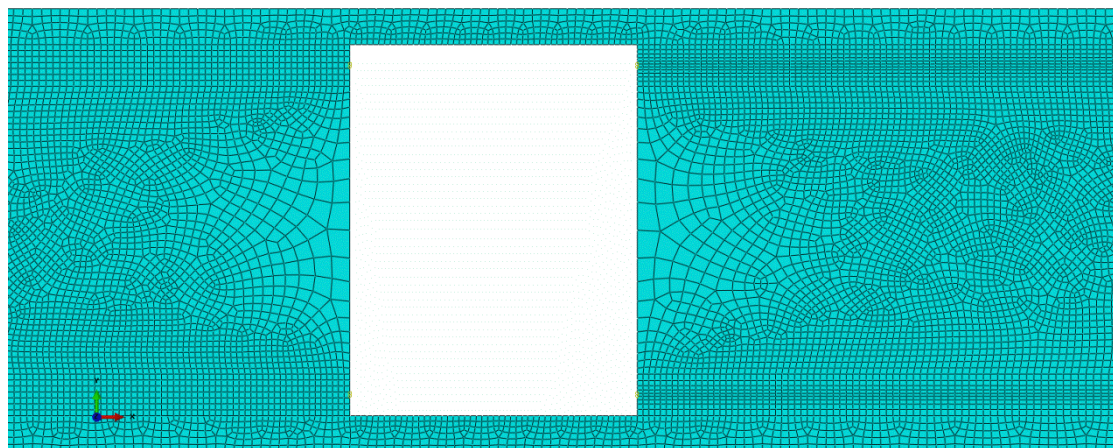

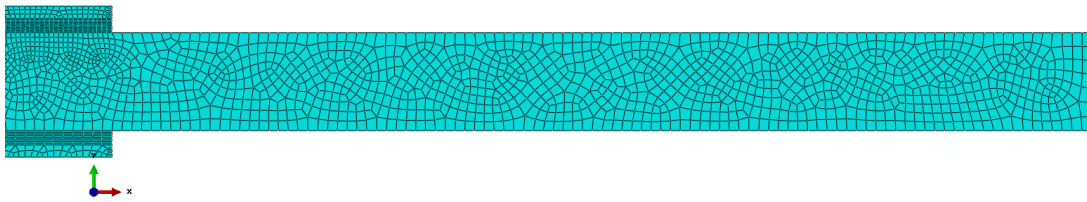**Figure 73** DLS 2 cracks same side tolerance mesh centre

Figure 74 DLS 2 cracks same side tolerance mesh side

Loading and boundary conditions: The DLS sample was fixed in one side and was being pulled from the other, so the boundary conditions assigned in this model were fixing all the displacements in one edge and assigning a displacement to the other edge. In the displacement side, instead of selecting the whole surface and get the values of RF for each node, in this model a constraint was included, selecting the bottom point of the surface as control point and assigning a kinematic coupling to the surface, so the RF was monitored my only checking this node.

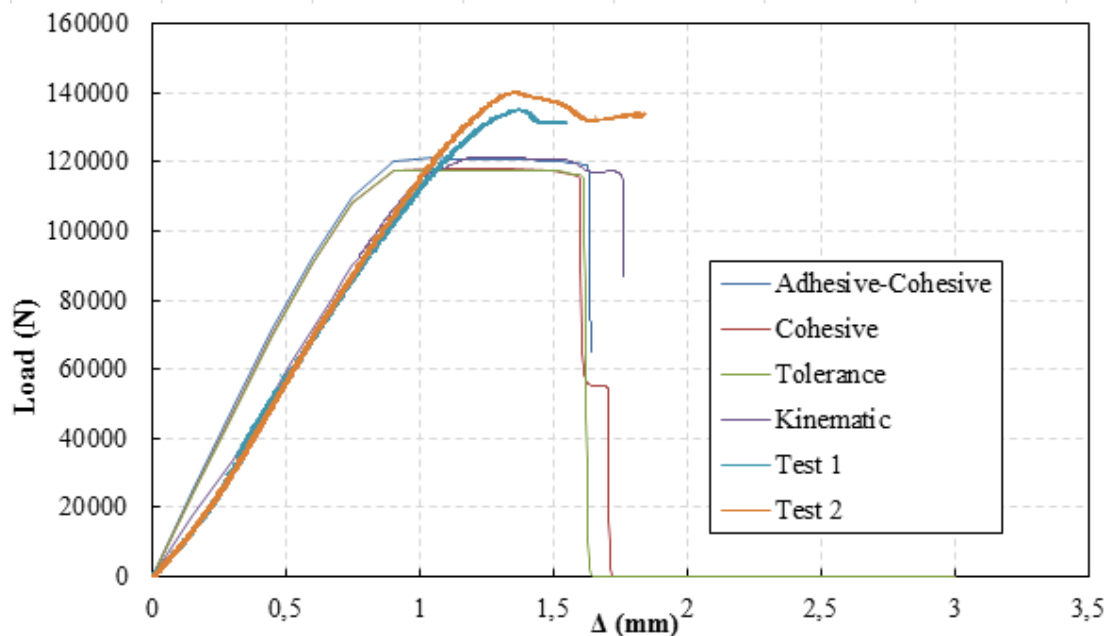**Figure 75** Kinematic model boundaries

6.4.1.3.5 Results

Figure 76 Test and simulation results for the 2 cracks same side models

6.4.2 Description of the 3D model

In order to predict the degradation of the adhesive, a 3D model is needed so it is possible to have different values of moisture in the adhesive layer. In this model, the mesh is thinner in the center of the specimen, and slowly gets bigger in the steel plate edges.
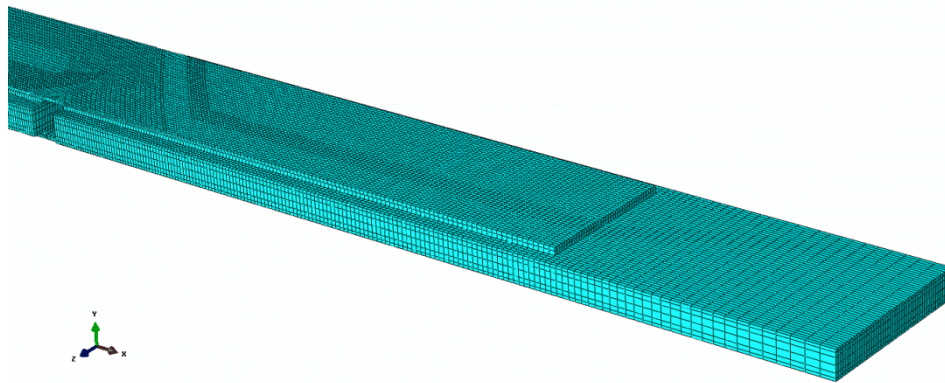

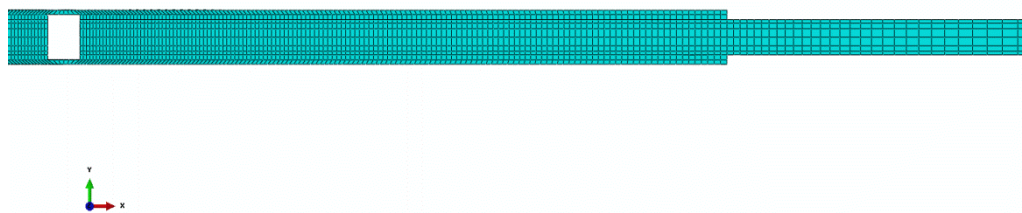**Figure 77** DLS 3D model mesh perspective

Figure 78 DLS 3D mesh from the side

To model the boundary conditions, a constraint is introduced in the face where the displacement is applied. To do this, in the interaction module, a kinematic coupling constraint is selected, and the control point is one of the corners of the edge surface, while the region selected as coupled is that edge surface.
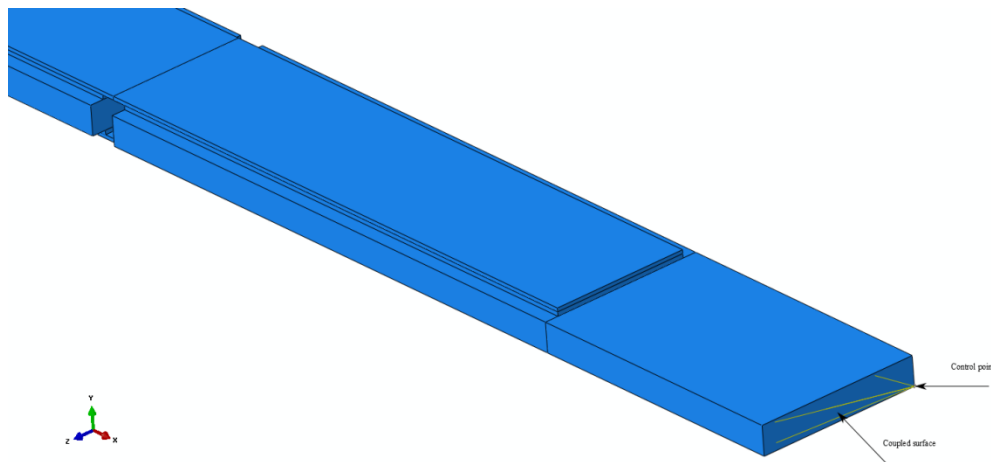
Figure 79 DLS 3D kinematic coupling

Coupling the displacement makes the process of obtaining the load applied very simple, as there is only need to read the reaction force in the control point. Therefore, the boundary conditions are completely fixed in one edge, and a displacement input in the control point of the other edge.

Figure 80 DLS 3D boundaries and loads

The results obtained with the 3D model are showed in next figure:

Figure 81 DLS 3D model compared with the test results

6.5 Coupled analysis

The coupled analysis consists in assigning a value of moisture at each node of the adhesive layer. To do this, ABAQUS can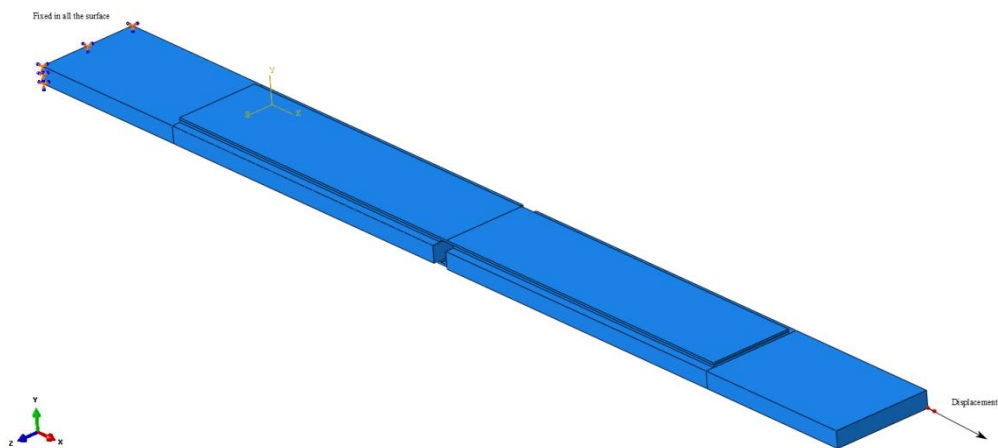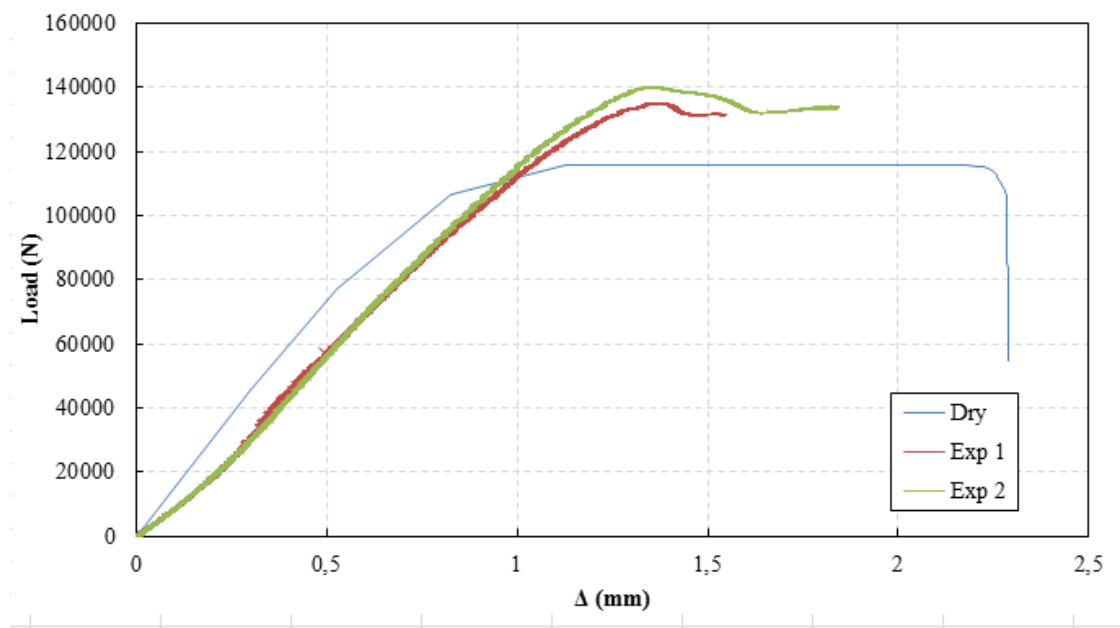't work with moisture amount values, so a change is made between moisture and temperature. This change is explained in the moisture part. The process is:

- Perform a moisture diffusion analysis with the same mesh that is going to be used in the stress analysis.
- In the stress model, in the load module, select predefined field, temperature, and select the output file from the diffusion analysis.
- In the stress analysis, introduce the properties of the adhesive as temperature-dependent.

6.5.1 Influence of moisture in the adhesive properties

To be able to quantify the ratio of degradation of the adhesive properties, some tests should be performed with aged samples in order to obtain the new values of the resistant properties. As the objective of this thesis is to give a methodology of doing this, and aging and performing tests require years of aging, a degradation of 50% in all the material properties is going to be assumed.

6.5.2 Simulation of wet DLS-test

The 3D model used for the wet DLS test is the same that the previous used. To be able to take in account the moisture content, previous moisture diffusion models, using the heat analogy, were performed in order to obtain the moisture content of the adhesive on different times. The following images show this moisture content:

Figure 82 Moisture concentration in 6 months aged DLS sample

Figure 83 Moisture concentration in 1 year aged DLS sample
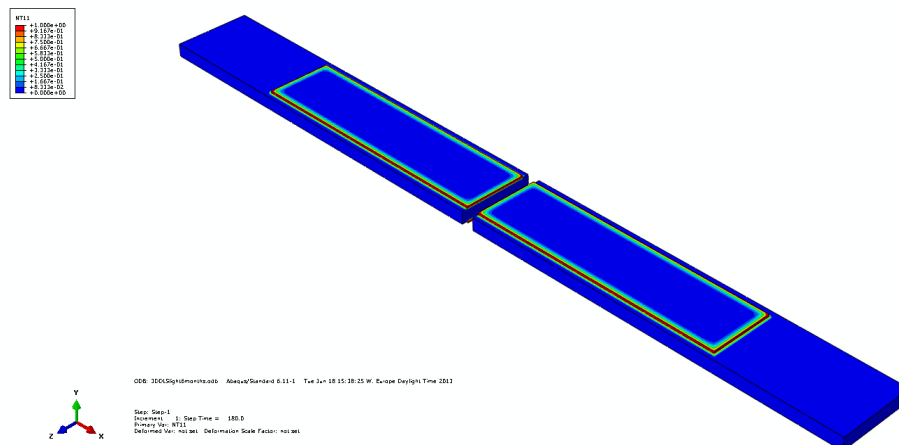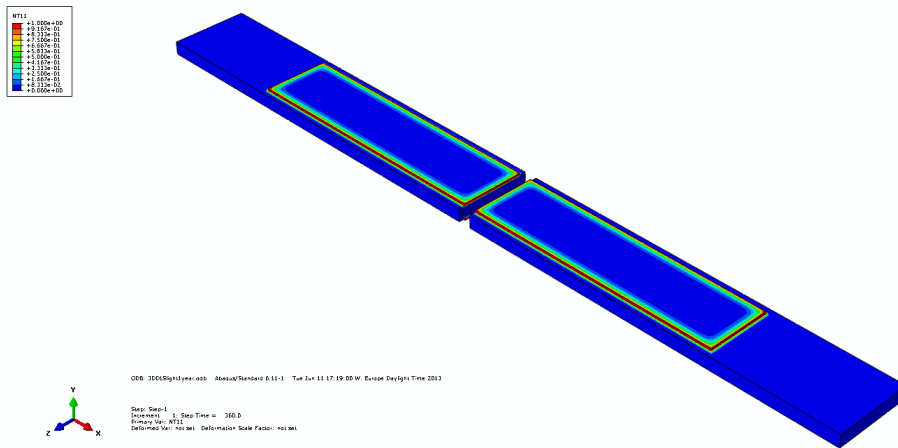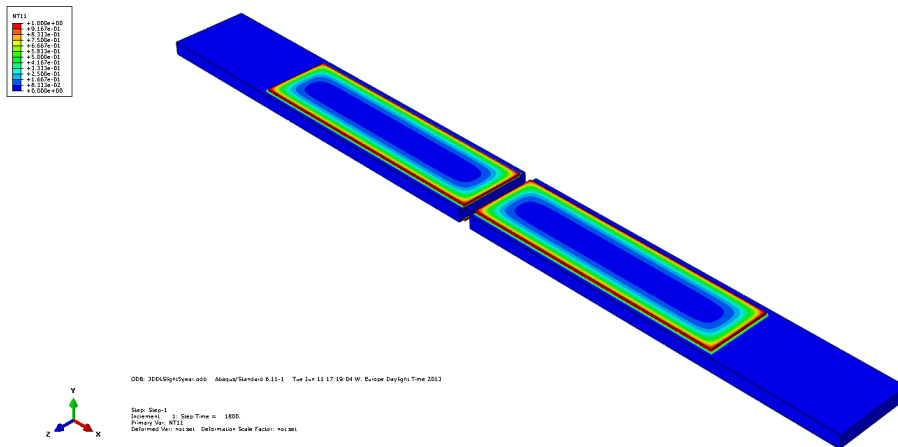

Figure 84 Moisture concentration in 5 years aged DLS sample
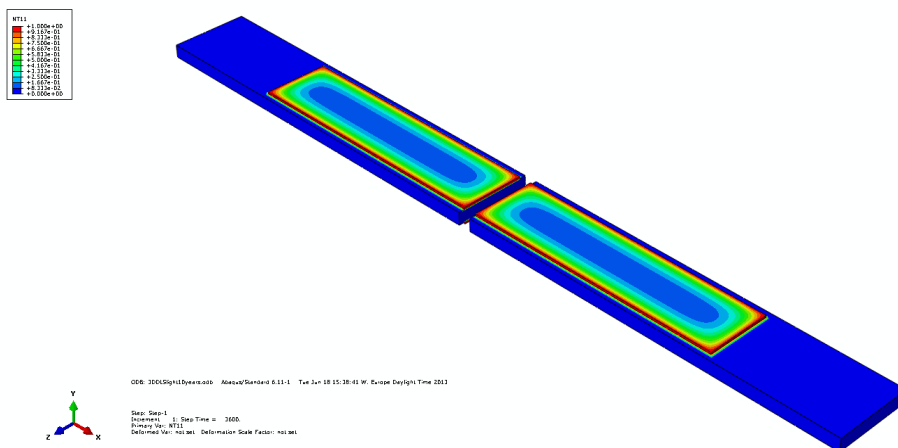

Figure 85 Moisture concentration in 10 years aged DLS sample
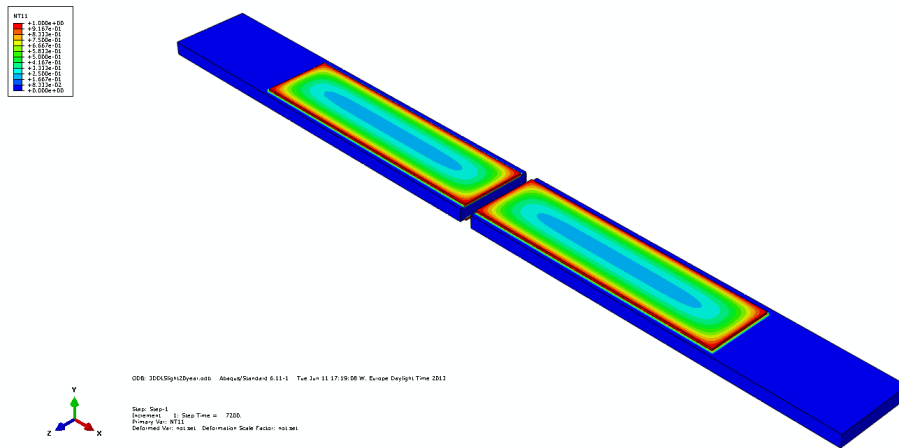
Figure 86 Moisture concentration in 20 years aged DLS sample

Using this time periods, and analyzing the behavior of the aged sample, the simulations give the following results:
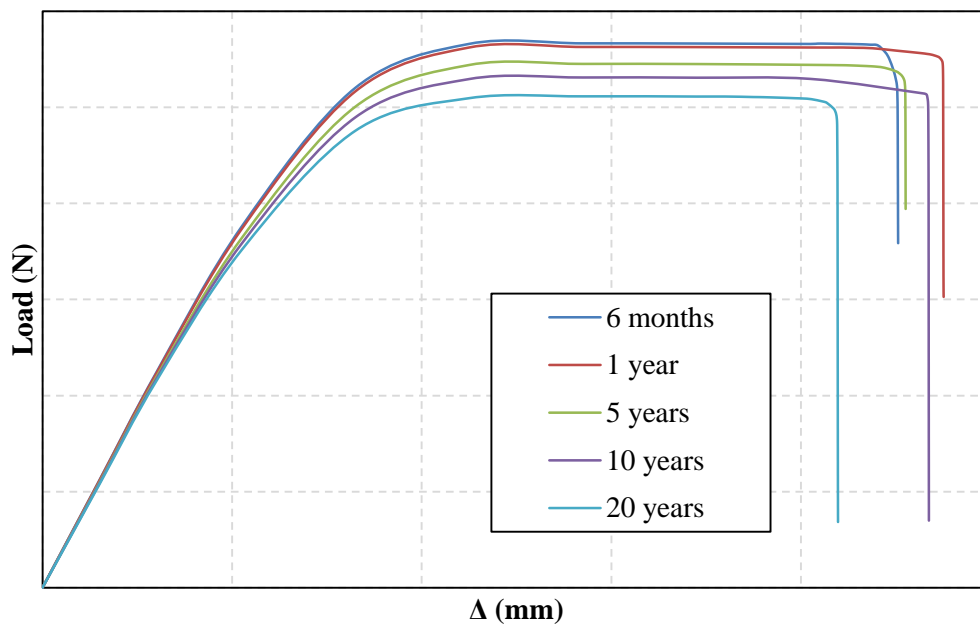

Figure 87 Decrease of ultimate load with the ageing time

7 Results and further investigation

After analyzing the results showed in the previous figures, it is remarkable that the closest approximation to the reality is the kinematic model. The initial slope of the curve is the same, but the simulations give lower ultimate loads than the test results. This may be due to the different speed of pulling between the damage mechanics tests and the DLS tests. For a first approximation, the 2D model gives better results than the 3D model. One possible way of improving this would be to make sure that assuming the third dimensional parameters to be the same as the second one is a correct approximation.

In order to improve the comprehension of the durability of this kind of joins, and to take in consideration more factors that could affect the degradation of the adhesive, the authors propose some different future investigation that should be made

7.1 Corrosion

To take in account corrosion is very important in future investigations. The content of clorures in the water that enters the joint may be high if the join is near the sea, for example. The corrosion brings a new problem to the durability of the union: the interface between the adhesive and the steel gets corroded, and the failure path may change from cohesive to adhesive. To quantify the corrosion, the FTIR test is proposed.

7.1.1 FTIR test

As the authors conclude in their study [60], the interfacial diffusion is different between the centre zone, the intermediate zone and the edge of the bonded joint, and has a significant difference with the adhesive layer diffusion. In order to have an accurate model of the diffusion in the interface, a Fourier Transform Infrared Spectroscopy (FTIR) has been performed.

Although it is not going to be used in this thesis, the authors believe that applying this test to the CFRP/steel case would give a better understanding of the degradation process of the interface and a better model would be achieved.

To separate the effect of moisture from the effect of corrosion, one way would be to immerse the samples in 2 different environments, one with deionised water and the other one with water with a specific concentration of salt. The differences between these 2 samples would mean the effect of corrosion.

7.2 Quantify the degradation of the adhesive

In order to model the degradation of the adhesive, this thesis assumed a degradation of 50% when the moisture content was 100%. Getting real values by making damage mechanics tests with aged samples would bring a more accurate approximation and a good prediction of the ultimate load and join degradation.

8   Conclusion

This thesis has given a methodology that is able to predict the adhesive degradation of a DLS joint strength due to moisture ingress. To be able to verify this methodology, two different tests were performed: TRB and DLS tests. In both of them, the models prediction is close to the real behavior of the samples. In order to do the coupled analysis, a moisture diffusion analysis was done on ABAQUS and was verified in MATLAB, with an analytical solution.

This work only considers the cohesive failure; hence all the models had the hypothesis of having the crack path in the middle of the adhesive. This is because, as the samples tested were un-aged, the interface between steel and adhesive was not affected by moisture or corrosion. Therefore, an interfacial failure was not supposed to appear. These hypotheses were confirmed with the 2 test samples.

Even though the gravimetric values have been taken from other works, the simulation of the aged samples showed that moisture affects the behavior of the joint, decreasing its properties, and it is something that must be taken in account.

The following main conclusions can be drawn:

- Moisture can be correctly modeled by both FEM and numerical software, and both give the same result.
- Moisture affects the durability of the adhesively bonded joints, and in this thesis the reduction of strength has been predicted and quantified.
- The effect of the salt has to be quantified in further investigation.
- Fracture mechanics tests are needed to be able to model and predict the behavior of the DLS and the TRB joints.
- Different ways of modeling the DLS and TRB joints have been investigated and compared.
- Both the 2D and the 3D models in ABAQUS give the same result.

9 References

1. Loh, W.K., et al., *Modelling interfacial degradation using interfacial rupture elements.* Journal of Adhesion, 2003. **79**(12): p. 1135-1160.

2. Liljedahl, C.D.M., et al., *Modelling the environmental degradation of the interface in adhesively bonded joints using a cohesive zone approach.* Journal of Adhesion, 2006. **82**(11): p. 1061-1089.

3. Britannica, E., *Encyclopaedia Britannica.* 1964: Encyclopaedia Britannica.

4. Cromwell, J.R., K.A. Harries, and B.M. Shahrooz, *Environmental durability of externally bonded FRP materials intended for repair of concrete structures.* Construction and Building Materials, 2011. **25**(5): p. 2528-2539.

5. Dawood, M. and S. Rizkalla, *Environmental durability of a CFRP system for strengthening steel structures.* Construction and Building Materials, 2010. **24**(9): p. 1682-1689.

6. Nguyen, T.-C., et al., *Durability of steel/CFRP double strap joints exposed to sea water, cyclic temperature and humidity.* Composite Structures, 2012. **94**(5): p. 1834-1845.

7. Crocombe, A.D., et al., *Predicting the residual strength for environmentally degraded adhesive lap joints.* International Journal of Adhesion and Adhesives, 2006. **26**(5): p. 325-336.

8. Bocciarelli, M., et al., *Prediction of debonding strength of tensile steel/CFRP joints using fracture mechanics and stress based criteria.* Engineering Fracture Mechanics, 2009. **76**(2): p. 299-313.

9. Silva, L.F.M. and R.D.S.G. Campilho, *Advances in Numerical Modelling of Adhesive Joints.* 2012: p. 1-93.

10. Meier, U., *Strengthening of structures using carbon fibre/epoxy composites.* Construction and Building Materials, 1995. **9**(6): p. 341-351.

11. Meier, U., *Carbon fiber-reinforced polymers: modern materials in bridge engineering.* Structural Engineering International, 1992. **2**(1): p. 7-12.

12. Bakis, C., et al., *Fiber-reinforced polymer composites for construction-state-of-the-art review.* Journal of Composites for Construction, 2002. **6**(2): p. 73-87.

13. Sung, N.H., Comyn, J., Bolger, J. C., *How Moisture Affects Adhesive and Sealant Joints _ Part I.*

14. Mubashar, A., et al., *Moisture absorption–desorption effects in adhesive joints.* International Journal of Adhesion and Adhesives, 2009. **29**(8): p. 751-760.

15. Hua, Y., et al., *Modelling Environmental Degradation in EA9321-Bonded Joints using a Progressive Damage Failure Model.* The Journal of Adhesion, 2006. **82**(2): p. 135-160.

16. Liljedahl, C.D.M., et al., *Modelling the Environmental Degradation of the Interface in Adhesively Bonded Joints using a Cohesive Zone Approach.* The Journal of Adhesion, 2006. **82**(11): p. 1061-1089.

17. Hohman, A.E.s., Charles M., *Durability of Adhesively Bonded Structure.* LTV AEROSPACE AND DEFENSE CO DALLAS TX, 1992: p. 80.

18. Comyn, J.S., S.J. Minford, J.D., *Improving the Moisture Resistance of Adhesives and Sealants - Part II.*

19. da Silva, L.F.M. and R.D. Adams, *Joint strength predictions for adhesive joints to be used over a wide temperature range.* International Journal of Adhesion and Adhesives, 2007. **27**(5): p. 362-379.

20. Sugiman, S., A.D. Crocombe, and I.A. Aschroft, *Experimental and numerical investigation of the static response of environmentally aged adhesively bonded joints.* International Journal of Adhesion and Adhesives, 2013. **40**: p. 224-237.

21. RAM RAGHAVA, R.M.C., *The macroscopic yield behaviour of polymers.*

22. Vable, M. and J. Reddy Maddi, *Boundary element analysis of adhesively bonded joints.* International Journal of Adhesion and Adhesives, 2006. **26**(3): p. 133-144.

23. BALDAN, A., *Adhesively-bonded joints in metallic alloys, polymers and composite materials Mechanical and environmental durability performance.*

24. Harris, R.D.A.a.J.A., *The influence of local geometry on the strength of adhesive joints.*

25. Peppiatt, N.A. and R.D. Adams, *Effect of poisson's ratio strains in adherends on stresses of an idealized lap joint.* The Journal of Strain Analysis for Engineering Design, 1973. **8**(2): p. 134-139.

26. J. Olvier, A.E.H., M.D.G. Pulido, *From continuum mechanics to fracture mechanics: The strong discontinuity approach.*

27. H.M. Westergaard, D.M.M., E. Orowan, *Linear Elastic Fracture Mechanics.*

28. Mei, H. and S. Gowrishankar, *INITIATION AND PROPAGATION OF INTERFACIAL DELAMINATION.*

29. Salimi, S., *Application of cohesive modeling in joining technology.* 2012(Thesis).

30. Bocciarelli, M. and P. Colombi, *Elasto-plastic debonding strength of tensile steel/CFRP joints.* Engineering Fracture Mechanics, 2012. **85**: p. 59-72.

31. Katnam, K.B., et al., *Characterisation of moisture-dependent cohesive zone properties for adhesively bonded joints.* Engineering Fracture Mechanics, 2010. **77**(16): p. 3105-3119.

32. Shah, S.P., Stuart E. Swartz, and Chengsheng Ouyang, *Fracture mechanics of concrete: applications of fracture mechanics to concrete, rock and other quasi-brittle materials.* . Vol. Vol. 552. 1995, New York.

33. Song, S.H., G.H. Paulino, and W.G. Buttlar, *A bilinear cohesive zone model tailored for fracture of asphalt concrete considering viscoelastic bulk material.* Engineering Fracture Mechanics, 2006. **73**(18): p. 2829-2848.

34. Turon, A., et al., *An engineering solution for mesh size effects in the simulation of delamination using cohesive zone models.* Engineering Fracture Mechanics, 2007. **74**(10): p. 1665-1682.

35. Thouless, Q.D.Y.a.M.D., *MIXED-MODE FRACTURE ANALYSES OF PLASTICALLY-DEFORMING ADHESIVE JOINTS.*

36. 570-98, A.D.D., *Standard Test Method for Water Absorption of Plastics.*

37. Liljedahl, C.D.M., et al., *Damage modelling of adhesively bonded joints.* International Journal of Fracture, 2006. **141**(1-2): p. 147-161.

38. Liljedahl, C.D.M., et al., *Modelling the environmental degradation of adhesively bonded aluminium and composite joints using a CZM approach.* International Journal of Adhesion and Adhesives, 2007. **27**(6): p. 505-518.

39. Sørensen, B.F. and T.K. Jacobsen, *Determination of cohesive laws by the< i> J</i> integral approach.* Engineering fracture mechanics, 2003. **70**(14): p. 1841-1858.

40. Rethore, J., et al., *Estimation of mixed-mode stress intensity factors using digital image correlation and an interaction integral.* International Journal of Fracture, 2005. **132**(1): p. 65-79.

41. Ortiz, M. and A. Pandolfi, *Finite-deformation irreversible cohesive elements for three-dimensional crack-propagation analysis.* International Journal for Numerical Methods in Engineering, 1999. **44**(9): p. 1267-1282.

42. Merkle, J. and H. Corten, *J integral analysis for the compact specimen, considering axial force as well as bending effects*, 1973, Oak Ridge National Lab., Tenn.(USA); Illinois Univ., Urbana (USA). Dept. of Theoretical and Applied Mechanics.

43. McMeeking, R.M., *Finite deformation analysis of crack-tip opening in elastic-plastic materials and implications for fracture.* Journal of the Mechanics and Physics of Solids, 1977. **25**(5): p. 357-381.

44. Growth, S.C., *Studies on crack initiation and stable crack growth.* Elastic-plastic fracture, 1983: p. 65.

45. Gowrishankar, S., et al., *A comparison of direct and iterative methods for determining traction-separation relations.* International Journal of Fracture, 2012. **177**(2): p. 109-128.

46. Ernst, H., P. Paris, and J. Landes. *Estimations on J-integral and tearing modulus T from a single specimen test record.* in *Fracture mechanics: thirteenth conference, ASTM STP.* 1981.

47. De Moura, M., et al., *Cohesive and continuum mixed-mode damage models applied to the simulation of the mechanical behaviour of bonded joints.* International Journal of Adhesion and Adhesives, 2008. **28**(8): p. 419-426.

48. Carka, D. and C.M. Landis, *On the path-dependence of the J-integral near a stationary crack in an elastic-plastic material.* Journal of Applied Mechanics, 2011. **78**(1): p. 011006.

49. Brocks, W. and H. Yuan, *Numerical investigations on the significance of J for large stable crack growth.* Engineering Fracture Mechanics, 1989. **32**(3): p. 459-468.

50. Brocks, W. and I. Scheider, *Reliable J-values: Numerical aspects of the path-dependence of the J-integral in incremental plasticity.* Materialprüfung, 2003. **45**(6): p. 264-275.

51.   Begley, J. and J. Landes, *The J-integral as a fracture criterion.* Astm Stp, 1972. **514**(514): p. 1-20.

52.   Katnam, K.B., et al., *Characterisation of Moisture Dependent Cohesive Zone Properies for adhesively bonded joints.* 2010.

53.   Mubashar, A., et al., *Strength prediction of adhesive joints after cyclic moisture conditioning using a cohesive zone model.* Engineering Fracture Mechanics, 2011. **78**(16): p. 2746-2760.

54.   Alfano, G., *On the influence of the shape of the interface law on the application of cohesive-zone models.* Composites Science and Technology, 2006. **66**(6): p. 723-730.

55.   Gustafson, P.A. and A.M. Waas, *The influence of adhesive constitutive parameters in cohesive zone finite element models of adhesively bonded joints.* International Journal of Solids and Structures, 2009. **46**(10): p. 2201-2215.

56.   Roy, S., et al., *Cohesive Layer Modeling of Time-Dependent Debond Growth in Aggressive Environments.* Journal of Engineering Materials and Technology, 2006. **128**(1): p. 11.

57.   Zhu, Y., K.M. Liechti, and K. Ravi-Chandar, *Direct extraction of rate-dependent traction–separation laws for polyurea/steel interfaces.* International Journal of Solids and Structures, 2009. **46**(1): p. 31-51.

58.   Jiang, X., H. Kolstein, and F.S.K. Bijlaard, *Moisture diffusion and hygrothermal aging in pultruded fibre reinforced polymer composite of bridge docks.* 2012.

59.   Mubashar, A., et al., *Moisture absorption-desorption effects in adhesive joints.* 2009.

60.   Ma, G.H., F.A. Zhang, and C.S. Gu, *Preparation of Polymer Microspheres Using Silane Coupling Agent Modified Nano-SiO$_2$ as Single Stabilizer.* Advanced Materials Research, 2011. **341-342**: p. 247-251.

Appendix A

```matlab
%----------------------------------------------------------------
% Ficks second law modeling using analytical solution.
%----------------------------------------------------------------
clc
clear all
close all


x0=50;
y0=200;
r=0;


x1=x0/2;
y1=y0/2;
D=0.0178848;
t=7200;
y=0;
    for x=-x1:2.38095:x1
         r=r+1;
        for j=0:100
              for m=0:100
               a(m+1)=((2*m+1)*pi*y)/(y0);
               b(m+1)=(-D*(2*m+1)^2*pi^2*t)/(y0^2);
               f(j+1)=((2*j+1)*pi*x)/(x0);
               g(j+1)=(-D*(2*j+1)^2*pi^2*t)/(x0^2);

aux(m+1)=(exp(g(j+1))*exp(b(m+1))*cos(f(j+1))*cos(a(m+1))...
                  *(((-1)^j)*((-1)^m)/((2*j+1)*(2*m+1))));


            end
                  aux2(j+1)=sum(aux);
           end
        h(r)=1-(16/pi^2)*sum(aux2);
        x2(r)=x;
    end


plot(x2,h);
ylim([0,1]);
```